NAVAL POSTGRADUATE SCHOOL
Monterey, California

DISSERTATION

NEARSHORE CURRENTS OVER A BARRED BEACH

by

Antonio Fernando Garcez Faria

June, 1997

Dissertation Supervisor and Committee Chairman:	Edward B. Thornton
Committee Members:	Timothy P. Stanton
	Thomas H.C. Herbers
	Roger T. Williams
	Thomas C. Lippmann

Approved for public release; distribution is unlimited.

REPORT DOCUMENTATION PAGE

Form Approved OMB No. 0704-0188

1. AGENCY USE ONLY *(Leave blank)*	2. REPORT DATE June 1997	3. REPORT TYPE AND DATES COVERED Doctoral Dissertation

4. TITLE AND SUBTITLE NEARSHORE CURRENTS OVER A BARRED BEACH

5. FUNDING NUMBERS

6. AUTHOR(S) Faria, Antonio Fernando Garcez

7. PERFORMING ORGANIZATION NAME(S) AND ADDRESS(ES)
Naval Postgraduate School
Monterey CA 93943-5000

8. PERFORMING ORGANIZATION REPORT NUMBER

9. SPONSORING/MONITORING AGENCY NAME(S) AND ADDRESS(ES)
Office of Naval Research
Coastal Sciences

10. SPONSORING/MONITORING AGENCY REPORT NUMBER

11. SUPPLEMENTARY NOTES The views expressed in this thesis are those of the author and do not reflect the official policy or position of the Department of Defense or the U.S. Government.

12a. DISTRIBUTION/AVAILABILITY STATEMENT
Approved for public release; distribution is unlimited.

12b. DISTRIBUTION CODE

13. ABSTRACT *(maximum 200 words)*

The objective of this dissertation is to develop numerical models and compare their predictions with data acquired during the DUCK94 experiment in order to improve our physical understanding of the hydrodynamic processes governing the vertical and cross-shore distributions of both longshore and cross-shore currents over a barred beach. The vertical structure of the mean longshore current is found to be well described by a logarithmic profile and a relationship between bed shear stress and bottom roughness, including the influence of ripples and mega-ripples, was also found. The vertical structure of the mean cross-shore current (undertow) is modeled using an eddy viscosity closure scheme to solve for the turbulent shear stress and includes contributions from breaking wave rollers (Lippmann and Thornton, 1997). These models of the vertical profiles of longshore and cross-shore mean currents are combined to formulate a quasi three-dimensional model to describe the cross-shore distribution of the longshore current. This model includes turbulent mixing due to the cross-shore advection of mean momentum of the longshore current by the mean cross-shore current (Putrevu and Svendsen, 1993) and contributions from wave rollers.

14. SUBJECT TERMS longshore current, nearshore, undertow, radiation stress, bottom stress, momentum mixing.

15. NUMBER OF PAGES 178

16. PRICE CODE

17. SECURITY CLASSIFICATION OF REPORT	18. SECURITY CLASSIFICATION OF THIS PAGE	19. SECURITY CLASSIFICATION OF ABSTRACT	20. LIMITATION OF ABSTRACT
Unclassified	Unclassified	Unclassified	UL

NSN 7540-01-280-5500

Standard Form 298 (Rev. 2-89)
Prescribed by ANSI Std. 239-18 298-102

Approved for public release; distribution is unlimited.

NEARSHORE CURRENTS OVER A BARRED BEACH

Antonio Fernando Garcez Faria
Lieutenant Commander, Brazilian Navy
B.S., Brazilian Naval Academy, 1983
M.S., Naval Postgraduate School, 1995

Submitted in partial fulfillment of the requirements for the degree of

DOCTOR OF PHILOSOPHY IN PHYSICAL OCEANOGRAPHY

from the

NAVAL POSTGRADUATE SCHOOL
June 1997

Author: _____
Antonio Fernando Garcez Faria

Approved by: _____
Edward B. Thornton
Professor of Oceanography, Dissertation Supervisor

_____
Timothy P. Stanton
Professor of Oceanography

_____
Thomas H. C. Herbers
Professor of Oceanography

_____
Thomas C. Lippmann
Professor of Oceanography

_____
Roger T. Williams
Professor of Meteorology

Approved by: _____
Robert H. Bourke, Chair, Department of Oceanography

Approved by: _____
Maurice D. Weir, Associate Provost for Instruction

ABSTRACT

The objective of this dissertation is to develop numerical models and compare their predictions with data acquired during the DUCK94 experiment in order to improve our physical understanding of the hydrodynamic processes governing the vertical and cross-shore distributions of both longshore and cross-shore currents over a barred beach. The vertical structure of the mean longshore current is found to be well described by a logarithmic profile and a relationship between bed shear stress and bottom roughness, including the influence of ripples and mega-ripples, was also found. The vertical structure of the mean cross-shore current (undertow) is modeled using an eddy viscosity closure scheme to solve for the turbulent shear stress and includes contributions from breaking wave rollers (Lippmann and Thornton, 1997). These models of the vertical profiles of longshore and cross-shore mean currents are combined to formulate a quasi three-dimensional model to describe the cross-shore distribution of the longshore current. This model includes turbulent mixing due to the cross-shore advection of mean momentum of the longshore current by the mean cross-shore current (Putrevu and Svendsen, 1993) and contributions from wave rollers.

TABLE OF CONTENTS

ACKNOWLEDGMENTS

This work, involving substantial field data acquisition and pre-processing, could not have been completed without the help of many people. In order to recognize all who helped, I would have to write almost another dissertation, and at this point I have to admit that I can barely finish these couple of sentences. Therefore, I would like to at least recognize those who contributed most.

First, I wish to express my appreciation to Prof. Edward B. Thornton, not only for his dedication and assistance as my dissertation supervisor, but also for being able to guide me through "rollers" and "mega-ripples" always with a smile on his face.

Secondly, my thanks to my committee: Prof. Tim Stanton, Tom Herbers, Tom Lippmann and Terry Williams for their support and advice, as well as for reading and critiquing several drafts of this dissertation. In addition, my thanks to Rob Wyland and Jim Stockel for their help in acquiring and pre-processing most of the data that I used.

I also wish to express my deep gratitude to my parents, Walter and Márcia, for all the unmeasurable sacrifices, and love throughout my entire life.

Last, but certainly not least, there is one more person that I would like to thank, withouth whose support, encouragement and understanding, I would certainly not have been able to finish this dissertation in less than two years. This person is my wife, Cláudia, and I would like to thank her not only for being there for me whenever and wherever I needed her, but also for not complaining (at least not a lot) when I was not able to be there for her. Cláudia, without your love and encouragement, I would not have been able to achieve this degree, and therefore I dedicate this work to you.

I. PREFACE

The nearshore currents generated by obliquely incident breaking waves within the surf zone can exceed 1 ms^{-1} during high energy conditions, and are some of the strongest currents with the greatest shear in all the oceans. These strong currents play a major role in oil spills and dispersion of other pollutants, and also transport significant amounts of sediment, having a dramatic effect on beach erosion. Additionally, the modeling of nearshore circulation assumes a special significance for military operations, where the success or failure of an amphibious assault, or a special forces operation is directly related to our ability to forecast the conditions within this unique operational theater.

The physical understanding and mathematical modeling of hydrodynamic processes in the nearshore zone have substantially improved during the last two decades. Yet, most existing models are formulated based on a monochromatic wave description and have been tested and calibrated with laboratory data, due to difficulties associated with measurements within this harsh environment. In this study, monochromatic formulations are extended to random wave fields by using a probabilistic approach (Thornton and Guza, 1983). The numerical models developed here are compared with data acquired during the DUCK94 (October 1994) experiment conducted on a barred ocean beach at the U.S. Army Corps of Engineers Field Research Facility near Duck, North Carolina. The objective of this dissertation is to improve our current understanding of the vertical and cross-shore distributions of both longshore and cross-shore currents, providing the first steps towards a comprehensive three-dimensional model.

In Chapter II, observed vertical structure of the mean longshore current over a barred

beach is examined to test the hypothesis that the turbulent bottom boundary layer of the mean longshore currents is logarithmic and to investigate the influence of wave-breaking generated turbulence on the mean longshore current profile. The relationship between bottom shear stress and bottom roughness, including the influence of ripples and mega-ripples is also investigated. This Chapter consists of a journal article accepted by the *Journal of Geophysical Research.*

The vertical structure of the mean cross-shore current (undertow) over a barred beach is investigated in Chapter III. A surface mass flux model, including contributions from white water surface rollers on breaking wave crests (Lippmann and Thornton, 1997), is used to predict the cross-shore distribution of depth-averaged undertow. The impact of using linear and non-linear wave theories to estimate surface mass flux is investigated. The vertical structure of the undertow is modeled using an eddy viscosity closure to estimate the turbulent shear stress. The effects of different depth-dependent formulations for the eddy viscosity as well different boundary conditions on the vertical structure of the undertow are evaluated.

In Chapter IV, the models of the vertical profiles of longshore and cross-shore mean currents developed in the preceding Chapters are combined to formulate a quasi three-dimensional model to describe the cross-shore distribution of the longshore current. This model includes turbulent mixing due to the cross-shore advection of mean momentum of the longshore current by the mean cross-shore current (Putrevu and Svendsen, 1994), and contributions from breaking wave rollers. The effect of introducing the observed cross-shore variation of bottom shear stress (Chapter I) on the longshore current prediction is investigated.

Each of the three dissertation Chapters represents a separate paper for publication. As such, they are self-contained with their own introduction, theory description, data results, conclusions, and references.

II. VERTICAL PROFILES OF LONGSHORE CURRENTS AND RELATED BED SHEAR STRESS AND BOTTOM ROUGHNESS

(This chapter consists of a journal article accepted by the *Journal of Geophysical Research* in May, 1997)

VERTICAL PROFILES OF LONGSHORE CURRENTS AND RELATED BED SHEAR STRESS AND BOTTOM ROUGHNESS

A.F. Garcez Faria, E.B. Thornton, T.P. Stanton, C.V. Soares[1] and T.C. Lippmann[2]

Naval Postgraduate School, Monterey, California 93940

ABSTRACT

The vertical structure of the mean wave-driven longshore current over a barred beach is examined on three strong current days during the DUCK94 experiment, and it is found that the bottom boundary layer is well described by a logarithmic profile (mean correlation coefficient for all 22 profiles, 0.98). The logarithmic profile fits better in the trough where turbulent bottom boundary layer processes predominate, than over the bar where breaking-wave induced turbulence generated at the surface modifies the profile. The surface layer in the presence of waves is well described by adjusting the logarithmic profile for the intermittent presence of water and adding the alongshore component of the mass transport velocity (slope of the least-squares linear regression between model predictions and observations, 1.005 and *rms* error of 7 percent).

Bed shear stresses calculated from logarithmic velocity profiles are equated to a quadratic bottom shear stress formulation. The associated bed shear stress coefficients vary by more than an order of magnitude across the surf zone (0.0006-0.012). Bottom roughness was measured throughout the nearshore using a sonic altimeter mounted on a moving platform. The bed shear stress coefficients are positively correlated with bottom roughness

---

[1]Presently at Marinha - Instituto Hidrográfico, 1296 Lisboa Codex, Portugal

[2]Presently at the Scripps Institution of Oceanography, La Jolla, California 92903

(linear correlation coefficient, 0.6). A higher linear correlation coefficient (0.8) is obtained by subtracting skin friction from the total bed shear stress.

INTRODUCTION

Knowledge of the bottom boundary and surface layers is fundamental to understanding nearshore hydrodynamics and sediment processes. For steady flow, such as in a river, the bottom boundary layer is well described by a logarithmic profile. Only limited wave-driven, longshore current vertical profiles have been measured. Visser (1986) measured wave-driven longshore currents in a laboratory experiment using micro-propeller and laser Doppler velocimeters and found profiles approached a logarithmic form. In a similar laboratory wave-driven longshore current experiment using laser velocimeters, Simons *et al.*(1992) verified that the vertical profiles tended to be logarithmic.

The velocity profile of a steady current is modified by the presence of waves. The superposition of waves on the mean current produces enhanced bottom friction (e.g., Grant and Madsen, 1979; Christoffersen and Jonsson, 1985; Myrhaug and Slaattelid, 1989; and Sleath, 1990). As a result, the vertical gradient of the mean current near the bed is increased and a more uniform profile can be expected throughout most of the water column. The influence of waves is inversely proportional to water depth and wave frequency, with decreasing importance of nonlinear interactions between waves and currents within the wave-bottom boundary layer with increasing depth and frequency.

Turbulence induced by breaking waves modifies the vertical profile of longshore currents. The downward momentum mixing produced from wave breaking-injected turbulence results in a more uniform velocity profile. Fredsoe and Deigaard (1992), and

Church and Thornton (1993) argue this would result in an increased bed shear stress.

In the following, mean longshore current profiles obtained over a barred beach are examined with the objectives of: 1) testing the hypothesis that the turbulent bottom boundary layer of the mean longshore currents is logarithmic, 2) investigating the influence of the surface layer on the mean longshore current profile, and 3) examining the relationship between bottom shear stress and bottom roughness, including the influence of ripples and mega-ripples.

THEORY

The vertical profile of longshore currents is significantly affected by the bottom boundary and surface layers. The bottom boundary layer assumes more importance since it determines the general logarithmic profile shape over most of the water column. However, processes in the surface layer can modify the profile in the presence of waves and wind.

Bottom Boundary Layer

Neglecting molecular viscous stresses, the alongshore momentum equation (y-direction) is written

$$\frac{\partial \rho v}{\partial t} + \frac{\partial \rho v u}{\partial x} + \frac{\partial \rho v^2}{\partial y} + \frac{\partial \rho w v}{\partial z} = -\frac{\partial p}{\partial y} \qquad \textbf{(1)}$$

The velocities are expanded into mean, turbulent, and wave-induced components, $u_i = U_i + \acute{u}_i + \tilde{u}_i$ and $w = \acute{w} + \tilde{w}$, where $(i = 1,2)$ refers to horizontal coordinates (x,y) and the mean vertical velocity is assumed equal to zero. After time averaging, (1) can be simplified with the aid of the following assumptions: 1) straight and parallel contours, e.g.,

$\frac{\partial}{\partial y}(\overline{\ }) = 0$ (overbar indicates time averaging); 2) steady state conditions, i.e., $\frac{\partial}{\partial t}(\overline{\ }) = 0$; 3) wave-induced and turbulent velocity components are statistically independent (uncorrelated), i.e., $\overline{\tilde{u}\tilde{v}} = 0$; 4) horizontal turbulent momentum flux is small compared to wave induced momentum flux (Stive and Wind, 1982), i.e., $\frac{\partial \overline{\rho \acute{v}\acute{u}}}{\partial x} \ll \frac{\partial \overline{\rho \tilde{v}\tilde{u}}}{\partial x}$, and can be neglected. Contributions due to momentum mixing caused by interactions between cross-shore and longshore currents $(\frac{\partial \overline{\rho VU}}{\partial x})$ are usually not negligible (Svendsen and Putrevu, 1994; and Garcez Faria *et al.*, 1996). Nevertheless, they are neglected here for simplicity sake. Applying these assumptions, the alongshore momentum equations can be written

$$-\frac{\partial \rho \overline{\acute{w}\acute{v}}}{\partial z} = \frac{\partial \rho \overline{\tilde{v}\tilde{u}}}{\partial x} + \frac{\partial \overline{\rho \tilde{w}\tilde{v}}}{\partial z} \qquad (2)$$

which says that the sum of cross-shore changes in the wave-induced alongshore momentum flux and vertical changes in the wave-induced Reynolds stress are balanced by vertical changes in alongshore turbulent shear stress.

Applying a first order turbulence closure, the alongshore turbulent shear stress can be defined

$$\tau_y(z) = -\rho \overline{\acute{w}\acute{v}} = \rho \mu_t \frac{\partial V}{\partial z} \qquad (3)$$

where μ_t is the turbulent eddy viscosity, which is assumed to be uniform with depth. Substituting (3) into (2)

$$\frac{\partial \tau_y(z)}{\partial z} = \frac{\partial \rho \overline{\tilde{v}\tilde{u}}}{\partial x} + \frac{\partial \overline{\rho \tilde{w}\tilde{v}}}{\partial z} \qquad (4)$$

The cross-shore gradient of $\overline{\tilde{v}\tilde{u}}$ is constant in the alongshore direction for straight and parallel contours. Within the surf zone, the shallow water approximation holds, thus $\overline{\tilde{v}\tilde{u}}$ is assumed independent of depth. The wave-induced Reynolds stress term ($\overline{\tilde{w}\tilde{v}}$) can arise from sloping bottom effects as well as from wave amplitude gradient effects and it would have a non-zero contribution even for linear wave theory (Deigaard and Fredsoe, 1989). Nevertheless, Rivero and Arcilla (1995), showed that $\overline{\tilde{w}\tilde{v}}$ is a linear function of depth, and hence its vertical gradient is a constant. Consequently, the right hand side of (4) is independent of depth and the shear stress profile is determined by integrating (4) over depth, to give

$$\tau_y(z) = [\tau_y(0) - \tau_y(-h)] \frac{z}{h} \tag{5}$$

Linearly varying shear stress occurs in flows driven by uniform hydrostatic pressure gradients, such as in steady open channel flows, which are well described by a logarithmic velocity profile. Therefore it is hypothesized that a steady, uniform, turbulent boundary layer flow over a rough surface in the alongshore direction can be described by a logarithmic profile:

$$V(z) = \frac{v_*}{\kappa} \ln \left(\frac{z + h}{z_o}\right) \tag{6}$$

where z is positive upwards from the surface, h is the mean water depth, κ is the Von Karman constant (0.4), v_* is the alongshore shear stress velocity and z_o is the physical roughness height, determined by bottom topography and sediment grain size. When waves

are present, nonlinear interactions between waves and currents within the bottom boundary layer increase the bottom shear stress. Following Grant and Madsen (1979), this additional stress can be modeled by an apparent roughness height z_a, that is analogous to, but larger than z_o.

The mean bottom shear stress ($\overline{\tau_y(-h)}$) is related to the longshore shear stress velocity (v_*) through

$$\overline{\tau_y(z=-h)} = \rho v_*^2 \tag{7}$$

In addition, a bed shear stress coefficient, C_f, can be calculated assuming a quadratic bed shear stress relationship

$$\overline{\tau_y(-h)} = \rho C_f \overline{(u^2+ v^2)^{1/2} v} \tag{8}$$

and combining with (7), gives

$$C_f = \frac{v_*^2}{\overline{(u^2 + v^2)^{1/2} v}} \tag{9}$$

which includes contributions from both steady (U,V) and non-steady ($\tilde{u},\tilde{v},\acute{u},\acute{v}$) velocity components.

Surface Layer

The surface layer is governed by waves and wind. Wave effects are manifested in three ways: 1) an undulating boundary is imposed on a mean current, which is being measured in an Eulerian frame; 2) the mass transport velocity in the crest-trough region due

to obliquely incident waves contributes to the longshore flow; 3) modifications of the profile associated with wave-breaking generated turbulence and the eventual contribution of wave rollers to the mass transport.

The shape of the mean current profile in this layer is determined mostly by the fact that the current meter is intermittently in and out of the water in the wave crest-trough region, e.g., for a linear wave the current meter is out of the water half the time at the mean sea level (MSL hereafter), and the time-averaged current is only 50 percent of the expected value from the logarithmic profile. To account for this, the surface elevation probability distribution function (*pdf* hereafter) is applied to the expected mean current profile in the absence of waves. The percent of time the current meter is in the water is given by 1-P(η), where P(η) is the cumulative surface elevation *pdf*. In an Eulerian frame of reference, the modified mean current within the surface layer is given by

$$V(z) = [1 - P(\eta)]\, V'(z) \qquad \textbf{(10)}$$

where V'(z) represents the logarithmic profile in the absence of waves (6). For moderate wave conditions in deep water, the surface elevation *pdf* is well described by the Gaussian *pdf*. As will be seen, the measured *pdf* in the surf zone are slightly positively skewed from the Gaussian distribution.

The mass transport velocity associated with obliquely incident waves can contribute to the longshore flow in the upper layer. Assuming irrotational flow, the mass flux (transport) in the direction of wave transport, M, can be evaluated by considering separately two regions in an Eulerian frame of reference (Philips, 1977). In the first region, from the bottom to the

MSL, the contribution is zero for irrotational flow. Within the second region, from the MSL to the water surface (η), $\tilde{u}$ is not defined for linear wave theory. A Taylor series expansion about $z=0$ is used to extend defined values of $\tilde{u}(0)$ at the surface, giving a second order approximation to M. The mass transport for a single wave is interpreted to this order, in an Eulerian reference frame, as due to a uniform velocity confined to the crest-trough region. Applying linear wave theory, a mass transport velocity is defined by

$$U = \frac{M}{\rho(2A)} \tag{11}$$

where A is the wave amplitude.

For random waves, the wave amplitudes can be described by the Rayleigh distribution to a first approximation, even within the surf zone (Thornton and Guza, 1983). The only waves that contribute at any elevation z, will have an amplitude $A \geq |z|$. Assuming directionally narrow banded waves, the ensemble averaged mass transport velocity profile in the direction of wave travel is obtained by applying the wave amplitude probability density function

$$\langle U(z) \rangle = \int_{|z|=A}^{\infty} U(A)p(A)dA \tag{12}$$

where $\langle\ \rangle$ represents ensemble averaging. The Rayleigh probability density function is given by

$$p(A) = \frac{8A}{H_{rms}^{\ 2}} e^{-\left(\frac{2A}{H_{rms}}\right)^2} \qquad where\ 0 < A < h \tag{13}$$

and H_{rms} is the *rms* wave height. Substituting (13) back into (12), applying linear wave theory, and performing the integration, gives

$$<U(z)> = \frac{\omega}{8}\frac{H_{rms}}{\tanh kh}\left[\frac{2|z|}{H_{rms}}\, e^{-\left(\frac{2|z|}{H_{rms}}\right)^2} + \frac{\sqrt{\pi}}{2}\, erfc\left(\frac{2|z|}{H_{rms}}\right)\right] \qquad for\ |z|<h \quad \textbf{(14)}$$

where *erfc(x)* is the complementary error function, ω is the wave radial frequency and k is the radial wavenumber. The alongshore component of the mass transport velocity is defined by

$$<V(z)> = <U(z)>\sin\bar{\theta} \qquad \textbf{(15)}$$

where $\bar{\theta}$ is the mean incident wave angle with respect to the beach normal, for the assumed directionally narrow banded waves.

The mean longshore current within the surface layer, as observed in an Eulerian reference frame, is modeled by adding the corrected logarithmic profile for the cumulative surface elevation *pdf* (10) with the alongshore component of the mass transport velocity (15)

$$V_{sfc}(z) = [1-P(\eta)]\,V'(z) + <U(z)>\sin\bar{\theta} \qquad \textbf{(16)}$$

DUCK 94 EXPERIMENT

The measurements described here are part of the comprehensive nearshore DUCK94 experiment conducted during October 1994 at the U.S. Army Corps of Engineers Field Research Facility (FRF), Duck, North Carolina. The FRF is located on the Outer Banks, a barrier island formation with no major coastal structures to obstruct nearshore flows. The

beach is a two-bar system with a dynamic inner bar (30-120 m offshore) and a secondary bar with lower amplitude (300-400 m offshore). The mean foreshore slope of the beach is approximately 0.08 (1:12) and the slope offshore of the bars is approximately 0.006 (1:170) (Lippmann *et al.*, 1993). The mean tidal range is 1.0 m. Sediments within the surf zone are well sorted with a mean grain size of 0.2 mm. Sediments on the foreshore are poorly sorted with larger mean grain size (>0.4 mm).

The data analysis presented is for the October phase of the DUCK94 experiment. The weather during October was climatologically characterized by three distinct phases: weak currents and winds from north (4-9 Oct.), relatively strong currents from north (0.6-1.0 m/s) caused by a storm with predominant winds and waves from north (10-17 Oct.), and variable currents and winds from north/south (17-21 Oct.). For the first phase (4-9 Oct.), the currents were weak and barely above sensor accuracy. During the last phase (17-21 Oct.), currents and winds were highly variable and a hole developed in the bar associated with a rip current system (observed with dye), such that the basic assumptions of steady state and straight and parallel contours are violated. Within the second phase (10-17 Oct.), observations were limited due to the Coastal Research Amphibious Buggy (CRAB) not being able to operate during the height of the storm on the 15th and being limited to the area inside the bar on the 13th, 14th, 16th, and 17th due to large waves. Therefore, the data selected for analysis are from 10-12 Oct. (Fig. 1), during the strong longshore currents period when observations spanned the entire surf zone and conditions approximate the assumptions of steady state and straight and parallel contours. Within this period a logarithmic profile is well defined.

A specially designed sled was used as a platform to mount instruments (Fig. 2). The sled is constructed of a 3 x 4 m six-inch aluminum-pipe frame with two 5 m length, 20 cm diameter pipe runners. This low-profile structure was stabilized by 180 Kg of lead weight plus approximately 450 Kg of sand inside the runners. In addition, there were four fins (45 cm wide) extending 60 cm into the sand to insure that the sled did not move while on station.

Currents were measured using a vertical stack of 8 Marsh-McBirney two-component electromagnetic current meters (ems, hereafter) with 2.5 cm diameter spherical probes mounted along a 2.5 m mast (Fig. 2). The ems elevations above the bed were 23, 42, 68, 101, 147, 179, 224 and 257 cm. The ems were displaced at least 1 m from the sled, and the sled was oriented such that the vertical stack of ems was on the "up-current" side of the sled to avoid flow contamination by the sled structure during observations. The ems were pre- and post-calibrated in a tow tank at the Naval Postgraduate School with an agreement of 1.9 percent in gain. An *in situ* determination for the offset is used, which was obtained by reversing the orientation of the ems on a very slow longshore current day (8 Oct.) by turning the sled around and returning it to the same location (within 1 m) within one hour. The *in situ* determined offsets were within 1 cm/s.

The sled orientation was determined using a digital compass mounted on the sled with accuracy O(1 degree). Measured two-component velocities were reduced to a shore normal right-handed coordinate system (positive offshore and to the south) by using compass data and adding at each sled position any deviation of the contour line, as measured by the CRAB, from a shore parallel direction. Velocity errors associated with the rotation of the coordinate system were smaller than the determined offsets, and therefore were neglected.

Waves and mean water level were measured using an array of five pressure sensors configured in a 3 m square with sensors at each corner and one in the center.

The data were digitally encoded on the sled to 14 bit precision at 36 samples/second and transmitted to shore via a fibre-optic cable where signals were monitored and recorded. Short cables from the sensors to the data acquisition system on the sled (< 7 m) resulted in low noise ems and pressure sensor signals. An armored cable, married to the sled chain tether, provided power and controller signals for the instruments via two conductors and returned the digitized signals and video via a fibre-optic line.

The sled was towed to the farthest offshore location for the first run (approximately 160 m from the shoreline) by the 11 m high, motorized, three-wheel CRAB. A four-wheel drive forklift pulled the sled shoreward 10 to 30 meters for subsequent runs (each run was nominally one hour). Five to eight runs were made across a transect each day. The data were acquired during daylight to early night, which happened to span the high tide during this period.

The morphology of the bottom (bathymetry) was measured at various scales from the CRAB. Large-scale variations of bathymetry were obtained by using an autotracking laser ranging system to measure the CRAB position approximately every meter with a vertical accuracy of less than 3 cm *rms*. Small-scale vertical bottom variations relative to the CRAB, including ripples and megaripples, were measured with a 1 MHZ sonic altimeter mounted on the CRAB, 70 cm from the bed. The altimeter has a 3.4 degree beam width which translates into an approximate 4 cm footprint and a nominal sampling rate of 25 Hz, which resulted in a sample spacing of 2-4 cm (dependent on CRAB speed) with mm vertical

resolution and accuracy less than 2 cm (Gallagher *et al.*, 1996). The decrease in accuracy relative to resolution is due to the changing reflective surface owing to the bed dialating or sediment transported along the bed as waves pass overhead. The CRAB survey and altimeter measurements were combined to obtain a high resolution description of the bottom (Thornton *et al.*, 1997). Contour plots of the bathymetry for the days selected for analysis show the alongshore contours in the vicinity of the sled measurements to be essentially straight and parallel (Fig. 3; 11 Oct. is typical). Bathymetry for the three selected days (Figs. 4-6, upper panel) show a pronounced bar progressively moving offshore and significant small-scale morphology in the trough. Areal variations were determined using a 500 KHz side-scan sonar also mounted on the CRAB.

Meteorological information of wind, air temperature, atmospheric pressure and sea surface temperature were recorded simultaneously at the seaward end of the 600 m long FRF pier and atop the FRF building in front of the pier.

DATA RESULTS

The data are qualitatively sorted by location into the two regions of over the bar and in the trough. This sorting allows a better identification of the possible correlations among variables, as wave-breaking, which is a major controlling factor within the surf zone, significantly changes for these regions.

Since the logarithmic velocity profile hypothesis is a bottom boundary layer concept, information from ems near the surface influenced by the effects of waves and wind as well as from coming in and out of the water are not included. A criterion is established such that only data from ems below (MSL- H_{rms}) are considered to define the logarithmic profile of

the bottom boundary layer. This criterion assures that the ems used in the analysis came out of the water less than 0.25 percent of the time based on a Gaussian distribution, which is conservative for the measured positively skewed distributions.

The *rms* wave height is approximated by $H_{rms} = \sqrt{8\sigma^2}$ where σ^2 is the variance calculated from the surface elevation time series. Surface elevation was calculated by Fourier transforming a one-hour pressure record, applying a linear wave theory transfer function to the complex Fourier amplitudes in the frequency domain, and inverse transforming to obtain the surface elevation time series (Thornton and Guza, 1982).

All 22 vertical profiles of longshore currents obtained during these three days are analyzed. The profiles are based on the measurements by four to seven ems over the vertical. The em closest to the sea bed was not used because of malfunction. Mean alongshore velocities are 1-hour averaged data with the exception of three runs, run 7 on 11 Oct. and runs 6 and 7 on 12 Oct., which are 40-minutes averaged data. In examining the bottom boundary and surface layers, the ems data are treated separately.

For the bottom boundary layer, logarithmic profiles are fit to the data based on a linear-regression least-squares method. The value of z_a is calculated from the z intercept of the linear-regression on a semi-log plot of z versus V(z), and the shear stress velocity v_* is calculated from the slope.

C_f values are calculated using measured velocities (u,v) in (9) time-averaged over the record length, with v_* determined by least-squares fit. C_f values are dependent on the elevation of the measured u,v values. Typically, C_f is calculated using measured u,v values referenced to one meter above the bed. A sensitivity analysis on the variation of C_f to the

elevation of the selected gage was performed, showing that the variation of C_f was dominated by the time-averaged alongshore velocity (V). This term was not only the largest in the denominator of (9), but also varied the most with depth. Therefore, to minimize the depth-dependence of C_f the depth-averaged velocity calculated from the logarithmic velocity profile ($V_d = \frac{v_*}{\kappa}[\ln(\frac{h}{z_a}) + \frac{z_a}{h} - 1]$) is used to specify the dominant time-averaged alongshore velocity. The em located at the elevation of 1 m above the bed is used to measure the smaller terms (total cross-shore velocity u and the non-steady component of the alongshore velocity $\tilde{v} + \acute{v} = v - V$), which have weak vertical variation outside the bottom boundary and surface layers. The total alongshore velocity is obtained by adding V_d to the measured non-steady component $\tilde{v} + \acute{v}$. The use of this method resulted in a mean variation of C_f with depth of only 7 percent with a standard deviation of 6 percent and a maximum variation of 24 percent, provided the gage used to measure the cross-shore velocity and non-steady component of the alongshore velocity was not in the surface layer ($z > MSL - H_{rms}$). Calculated C_f, z_a and v_* values are listed in Table 1.

Error estimates of z_a and v_* based on the linear regression correlation coefficients (C) are calculated using (Gross and Nowell, 1983 and Cacchione *et al.*, 1987)

$$v_* \pm v_* \, t_{(n-2,1-\alpha/2)} \, (\frac{C^{-2}-1}{n-2})^{1/2} \tag{17}$$

$$\ln z_a \pm t_{(n-2,1-\alpha/2)} \, (\frac{1}{n}\sum_{i=1}^{n} [\ln(z_i)]^2)^{1/2} \, (\frac{C^{-2}-1}{n-2})^{1/2} \tag{18}$$

where n is the number of ems used for the regression, and $t_{(n-2,1-\alpha/2)}$ is the Student's t distribution for $(1-\alpha)$ confidence interval with $(n-2)$ degrees of freedom.

The uncertainties of C_f values can be determined from the error estimates of v_* and the time and depth-averaged velocity calculated from the measurements $Vm = \frac{1}{h}\int_{-h+z_a}^{0} [\overline{(v^2+u^2)^{1/2}v}]^{1/2} dz$ (mean velocity, hereafter)

$$C_f \pm C_f \left[\frac{1+2v_{*_{err}}+(v_{*_{err}})^2}{1+2V_{m_{err}}+(V_{m_{err}})^2}-1\right] \qquad \textbf{(19)}$$

where $v_{*_{err}}$ is the relative error of the shear stress velocity at a given confidence level calculated from (17) and $V_{m_{err}}$ is the relative error of the mean velocity determined by $V_{m_{err}} = \frac{1(cm/s)}{V_m}$, assuming that the mean velocity has a constant absolute error equal to the *in situ* determined offset (1 cm/s). Error estimates for C_f, z_a, and v_* are listed in Table 2, for a 95 percent confidence interval.

The measured cumulative surface elevation *pdf* is used to describe the surface layer, and compares reasonably well with the Gaussian cumulative *pdf* (Fig. 7). The Gaussian distribution has zero skewness and kurtosis equal to three. The measured skewness values ranged from 0.26-0.57 and kurtosis values ranged from 2.7-3.5, indicative of weakly nonlinear waves.

In the surface layer, the upper ems sometimes came in and out of water, which causes noise in the ems outputs. To eliminate this noise, the current velocities were set to zero when the ems were within 5 cm of the surface as determined from the surface elevation

time series.

The combined surface and bottom boundary layer solution is the logarithmic profile given by (6) from z_a up to (MSL - H_{rms}), and the modified logarithmic profile by the observed cumulative surface elevation *pdf* plus the alongshore component of the mass transport velocity given by (16) above this level. As a typical example, the profile for the seventh run of 10 Oct. is enlarged in Fig. 8, where the solid line is the logarithmic profile and the dashed line the modified profile within the surface layer.

The observed and model predicted velocity profiles at successive offshore positions (runs) that the sled occupied during a transect are shown in the upper panels of Figs. 4-6. The largest deviation occurs for the fourth run of 11 Oct., which generates an outlier in the parameter estimates if the data from the em at an elevation of 42 cm above the sea bed (Fig. 5) is included in the linear regression. A comparative analysis for all ems for this run showed the energy density spectra to be nearly uniform (average variance of 0.072 m^2 and standard deviation of 0.013 m^2) with exception of this em (variance of 0.021 m^2). Thus, data from this em is disregarded and a new regression is calculated with the remaining six ems. This procedure eliminates the outlier.

DISCUSSION

Three days of the DUCK94 experiment are examined when strong longshore currents occurred. Mean longshore current profiles obtained using four to seven ems spaced from 42 to 257 cm above the sea bottom are used to test the validity of the logarithmic profile hypothesis within the energetic surf zone region.

Bottom Boundary Layer

A high correlation coefficient for the linear regression, is commonly accepted as an indicator of the validity of the logarithmic approach (Grant *et al.*, 1984; Gross *et al.*, 1994; Li, 1994). The linear correlation coefficients for all profiles ranged from 0.95 to 0.99 (Table 2), with an average value of 0.98, and the largest deviations occurring over the bar, where wave breaking was strong. Anomalous high correlation coefficients can be obtained for profiles calculated using a small number of ems for the linear regression, such as occurred for stations very close to the shoreline due to shallow water. Thus, a high correlation coefficient, although necessary, is not sufficient to validate the logarithmic profile approach.

Other measures of how well the logarithmic model describes the mean alongshore current profile within the bottom boundary layer are the uncertainties of the calculated shear stress velocity v_* (17) and apparent roughness height z_a (18). These uncertainties reflect both the correlation coefficients and the number of ems used in the regression. An example is comparing the fourth run of 11 Oct. with the seventh run of 10 Oct. (Table 2) . The latter has a higher correlation coefficient (0.991), but only 4 ems were used in the linear regression; thus uncertainties in the calculated v_* and z_a values are larger for this run, even though the former has a lower correlation coefficient (0.987). Therefore, the uncertainties are not biased by an anomalous high correlation coefficient due to a small number of ems used in the regression. The degenerate case is when only two ems are used for the linear regression (eighth run of 11 Oct.), resulting in a correlation coefficient of one, which does not allow the calculation of the uncertainties for v_* and z_a. Consequently, data from this run are disregarded.

There is some uncertainty of the exact distance of the ems from the bed, because the sled runners sank into the sand an unknown amount depending on the bearing capacity of the bed (theory and divers suggest 3-8 cm) and owing to the undulating bottom, particularly over mega-ripples. To test the sensitivity of the logarithmic profile due to the uncertainty in elevation, the elevation of the ems was shifted ±5 cm in steps of 1 cm and the linear regression least-squares-fit recalculated until the best correlation between the data and the logarithmic model predictions was obtained for each run (Grant *et al.*, 1984).

As the bathymetry is not uniform over the transect covered by the sled, no unique zero-shift value should be expected to optimize the correlation coefficient for all runs. Another effect on the error calculation to be considered with an *ad hoc* decrease (increase) in the elevation of the ems is that an em previously located above (below) the model cut-off level (MSL - H_{rms}) can be relocated to a new elevation below (above) this level. For example, an em previously neglected by the model is now included in the linear regression. The zero-shifting modifies the error estimates of v_* , z_a, and C_f (17, 18, and 19) by changing the correlation coefficients and the number of ems used for the regression.

With the uncertainties involved, the zero-shifting method was only applied whenever a significant reduction (greater than 10 percent) was obtained in the shear stress velocity error estimate. Applying this criteria, only three runs were shifted (by the same - 5 cm): seventh runs of 10 and 11 Oct., and third run of 12 Oct. The sensitivity of the ems to elevation from the bed as inferred from the zero-shifting method for these three runs is shown in Table 3. The general trend being that both the shear stress velocity and apparent roughness height errors decreased with increased negative shift, although the improvement

is only significant for the shear stress velocity. The values listed in Tables 1 and 2 for these runs were calculated after applying the zero-shift.

The observed and model predicted velocity profiles at successive offshore positions (runs) that the sled occupied during a transect are shown in the upper panels of Figs. 4-6. The data agree well with the model indicating that the contribution from momentum mixing arising from interactions between cross-shore and longshore currents ($\frac{\partial \overline{\rho VU}}{\partial x}$) neglected for simplicity sake, does not significantly modify the vertical profile of longshore currents, suggesting that $\frac{\partial \overline{\rho VU}}{\partial x}$ is independent of depth.

The largest discrepancies between measured and modeled profiles occur over the bar, where wave breaking is most intense (x-distance between 220 and 240 m). The surface layer during wave breaking is typified by an intense production of turbulence that eventually is dissipated in the shear layer at the lower boundary of the surface roller for spilling type breakers and more intense injection of turbulence for plunging type breakers. The increase of turbulent mixing due to wave breaking produces a more uniform vertical profile of the mean longshore current within the bottom boundary layer for a given bottom shear stress, compared with profiles in the absence of breaking. Therefore, larger discrepancies between observations and logarithmic profile predictions (lower correlation coefficients) would be expected for increased turbulent mixing caused by wave breaking.

To test this hypothesis, percentages of waves breaking were determined from video recordings. The number of waves breaking is determined using the methods of Lippmann and Holman (1991), while the total number of waves is found applying the zero-up-crossing method to the surface elevation time series (see Lippmann and Thornton, 1997, for details).

The general decrease of the correlation coefficient between observations and logarithmic profile predictions with increasing percentage of wave breaking (Fig. 9) supports this conclusion.

Surface Layer

The mean current profile within the surface layer is modified in the presence of winds and waves. The winds act directly to generate longshore currents via the alongshore surface wind stress component, and indirectly by generating obliquely incident waves which then force the longshore currents via changes in the radiation stress. Whitford and Thornton (1993) measured the various terms in the alongshore momentum balance including wind stress and wave forces during the SUPERDUCK experiment (15-18 October 1986) at the same location as the DUCK94 experiment. They found an average wind force to wave force ratio for this four-day period of 0.11 (range 0.02 - 0.33) for a mean alongshore component of wind speed of 3.6 m/s (range 1.9 - 5.3 m/s). During the three-day period studied here the mean alongshore wind speed was 9.1 m/s (range 7.7 - 12.6 m/s) resulting in an average wind force to wave force ratio of 0.21 (0.10 - 0.50). Despite the wave force dominance characterizing wave-driven longshore currents, the wind force contribution is not negligible.

Winds and currents are approximately from the same direction (Fig. 1), thus the wind force effect is to increase the alongshore currents. As the logarithmic profiles are fit to the data based on a linear-regression least-squares method, the direct wind force effect is already included in the logarithmic profile. The indirect wind force effect of wave generation resulting in increased wave heights (higher H_{rms} values) is also included in the alongshore component of mass transport velocity. The theoretical exponential decay of wind-induced

current speed with depth was not observed within the surface layer due to the dominant effect of the ems intermittently being out of the water, and therefore is not included in the model.

The modification of the mean current profile within the surface layer is modeled here by correcting the logarithmic profile predictions for measurements in an Eulerian frame with an undulating boundary and adding the alongshore component of the mass transport velocity (16). As few ems were located above the (MSL - H_{rms}) level for each run, a local correlation coefficient as an indicator of the validity of this approach is meaningless. Therefore, the validity of the model is evaluated by comparing model predictions with observations for the ensemble of ems located within the surface layer.

The linearity of (16) allows an evaluation of the contribution of each term (intermittent-wetting and alongshore component of mass transport velocity) separately. For the intermittent-wetting term only, a plot of predicted versus observed velocities (Fig. 10) shows good agreement, but with the modified logarithmic profile by the cumulative surface elevation *pdf* slightly under-predicting the observed velocities. The *rms* error and slope of the least-squares linear regression between predictions and observations are respectively 13 percent and 0.96, giving a slope-error of -4 percent. Next, including the alongshore component of the mass transport velocity (Fig. 11) results in reduced *rms* and slope errors of 7 percent and 0.5 percent. Despite the small magnitude of the mass transport term (on average only 11 percent of the intermittent-wetting term), its addition corrects the small under-prediction of using only (10) and improves the overall agreement with the data by reducing both the *rms* and slope errors.

Although the results obtained by this first attempt (to the knowledge of the authors)

to model mean longshore currents within the surface layer are encouraging, improvements can be achieved by including contributions from at least two physical processes. The first, arises from the additional mass transport associated with the presence of wave-breaking generated rollers, and will increase the model-predicted velocity within the surface layer. The second is associated with the directional spreading of random waves and it will have an opposite effect, reducing the model-predicted velocity. Preliminary calculations indicate that these terms are of the same order of the mass transport term, and thus an order of magnitude smaller than the intermittent-wetting. The good agreement with the data obtained by applying this simple model is attributed to the dominance of the intermittent-wetting term and compensating effects of neglected contributions from the presence of wave rollers and directional spreading.

Bed Shear Stress Coefficient

The bed shear stress coefficient (C_f) from the quadratic friction model is an important parameter in both nearshore hydrodynamics and sediment transport. The simplest formulation for longshore currents assumes steady state wave conditions and straight and parallel bottom contours, and results in an alongshore balance between cross-shore changes in wave-induced momentum (radiation stress, S_{yx}) with the bottom shear stress, to give (Thornton, 1970)

$$V = \frac{1}{\rho C_f \overline{|\vec{u}|}} \frac{\partial S_{yx}}{\partial x} \qquad \textbf{(20)}$$

where $|\vec{u}|$ is the magnitude of the total velocity vector. The sediment transport formulation

of Bailard and Inman (1981), based on the work by Bagnold (1966), states that the immersed-weight sediment transport rate is proportional to the local rate of energy dissipation

$$\vec{i}_t = \rho C_f |\vec{u}_t|^3 (\vec{K}_{bt} + \vec{K}_{st}) \quad \textbf{(21)}$$

where $\vec{K}_{bt}$ and $\vec{K}_{st}$ are dimensionless time-varying vectors associated with the bedload and suspended load transport rates. It is noted that both the longshore currents and sediment transport rates are direct functions of C_f. Nevertheless, the physical processes governing these phenomena are inherently different. The longshore currents are mainly controlled by form drag of the bed forms and non-linear interactions between waves and mean current. Sediment transport is mainly related to skin friction due to sediment grains (Smith, 1977; Dyer, 1980), although the presence of waves increases the sediment entrainment rate (Grant and Madsen, 1979), thus increasing the transport rate.

The bottom shear stress coefficient (C_f) varied by an order of magnitude across the surf zone, with the values offshore and over the bar in the order of 10^{-3}, while the values in the trough were in the order of 10^{-2}. An attempt was made to find empirical relationships between C_f and measured physical parameters commonly used throughout the literature such as $\frac{|\vec{u}_b|}{V}$ (ratio of near-bottom wave velocity magnitude from linear wave theory to mean current speed), the *rms* bottom roughness (r) and percent of wave breaking. Surprisingly, no statistically significant correlation was found between C_f and $\frac{|\vec{u}_b|}{V}$.

C_f was found to be negatively correlated with percentage of wave breaking, with a linear correlation coefficient of -0.71, which is statistically significant at the 99 percent confidence level (Fig. 12). This is contrary to the theoretical analyses of Fredsoe and

Deigaard (1992) and Church and Thornton (1993). An effect associated with wave breaking in the surf zone is the generation of surface rollers that increases the mass transport within the surface layer, thus increasing the cross-shore return flow, or undertow, and consequently the average total velocity $\overline{(u^2+ v^2)^{1/2}v}$. This effect reduces the C_f values calculated using (9) for increasing wave breaking. In addition, decreased C_f with increased wave breaking may be physically related to the planing-off of wave-ripples due to increased near-bottom velocities associated with wave breaking and consequent reduction of form drag, as well as to stratification caused by an intense vertical gradient of suspended sediment near the sea bed. This stratification can diminish the turbulent flow intensity in the bottom boundary layer, leading to reduced bottom stress (Smith and McLean, 1977a; and Taylor and Dyer, 1977).

C_f would be expected to be related to bottom roughness due to enhanced form drag. The bottom roughness is examined by calculating wavenumber spectra of the bed. To calculate wavenumber spectra, the unevenly spaced data from the combined CRAB surveys and altimeter measurements are linearly interpolated to evenly spaced 2 cm increments of the cross-shore distance. The small-scale morphology in general shows large cross-shore variation; as a consequence, the condition of spatial homogeneity (stationarity) required for calculating averaged spectra is not met. Therefore, continuous bottom roughness wavenumber spectra are calculated for 20 m cross-shore segments at increments of 1 m across the surf zone.

Lowest wave numbers are filtered by subtracting a third-order polynomial best-fit curve from each 20 m section. A 10 percent cosine-taper data window is applied to decrease

spectral leakage. The spectra are summed over three wavelength bands (0.2 - 1.0 m, 1.0 - 3.33 m, and 3.33 - 20 m) plus the total band (0.2 - 20 m), resulting in 160, 28, 10, and 198 degrees of freedom for each band respectively. The wavelength bands chosen are based on examination of individual spectra. The spectra were generally broad, indicating that several ripple wavelengths coexisted as a result of newly formed ripples combined possibly with residual ripples from the past to form a complex series of ripple patterns, plus the effects of alignment of ripples relative to the cross-shore measurement axis. The *rms* height of each band is calculated as the square root of the variance within each band. Note that variances sum, not *rms* heights, such that the *rms* height of the sum of the three bands is calculated from the square root of the sum of their variances. The *rms* bottom roughness (Figs. 4-6, lower panel) is dominated by longer wavelength features primarily associated with mega-ripples, with a small contribution from the superimposed shorter wavelength ripples O(1 m). The general trend being that bottom roughness was smoothest offshore and over the bar where wave ripples were planed-off due to higher near-bottom velocities, with increased roughness within the trough associated with mega-ripples (see Thornton, *et al.*, 1997, for details). The *rms* bottom roughness (r) is calculated from the total band (0.2 - 20 m), and thus includes contributions from both large and small-scale morphology. Calculated values are listed in Table 1.

Roughness measurements were made in the cross-shore direction only. To relate C_f, calculated from the alongshore bed shear stress, to roughness, it is assumed that the bed forms are quasi-isotropic, which is not unreasonable for mega-ripples in the trough. However, this assumption is violated for long-crested wave ripples, such as occurred for the

seventh run of 11 Oct. when large wave ripples (observed in the side-scan sonar) were oriented parallel to the flow (alongshore direction) which results in over-estimating the *rms* roughness associated with longshore currents at this cross-shore position. Altimeter data for 12 Oct. is not available from 210-260 m due to the high false return levels induced by strong scattering of the acoustic pulses from air-bubbles entrained by waves breaking over the bar. Therefore, the CRAB survey data is used as the profile in this section, and hence the bottom is not as highly resolved in this area, compromising roughness estimates for the third, fourth, and fifth runs of 12 Oct. Thus, roughness data from these four runs, as well data from the eighth run of 11 Oct. (only two ems below the MSL - H_{rms} level) are disregarded.

If data from runs with logarithmic profile correlation coefficients less than 0.98 with resulting relative errors for C_f greater than 50 percent (Table 2) are also disregarded, only 9 profiles could be used, making the ensemble too small to infer any statistically reliable relationship between C_f and bottom roughness. Therefore, it was decided to use data from the remaining 17 profiles with the associated 95 percent confidence error estimates to examine the relationship between C_f and r. The bed shear stress coefficients are positively correlated with bottom roughness normalized by mean water depth (Fig. 13), with a linear correlation coefficient of 0.63, which is statistically significant at the 99 percent confidence level.

The scatter of data observed in Fig. 13 may be due to correlating the non-synoptic velocity measurements with bottom roughness measured once in the morning, prior to the positioning of the sled for the first station. Wave forcing quantified by deep water wave height (H_o), period of peak wave frequency (T), and wave direction (θ) changed during the

period of observation (Fig. 1) due to both wind and tidal variations. Changes in wave forcing have a direct effect in the measured velocities and an indirect effect in bottom roughness due to modification of wave ripples associated with variations in wave height.

For steady currents (open channel flows) C_f depends only on bottom roughness when the bed is hydraulically rough, and several empirical relationships (power-laws) are available throughout the literature. One of the most widely used is the Manning-Strickler equation (Sleath, 1984, equation 5.86)

$$C_f = \frac{f_{DW}}{8} = 0.015 \left(\frac{k_s}{h}\right)^{\frac{1}{3}} \tag{22}$$

where f_{DW} is the Darcy Weisbach friction coefficient and k_s is the bed roughness length scale or equivalent Nikuradse roughness of the bed.

In our definition of C_f (9), contributions from both steady and non-steady velocity components were taken into account, whereas (22) applies to steady flow only. Nevertheless, during the period being analyzed the observed strong longshore current is not only the dominant term, but is also well represented by a logarithmic profile (6). The flow can be classified as hydraulically rough as calculated Reynolds numbers ($\frac{k_s v_*}{\mu}$, in which μ = molecular kinematic viscosity coefficient) were greater than 70 for all runs (Schlichting, 1979). Thus, if measured *rms* bottom roughness is representative of the equivalent Nikuradse roughness of the bed ($k_s \approx r$), one might expect C_f to be related to $\left(\frac{r}{h}\right)$ by a power law similar to (22). A plot of predicted C_f by the Manning-Strickler equation (22) is included in Fig. 13, which shows an order of magnitude agreement between the data and predictions.

These results suggest that the calculated *rms* bottom roughness (r) is representative of the bed roughness length scale or equivalent Nikuradse roughness of the bed (k_s).

The structure of the flow inside the wave boundary layer (WBL hereafter) is out of the scope of this paper as no measurements were made within this region. Outside the WBL, z_a is the proper length scale and not z_o (Grant and Madsen, 1986). Therefore, the equivalent Nikuradse roughness of the bed (k_s) is replaced by an apparent bed roughness length scale (k_a). The flow is hydraulically rough during the period being analyzed, and thus k_a can be assumed to be given by $\frac{k_a}{30} = z_a$ (Nikuradse, 1933). Assuming that k_a is representative of the bed roughness length scale when waves and currents are present, an empirical relation (power law) between C_f and $\frac{k_a}{h}$ is obtained by applying a linear regression least-squares fit to the data to give

$$C_f = 0.011 \left(\frac{k_a}{h}\right)^{\frac{1}{2.75}} \tag{23}$$

which is plotted in Fig. 14. The *rms* error between measured and predicted C_f by (23) is 18 percent, which is within the 95 percent confidence band of the measurements. This is not surprising as the coefficients of (23) were determined by fitting the data in a least-squares sense. Nevertheless, the correlation between measured C_f and $\frac{k_a}{h}$ is 0.80 which is statistically significant at the 99.5 percent confidence level indicating that a power law relation between these parameters is not fortuitous.

An independent check of (23) is obtained by including the results from velocity profiles measured by Grant *et al.* (1984) on the northern California continental shelf in

90 m depth during the Coastal Ocean Dynamics Experiment (CODE) using four vertically stacked acoustic-travel-time current meters (BASS) mounted on tripods. A plot of measured C_f versus $\frac{k_a}{h}$ for the CODE data (listed in table 2 of their paper) is included in Fig. 14. The agreement between C_f predicted by (23) and measured for the CODE data set is even better (*rms* error of 3.5 percent) than for the DUCK94 data set which was used to determine the coefficients of (23).

These results indicate that a single roughness length scale can be used to characterize combined flows over a movable bed, which is a basic assumption for all existing theoretical models. This assumption was shown to be valid for waves, currents, and combined flows over a fixed rippled bed by Mathisen and Madsen (1996).

Another reason for the scatter of data observed in Fig. 13 arises from C_f values being calculated from the total bottom shear stress, which has stress contributions from skin friction related to sediment grains, waves-current nonlinear interactions within the bottom boundary layer as well as form drag related to bed forms. Smith and McLean (1977b) linearly partitioned the total bed shear stress into skin friction and form drag, and found good agreement with data from the Columbia River. Nelson and Smith (1989), Wiberg and Nelson (1992), and Li (1994) subsequently applied the linear partition concept to several flume experiments with good results. Extending this concept to the surf zone environment requires including an additional component due to non-linear interactions between waves and currents within the bottom boundary layer to the total bed shear stress. Assuming that the linear stress partition is valid within the surf zone, the skin friction contribution can be removed from the total bottom stress and a new bed shear stress coefficient C_f' is defined

$$C_f' = \frac{v_{*_d}^2 + v_{*_{wc}}^2}{(u^2 + v^2)^{1/2} v} \tag{24}$$

where v_{*_d} and $v_{*_{wc}}$ are the form drag and waves-current interactions shear stress velocities. The relationship between C_f' and the total bed shear stress coefficient (C_f) can be determined from (9) and (24)

$$C_f' = [1 - (\frac{v_{*_s}}{v_*})^2] \, C_f \tag{25}$$

where v_{*_s} is the skin friction related shear stress velocity.

As skin friction was not measured during the DUCK94 experiment, an attempt is made to isolate its contribution from the total bottom shear stress by applying a stress partitioning model. The probabilistic approach used to quantify bottom roughness does not allow the adjustment of the two empirical coefficients C_D and a_1 necessary to apply the Smith and McLean (1977b) model. Therefore, the empirical relationships obtained by Li (1994) by applying linear regression to the mean flow laboratory data of Kapdasli and Dyer (1986), Paola (1983) , as well as his own data obtained from mobile sand ripples, are used to estimate skin friction shear stress velocity from the total shear stress velocity obtained from the logarithmic profile

$$\frac{v_{*_s}}{v_*} = 0.125(\frac{v_*}{R}) + 0.373 \qquad for \quad \frac{v_*}{R} < 2.3 \tag{26}$$

$$\frac{v_{*_s}}{v_*} = 0.107\left(\frac{v_*}{R}\right) + 0.266 \qquad for \quad \frac{v_*}{R} \geq 2.3 \qquad (27)$$

where R is ripple height, that is assumed here to be equal to the measured *rms* bottom roughness ($R = r$) . For $\frac{v_*}{R} > 6.86$, the predicted v_{*_s} by (27) is greater than the total measured shear stress velocity, and it is assumed that v_{*_s} is equal to 99 percent of the total shear stress whenever this occurred. Calculated values of v_{*_s} are listed in Table 1.

The recalculated bed shear stress coefficients C_f' by (25) show a higher linear correlation coefficient (0.76) with bottom roughness normalized by mean water depth (Fig. 15). Theoretically this is expected as the removal of the skin friction component from the total stress should enhance the form drag contribution, and consequently increase the correlation between bed shear stress and bottom roughness. The improved correlation obtained by applying Li (1994) empirical relationships indicates that the linear stress partition concept introduced by Smith and McLean (1977b) can be extended to the surf zone environment, although a more detailed data set is necessary to validate these expressions.

Apparent Roughness Height

The change of mean current velocity profile due to the superposition of waves has been theoretically investigated over the last two decades and several models have been presented (Lundgren, 1972; Smith, 1977; Bakker and Van Doorn, 1978; Grant and Madsen, 1979; Fredsoe, 1984; Christoffersen and Jonsson, 1985; Myrhaug and Slaattelid, 1989; Sleath, 1991). A general approach common to all these works is splitting the mean velocity

profile in an inner region close to the bed affected by turbulence produced in the wave boundary layer, and an outer region above it, where the current is not directly affected by wave-current non-linear interactions so that the logarithmic profile (6) may be assumed to apply. The increased bed shear stress associated with wave-current interactions is modeled by replacing z_o with z_a in (6).

The apparent roughness increase $\frac{z_a}{z_o}$ is theoretically expected to depend on the relative current strength $\frac{|\vec{u}_b|}{V}$, the relative roughness $\frac{A_d}{k_s}$ (ratio of the near-bottom wave semi-orbital excursion from linear wave theory to equivalent Nikuradse roughness), and the angle between wave and current direction (ϕ). Several empirical relations for $\frac{z_a}{z_o}$ based on these parameters have been obtained from laboratory experiments. Nevertheless, the applicability of these empirical relations to field data has not been verified, as previous field experiments, although containing reliable data on z_a, lack corresponding measurements of bottom roughness (Grant *et al.*, 1984; Cacchione *et al.*, 1987; Lambrakos *et al.*, 1988; Slaattelid *et al.*, 1990).

Three widely applied empirical relationships for $\frac{z_a}{z_o}$ (Coffey and Nielsen, 1986; Sleath, 1991; and Van Rijn, 1993) are tested using DUCK94 data, as measurements of both z_a and bottom roughness were made during this experiment. For hydraulically rough flows, the physical roughness height can be estimated from $z_o = \frac{k_s}{30}$ (Nikuradse, 1933), and once again the measured rms bottom roughness is used to represent the equivalent Nikuradse roughness of the bed ($k_s = r$).

No statistically significant correlation was found between observed $\frac{z_a}{z_o}$ and the parameters $\frac{|\vec{u}_b|}{V}$, $\frac{A_d}{k_s}$, and ϕ. Consequently, none of these empirical relations are able to

accurately predict the apparent roughness increase for this data. These results, together with the scatter of available laboratory data on $\frac{z_a}{z_o}$ (Nielsen, 1992, Fig. 1.5.13) and difficulties associated with bottom roughness and velocity measurements within the WBL in the field, indicate that much remains to be done before a reliable empirical or theoretical relation for the apparent roughness height increase experienced by the mean current profile in the presence of waves is obtained.

CONCLUSIONS

The vertical structure of mean longshore currents on a barred beach is well described by a logarithmic profile for the three strong longshore current days examined. This hypothesis works better in the trough where turbulent bottom boundary layer processes are more dominant than over the bar, where breaking-wave induced turbulence generated at the surface modifies the profile.

The modification of the mean longshore current profile within the surface layer in the presence of winds and waves is modeled by correcting the logarithmic profile predictions for measurements in an Eulerian frame with an undulating boundary for all ems located above the (MSL - H_{rms}) level. The addition of the alongshore component of the mass transport velocity corrects the under-prediction of the modified logarithmic profile and improves the overall agreement with the data. Therefore, it can be concluded that this simple model provides a first order approximation that is sufficiently accurate to predict mean longshore currents within the surface layer.

The data indicates that wave breaking inside the surf zone decreases the bottom shear stress coefficient which is contrary to the theoretical analysis of Fredsoe and Deigaard

(1992), and Church and Thornton (1993). This may be physically related to wave-breaking generated surface rollers that increases the cross-shore return flow (undertow) and consequently the average total velocity, decreasing C_f values calculated using (9); as well as to the planing-off of wave-ripples due to increased near-bottom velocities and consequent reduction of form drag, and to stratification caused by an intense vertical gradient of suspended sediment near the sea bed.

The bed shear stress coefficient (C_f) varied by an order of magnitude across the surf zone (0.0006-0.012), with the values offshore and over the bar $O(10^{-3})$, while the values in the trough were $O(10^{-2})$. Thus, longshore current and sediment transport models that assume C_f to be constant or mildly changing should be revised.

C_f was found to be directly proportional to bottom roughness, and hence, bottom roughness is an important parameter to characterize the bottom boundary layer. The empirical relationships obtained by Li (1994) were used to remove the skin friction contribution from the total bottom shear stress. The improved correlation between bottom shear stress and bottom roughness obtained, although not conclusive to validate these simple expressions, indicates that the linear stress partition concept introduced by Smith and McLean (1977b) can be extended to the surf zone environment.

An empirical relation between C_f and apparent roughness length scale of the bed normalized by water depth ($\frac{k_a}{h}$) was obtained by applying a linear regression least-squares fit to the DUCK94 data. Good agreement was also found between this relation and CODE data (Grant *et al.*, 1984), indicating that a single roughness length scale can be used to characterize combined wave-current flows over a movable bed.

Surprisingly, no statistically significant correlation was found between observed apparent roughness increase ($\frac{z_a}{z_o}$) and the parameters $\frac{|\vec{u}_b|}{V}$, $\frac{A_d}{k_s}$, and ϕ. Consequently, none of the three most used empirical relations for $\frac{z_a}{z_o}$ (Coffey and Nielsen, 1986; Sleath, 1991; and Van Rijn, 1993) were able to accurately predict the apparent roughness increase. These results indicate that despite improvements in our knowledge of turbulent boundary layers during the last two decades, we are still not able to estimate bottom roughness for field applications, which prevents the use of an empirical relation such as (23) or any other theoretical expression to predict friction factor for combined waves and current flows.

ACKNOWLEDGMENTS

This research was funded by the Office of Naval Research, Coastal Sciences Program, under contract N00114-95-AF-002. The authors wish to express their appreciation to all those who participated in DUCK94 experiment, particularly the staff of the U.S. Army Field Research Facility under the direction of B. Birkemeier. In addition, special appreciation is expressed to R. Wyland, Naval Postgraduate School for his role in acquisition of wave and current data, and to Jim Stockel and Mary Bristow, Naval Postgraduate School, for help in processing data. We also would like to thank Prof. W. Dally, Florida Institute of Technology, for his thoughtful suggestions which resulted in an improved paper.

REFERENCES

Bagnold, R.A., An approach to the sediment transport problem from general physics. U.S. Geological Survey, Professional Paper No. 422-I. Washington, D.C., 1966.

Bailard, J.A., and D.L. Inmann, An energetics bedload transport model for a plane sloping beach; local transport, *Journal of Geophysical Research*, 86(C3), 2035-2043 , 1981.

Bakker, W.T., and T. Van Doorn, Near bottom velocities in waves with a current, *Proceedings 16th Coastal Engineering Conference, ASCE*, 1394-1413, 1978.

Cacchione, D.A., W.D. Grant, D.E. Drake, and S.M. Glenn, Storm-dominated bottom boundary layer dynamics on the northern California continental shelf: Measurements and predictions, *Journal of Geophysical Research*, 92(C2), 1817-1827, 1987.

Christoffersen, J.B., and I.G. Jonsson, Bed friction and dissipation in a combined current and wave motion, *Ocean Engineering*, 12(5), 387-423, 1985.

Church, J.C., and E.B. Thornton, Effects of breaking wave induced turbulence within a longshore current model, *Coastal Engineering*, 20, 1-28, 1993.

Coffey, F.C., and P. Nielsen, The influence of waves on current profiles, *Proceedings 20th Coastal Engineering Conference, ASCE*, 82-96, 1986.

Deigaard, R. and J. Fredsoe, Shear stress distribution in dissipative water waves, *Coastal Engineering*, 13, 357-378, 1989.

Dyer, K.R., Velocity profiles over a rippled bed and the threshold of movement of sand, *Estuarine Coastal Ma. Sci.*, 10, 181-199, 1980.

Fredsoe, J., Turbulent boundary layer in wave-current motion, *Journal of Hydraulic Engineering*, Vol. 110, No. 8, 1103-1120, 1984.

Fredsoe, J. and R. Deigaard, Mechanics of coastal sediment transport, *World Scientific Publishing Co. Pte. Ltd.*, Singapore, 1st edition, pp. 144, 1992.

Gallagher, E.L., W. Boyd, S. Elgar, R.T. Guza, and B. Woodward, Performance of a sonar altimeter in the nearshore, *Marine Geology*, 133, 241-248, 1996.

Garcez Faria, A.F., E.B.Thornton, and T.P. Stanton, A quasi-3D model of longshore currents, *Proceedings of Coastal Dynamics'95, ASCE*, 389-400, 1996.

Grant, W.D., and O.S. Madsen, Combined wave and current interaction with a rough bottom, *Journal of Geophysical Research*, 84(C4), 1797-1808, 1979.

Grant, W.D., and O.S. Madsen, The continental-shelf bottom boundary layer, *Ann. Rev. Fluid Mechanics*, 18, 265-305, 1986.

Grant, W.D., A.J. Williams III, and S.M. Glenn, Bottom stress estimates and their prediction on the northern California continental shelf during CODE-1: the importance of wave-current interaction, *Journal of Physical Oceanography*, 14, 506-527, 1984.

Gross, T.F., and A.R.M. Nowell, Mean flow and turbulence scaling in a tidal boundary layer, *Continental shelf Research*, 2, 109-126, 1983.

Gross, T.F., A.J. Williams III, and E.A. Terray, Bottom boundary layer spectral estimates in the presence of wave motions, *Continental shelf Research*, 14, 1239-1256, 1994.

Kapdasli, M.S., and K.R. Dyer, Threshold conditions for sand movement on a rippled bed, *Geo. Mar. Lett.*, 10, 45-49, 1986.

Lambrakos, K.F., D. Myrhaug, and O.H. Slaattelid, Seabed current boundary layers in wave-plus-current flow conditions, *J. Waterway Port Coastal and Ocean Eng.*, 114, 2, 161-174, 1988.

Li, M.Z., Direct skin friction measurements and stress partitioning over movable sand ripples, *Journal of Geophysical Research*, 99(C1), 791-799, 1994.

Lippmann, T.C., and R.A. Holman, Quantification of sand bar morphology: a video technique based on wave dissipation, *Journal of Geophysical Research*, 94(C1), 995-1001, 1991.

Lippmann, T.C., R.A. Holman, and K.K. Hathaway, Episodic, nonstationary behavior of a double bar system at Duck, North Carolina, U.S.A., 1986-1991, *Journal of Coastal Research*, 15(SI), 49-75, 1993.

Lippmann, T.C., and E.B.Thornton, The spatial distribution of wave breaking on a barred beach, submitted to *Journal of Geophysical Research*, 1997.

Lundgren, H., Turbulent currents in the presence of waves, *Proceedings 13th Coastal Engineering Conference, ASCE*, 623-634, 1972.

Mathisen, P.P., and O.S. Madsen, Waves and currents over a fixed rippled bed 1. Bottom roughness experienced by waves in the presence and absence of currents, *Journal of Geophysical Research*, 101(C7), 16533-16542, 1996.

Myrhaug, D., and O. Slaattelid, Combined wave and current boundary layer model for fixed rough seabeds, *Ocean Engineering*, 16(2), 119-142, 1989.

Nelson, J.M, and J.D. Smith, Mechanics of flow over ripples and dunes, *Journal of Geophysical Research*, 94(C6), 8146-8162 , 1989.

Nielsen, P., Coastal bottom boundary layers and sediment transport, *World Scientific Publishing Co. Pte. Ltd.*, NJ, 1st edition, 1992.

Nikuradse, J., Stromungsgesetze in glatten und rauhen rohren, *Forschung Arb. Ing. Wesen*, 361, 1933.

Paola, C., Flow and skin friction over natural rough beds, Sc.D. dissertation, MIT-WHOI Joint Program in Oceanogr., Mass. Inst. Of Technol./Woods Hole Oceanogr. Inst., Woods Hole, Mass., 1983.

Philips, O.M., The dynamics of the upper ocean, *Cambridge University Press*, NY, 2nd edition, pp. 316, 1977.

Rivero, F.J. and A.S. Arcilla, On the vertical distribution of $<\tilde{u}\tilde{w}>$, *Coastal Engineering*, 25, 137-152, 1995.

Schlichting, H., Boundary layer theory, *McGraw-Hill*, NY, 7th edition, 1979.

Simons, R.R., T.J. Grass, and M. Mansour-Tehrani, Bottom shear stresses in the boundary layers under waves and currents crossing at right angles, *Proceedings 23th Coastal Engineering Conference, ASCE*, 604-617, 1992.

Slaattelid, O.H., D. Myrhaug, and K.F. Lambrakos, North sea bottom steady boundary layer measurements, *J. Waterway Port Coastal and Ocean Eng.*, 116, 5, 614-633, 1990.

Sleath, J.F.A., Sea bed mechanics, *John Wiley & Sons Inc.*, NY, 1st edition, pp. 220, 1984.

Sleath, J.F.A., Velocities and bed friction in combined flows, *Proceedings 22th Coastal Engineering Conference, ASCE*, 450-463, 1990.

Sleath, J.F.A., Velocities and shear stresses in wave-current flows, *Journal of Geophysical Research*, 96(C8), 15237-15244, 1991.

Smith, J.D., Modeling of sediment transport on continental shelves, in *The Sea*, vol. 6, edited by E.D. Goldberg et al., Wiley-Interscience, pp. 539-577, New York, 1977.

Smith, J.D., and S.R. McLean, Boundary layer adjustments to bottom topography and suspended sediment, in *Bottom Turbulence*, edited by J.C.J. Nihoul, Elsevier, pp. 123-151, New York, 1977a.

Smith, J.D., and S.R. McLean, Spatially averaged flow over a wavy surface, *Journal of Geophysical Research*, 82(C12), 1735-1746, 1977b.

Stive, M.J.F., and H.G. Wind, A study of radiation stress and set-up in the nearshore region, *Coastal Engineering*, 6, 1-25, 1982.

Svendsen, I.A., and U. Putrevu, Nearshore mixing and dispersion, *Proc. R. Soc. London*, A 445, 561-576, 1994.

Taylor, P.A., and K.R. Dyer, Theoretical models of flow near the bed and their implications for sediment transport, in *The Sea*, vol. 6, edited by E.D. Goldberg et al., Wiley-Interscience, pp. 579-601, New York, 1977.

Thornton, E.B., Variation of longshore currents across the surf zone, *Proceedings 12th Coastal Engineering Conference, ASCE*, 291-308, 1970.

Thornton, E.B., and R.T. Guza, Energy saturation and phase speeds measured on a natural beach, *Journal of Geophysical Research*, 87(C12), 9499-9508, 1982.

Thornton, E.B., and R.T. Guza, Transformation of wave height distribution, *Journal of Geophysical Research*, 84(C8), 4931-4938, 1983.

Thornton, E.B., J.L. Swayne, and J.R. Dingler, Small-scale morphology related to waves and currents across the surf zone, *Marine Geology* (accepted), 1997.

Van Rijn, L.C., Principles of sediment transport in rivers, estuaries and coastal areas, *Aqua Publications*, The Netherlands, 1st edition, 1993.

Visser, P.J., Wave basin experiments on bottom friction due to current and waves, *Proceedings 20th Coastal Engineering Conference, ASCE*, 807-821, 1986.

Whitford, D.J., and E.B. Thornton, Comparison of wind and wave forcing of longshore currents, *Continental Shelf Research*, 13, 1205-1218, 1993.

Wiberg, P.L., and J.M. Nelson, Unidirectional flow over asymmetric and symmetric ripples, *Journal of Geophysical Research*, 97(C8), 12745-12761, 1992.

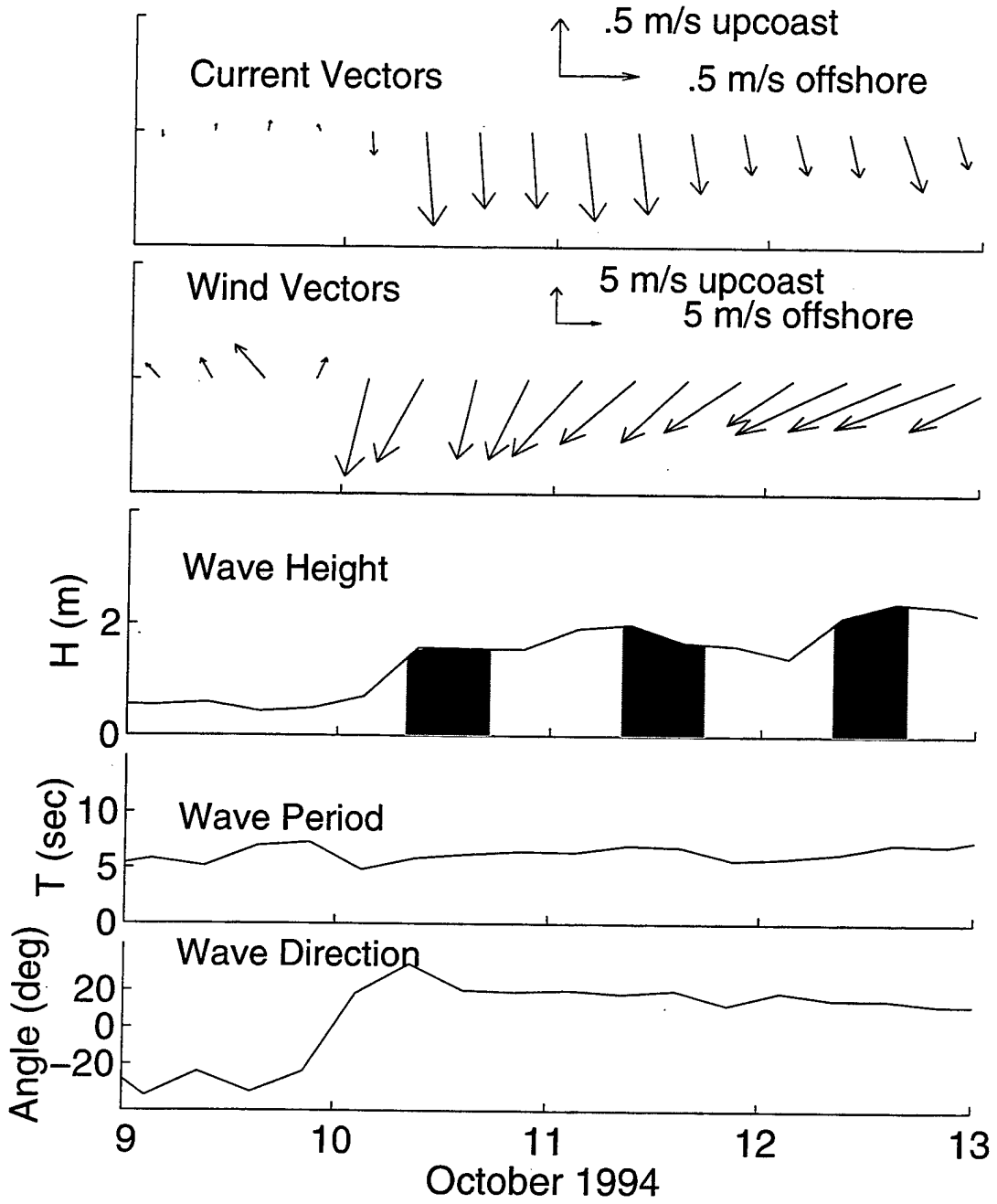

Figure 1. Climatology for the three days considered (10, 11 and 12 Oct.). Currents were measured in the middle of the trough. H is the significant wave height, T is the period of peak frequency, and Angle is the mean wave angle relative to beach normal (θ).

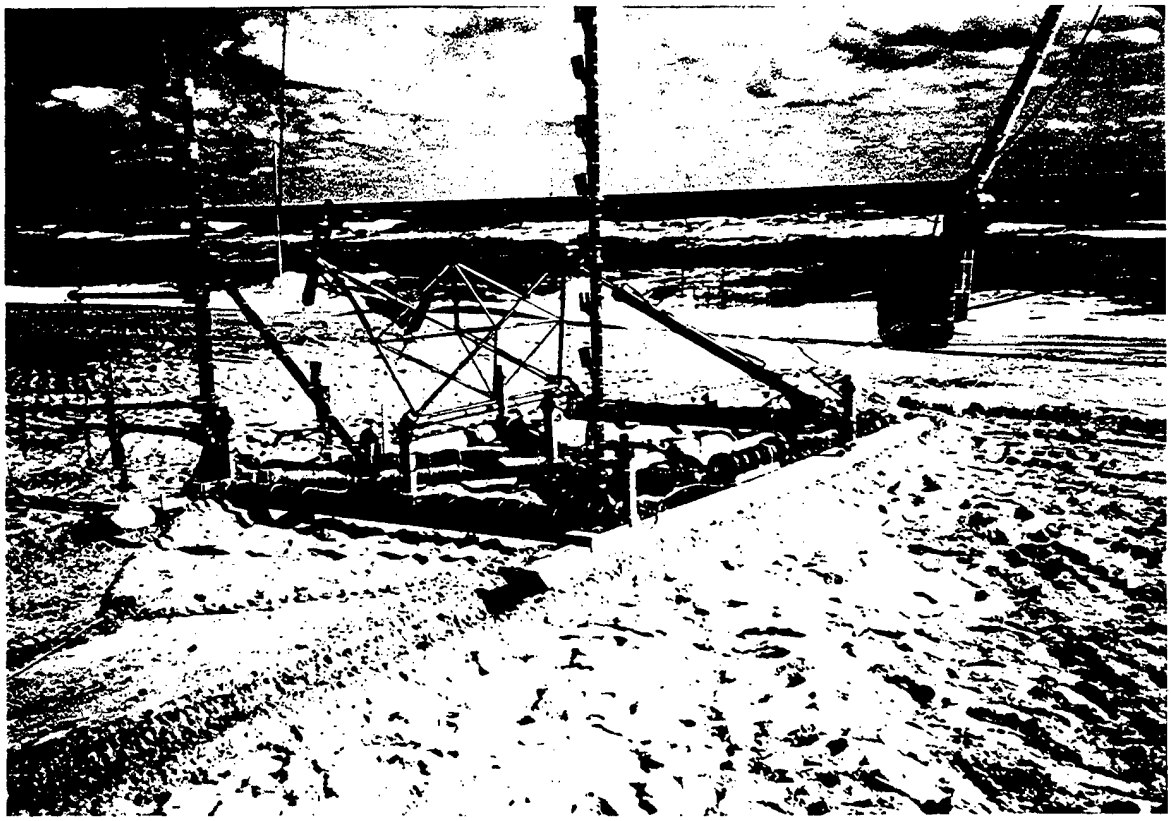

Figure 2. Photograph of the Sled being pulled off the beach by the CRAB (upper right) during DUCK94 experiment. Vertical array of ems are mounted along Sled mast (center left).

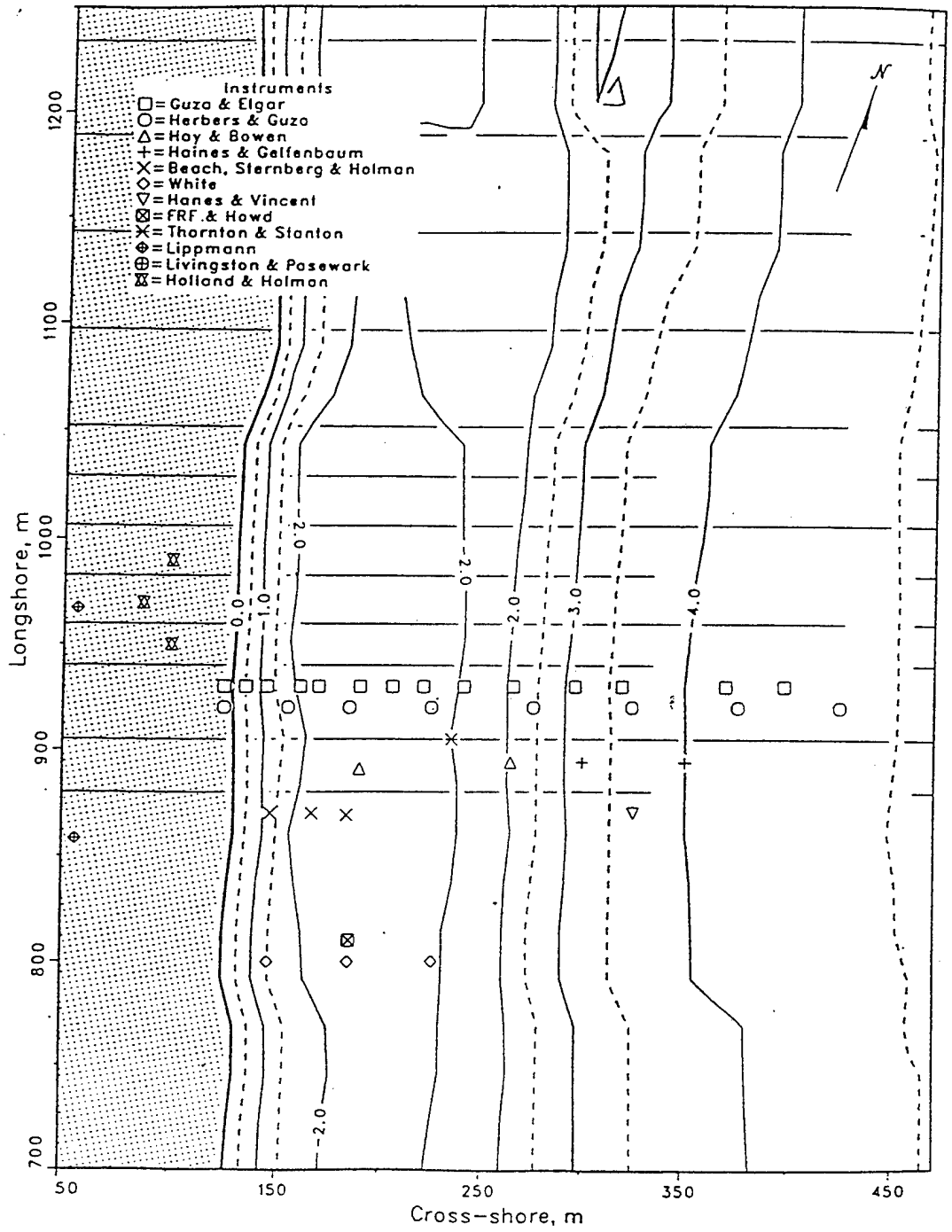

Figure 3. Bathymetry and instrument locations during DUCK94 experiment (11 Oct.). Sled transect line was 940 m alongshore.

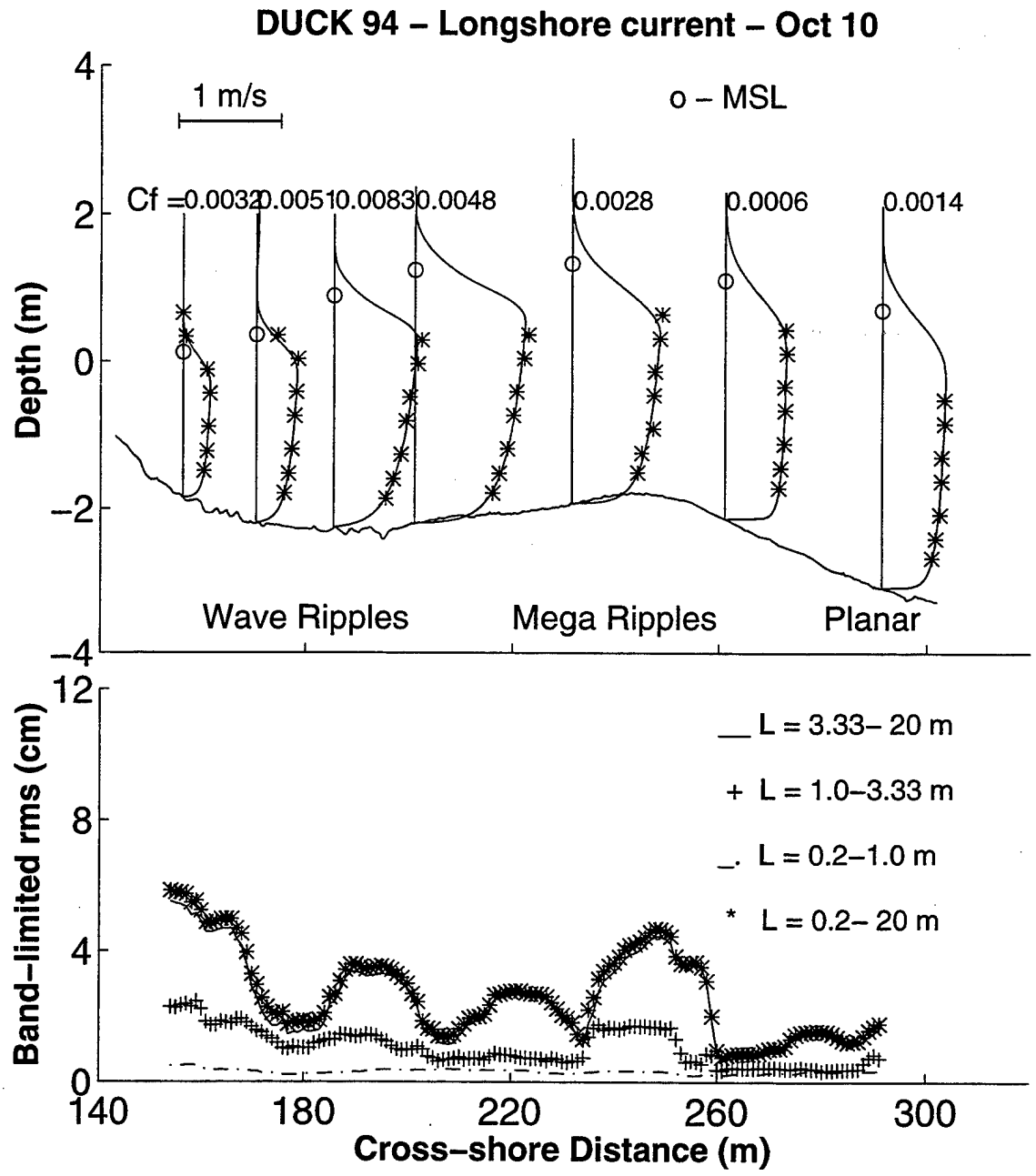

Figure 4. Measured (*) and predicted (−) vertical profiles of mean longshore currents superposed on bottom profile with tide elevation indicated by (o) and measured C_f values (upper panel). Variation of band-limited *rms* bottom roughness with cross-shore distance for 10 Oct (lower panel).

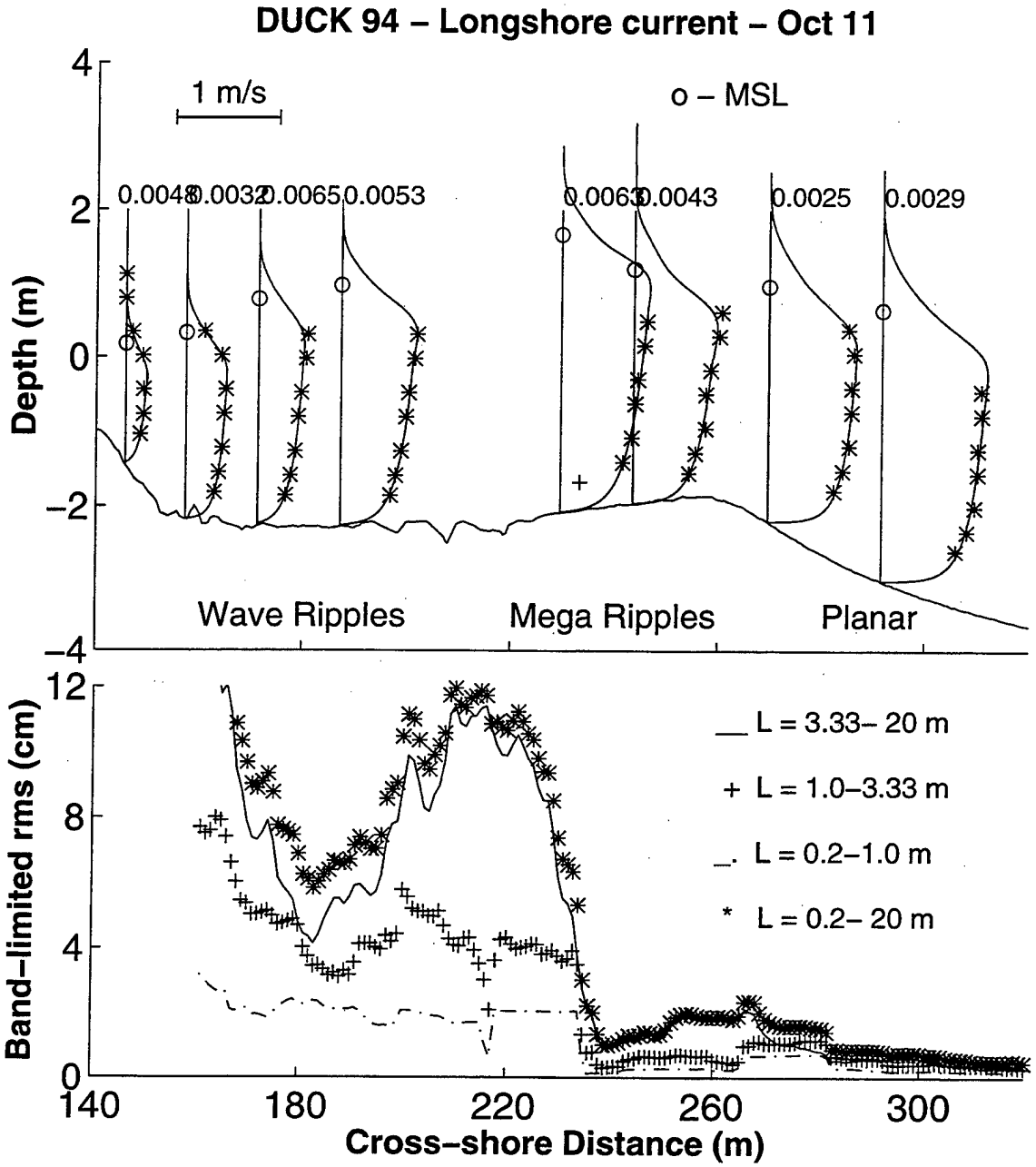

Figure 5. Same as in Figure 4 but for 11 Oct. The anomalous measurement point indicated by + in the fourth run (upper panel) is not included in the linear regression.

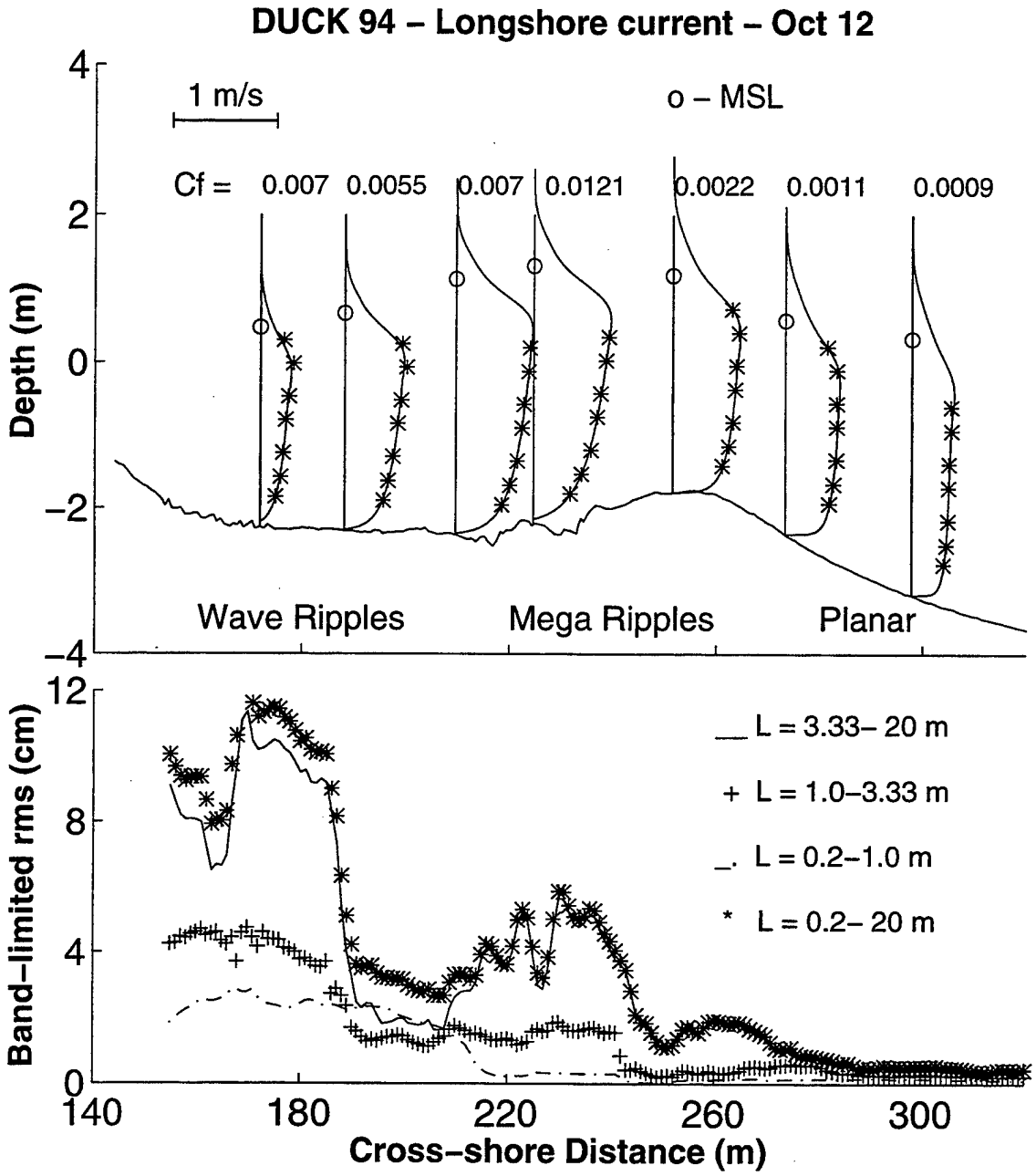

Figure 6. Same as in Figure 4 but for 12 Oct.

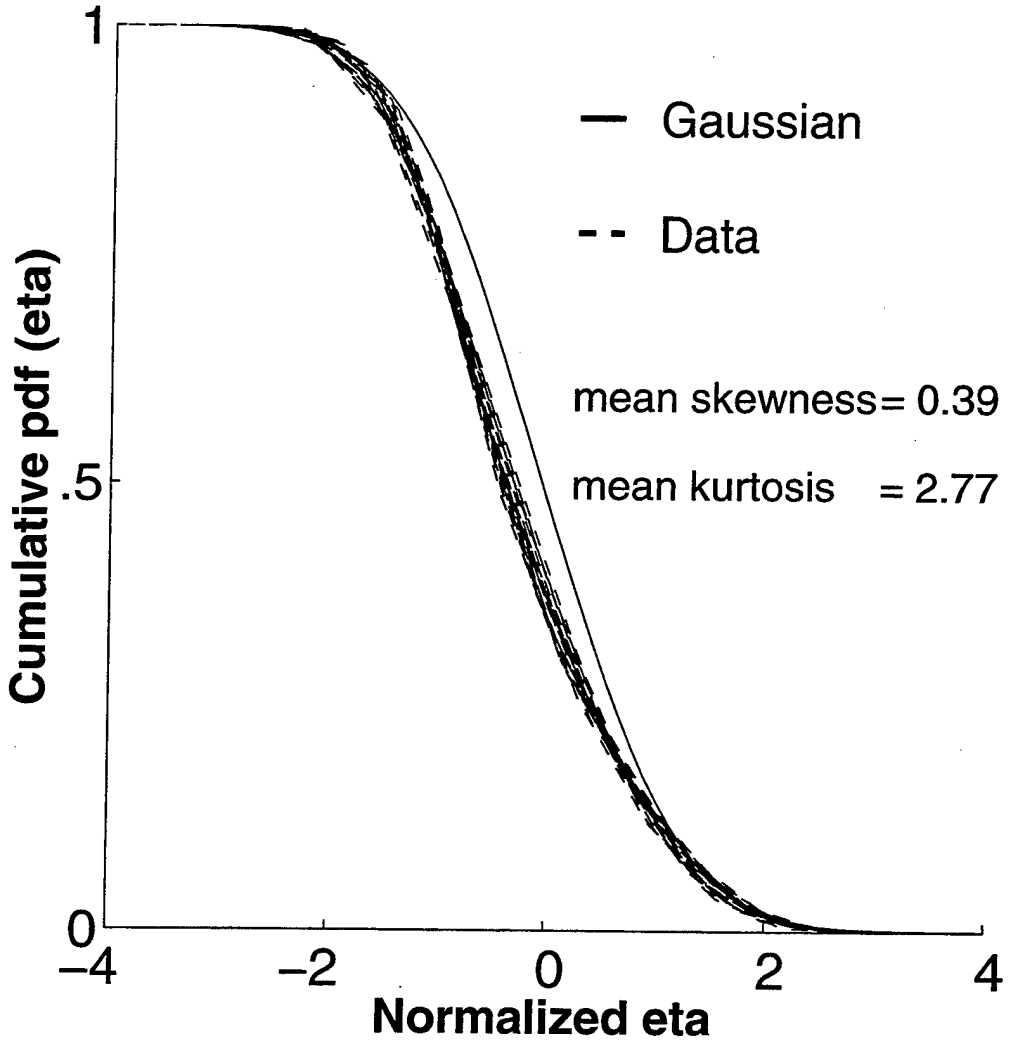

Figure 7. Comparison between measured and Gaussian cumulative surface elevation *pdf* for all the runs during the three days considered (10, 11 and 12 Oct.). Mean skewness and kurtosis for the three days are indicated.

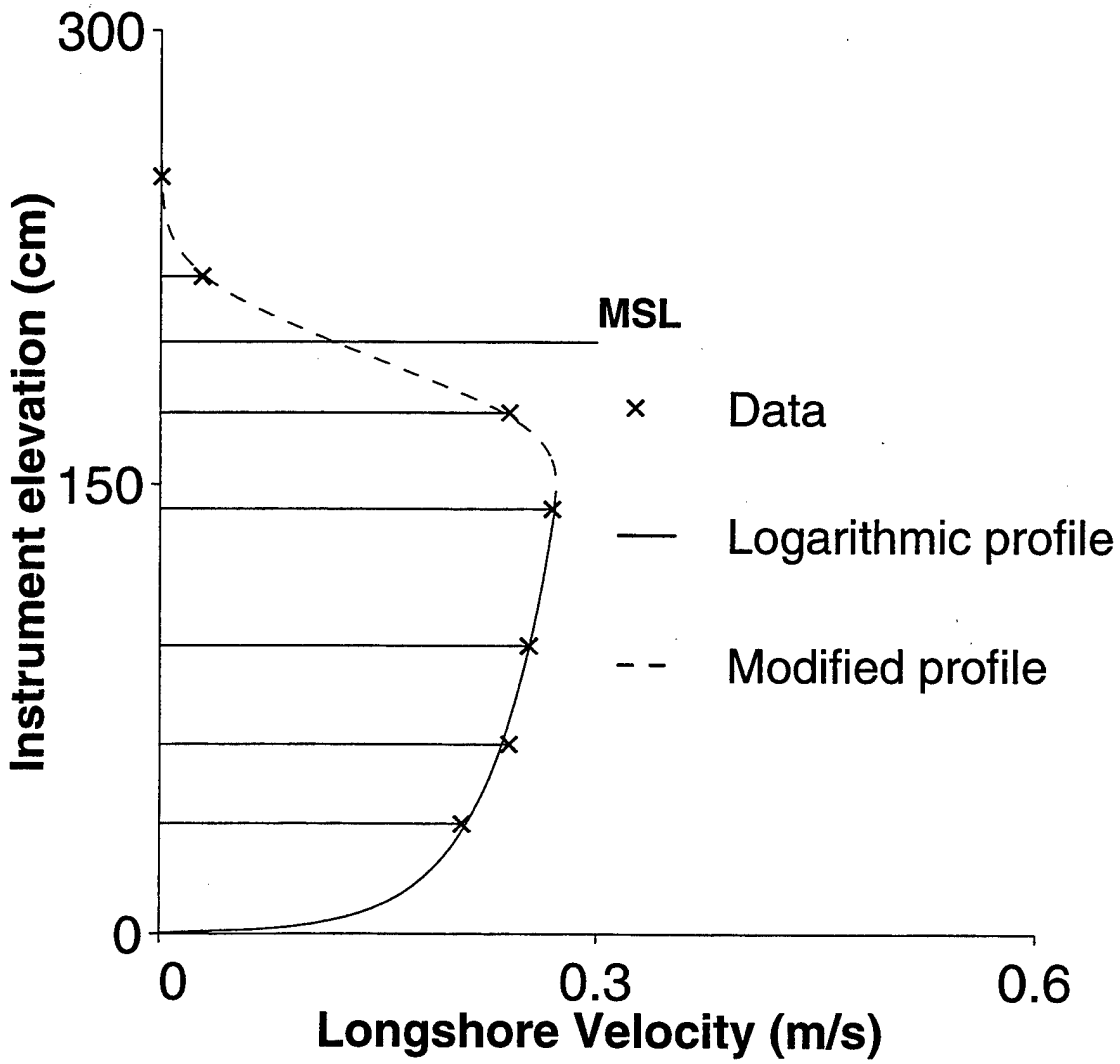

Figure 8. Vertical profile combining bottom boundary and surface layer models for the seventh run of 10 Oct. The upper three ems sometimes were out of the water.

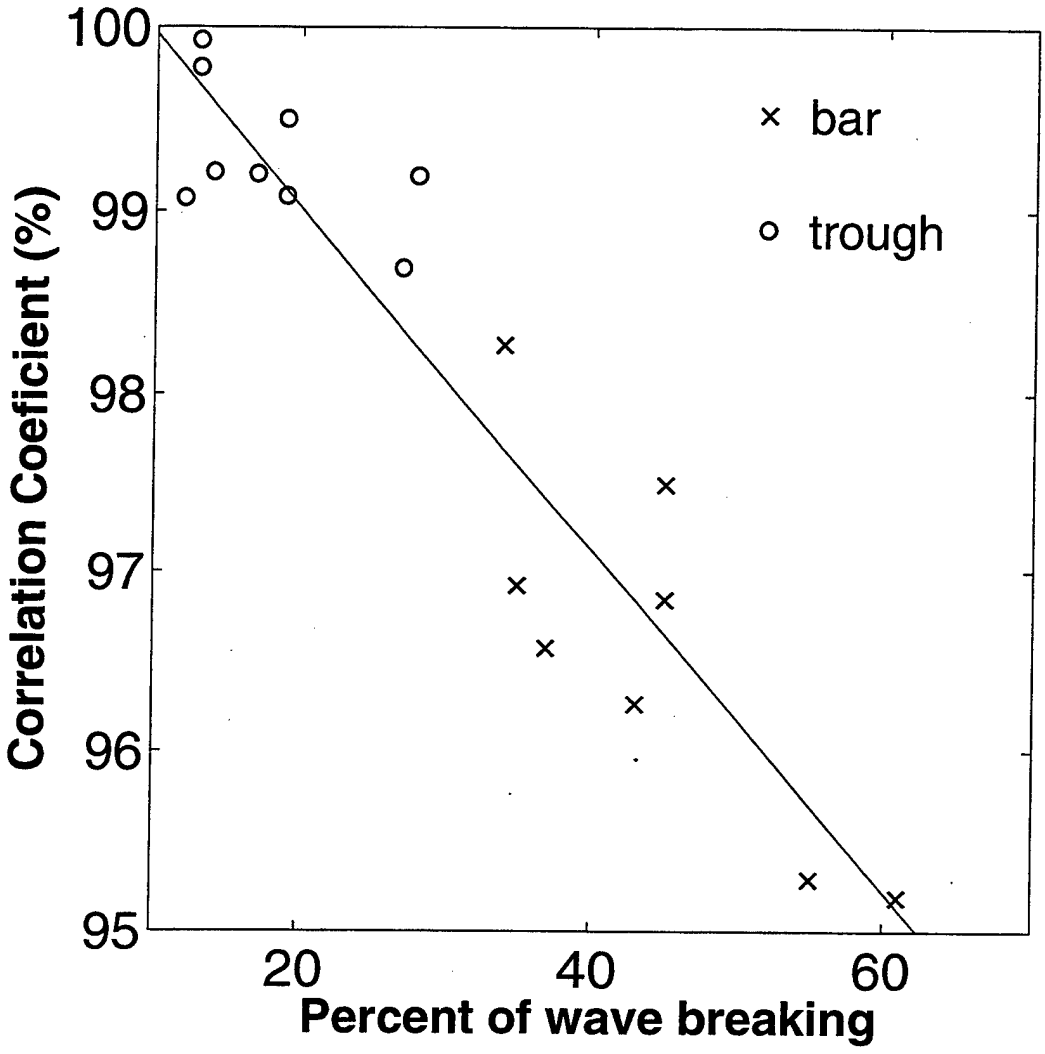

Figure 9. Correlation coefficient between observations and logarithmic profile predictions versus percentage of wave-breaking calculated from video data. The line represents a linear regression with a regression coefficient of -0.94.

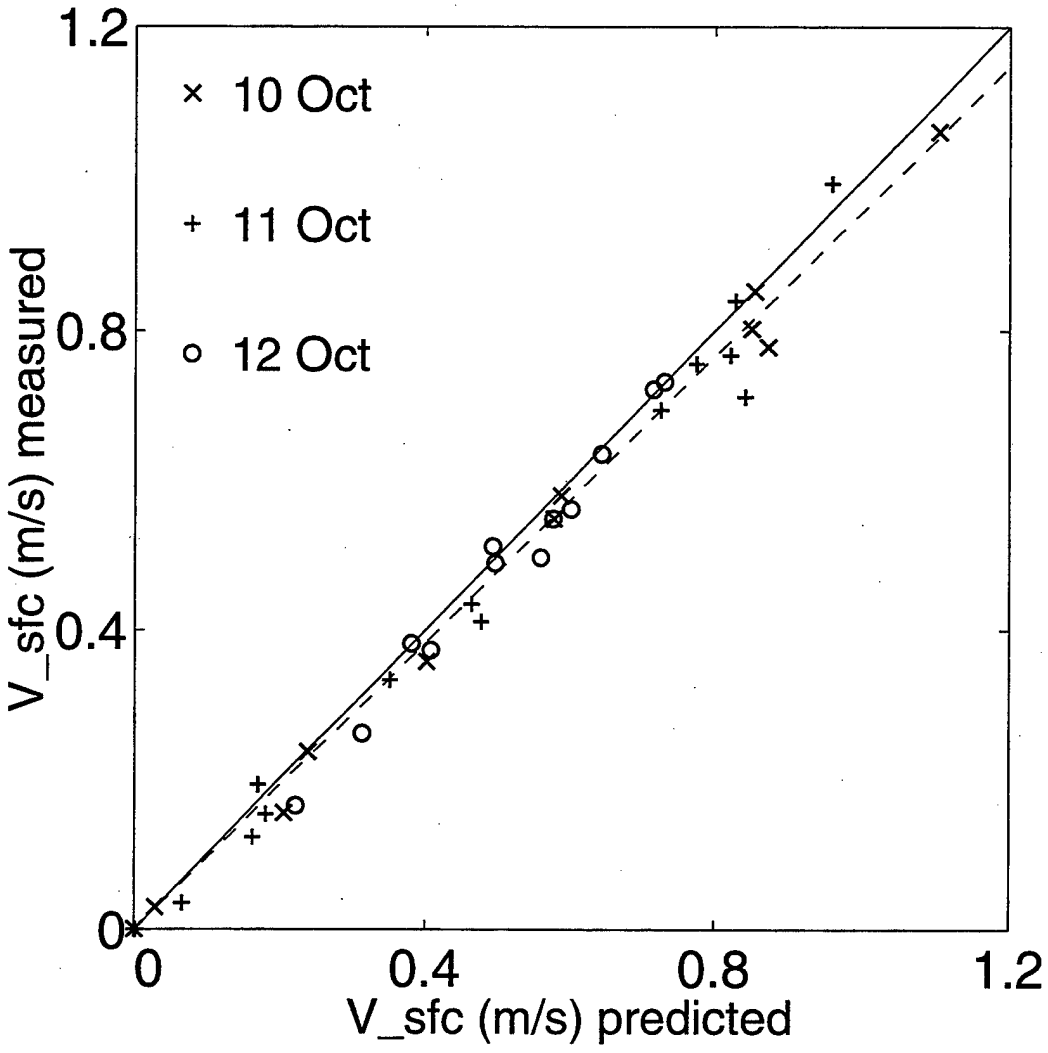

Figure 10. Predicted (equation 10) versus observed longshore velocities within the surface layer. The solid line represents perfect agreement (slope=1) and the dashed line represents a linear regression with a slope of 0.96.

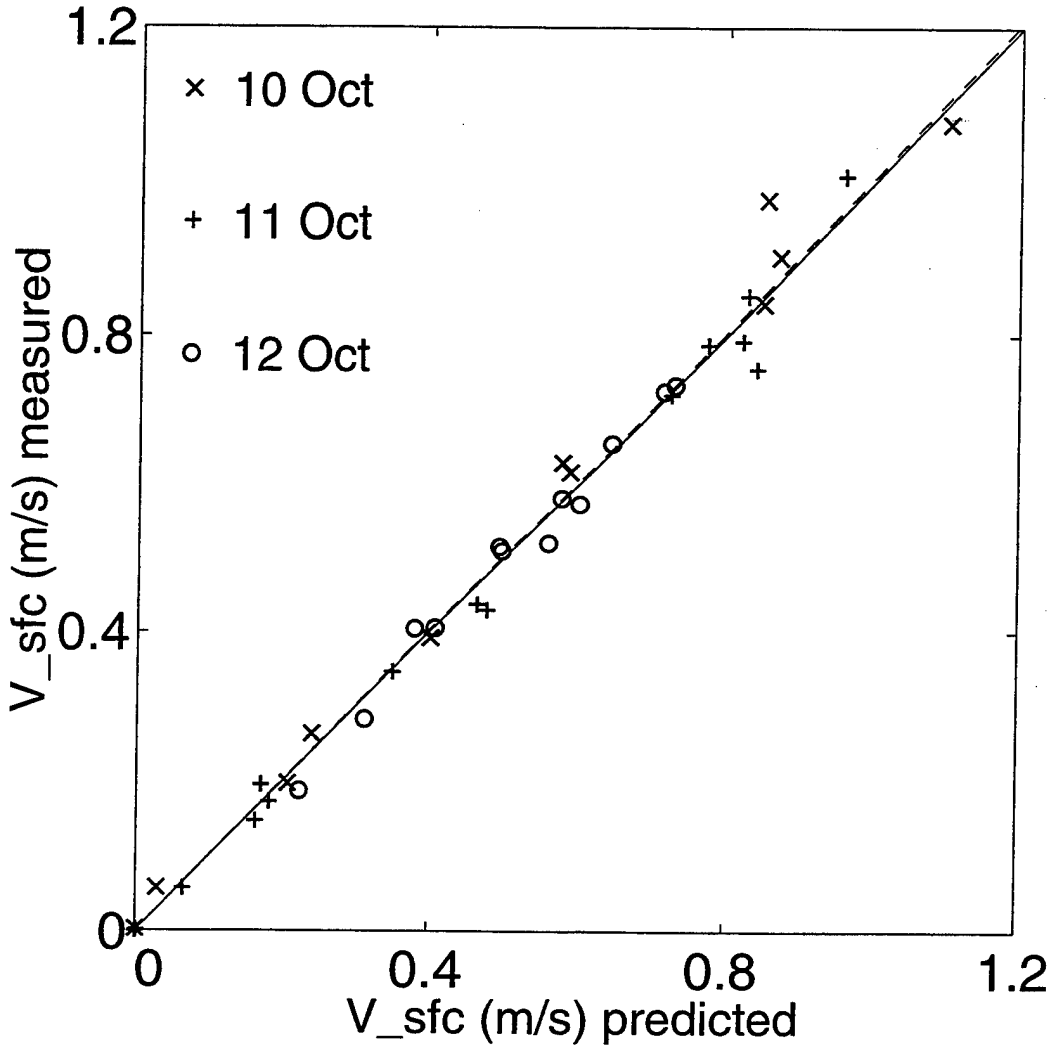

Figure 11. Same as in Figure 10 but including the alongshore component of mass transport velocity (equation 16). The slope of the linear regression is 1.005.

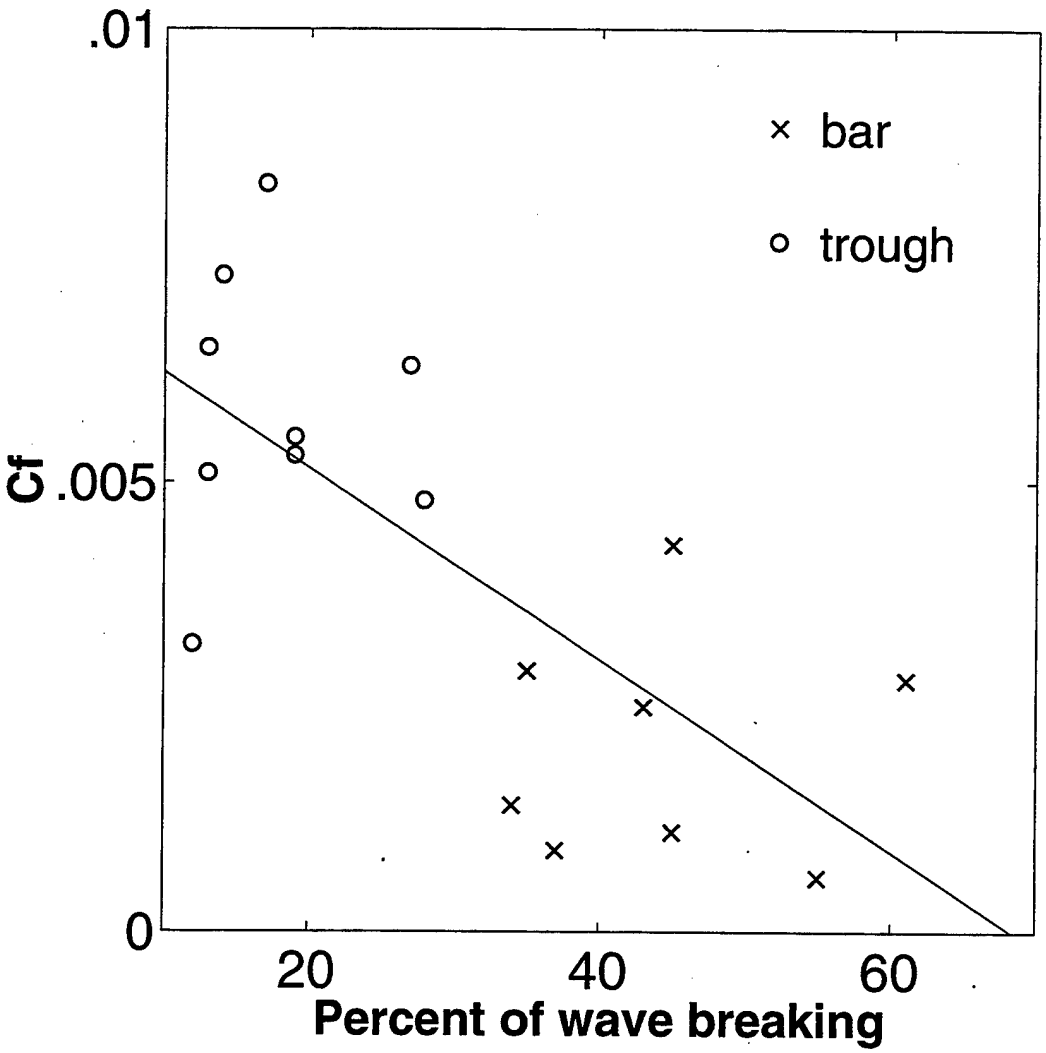

Figure 12. Bed shear stress coefficient (C_f) versus percentage of wave-breaking calculated from video data. The line represents a linear regression with a regression coefficient of -0.71.

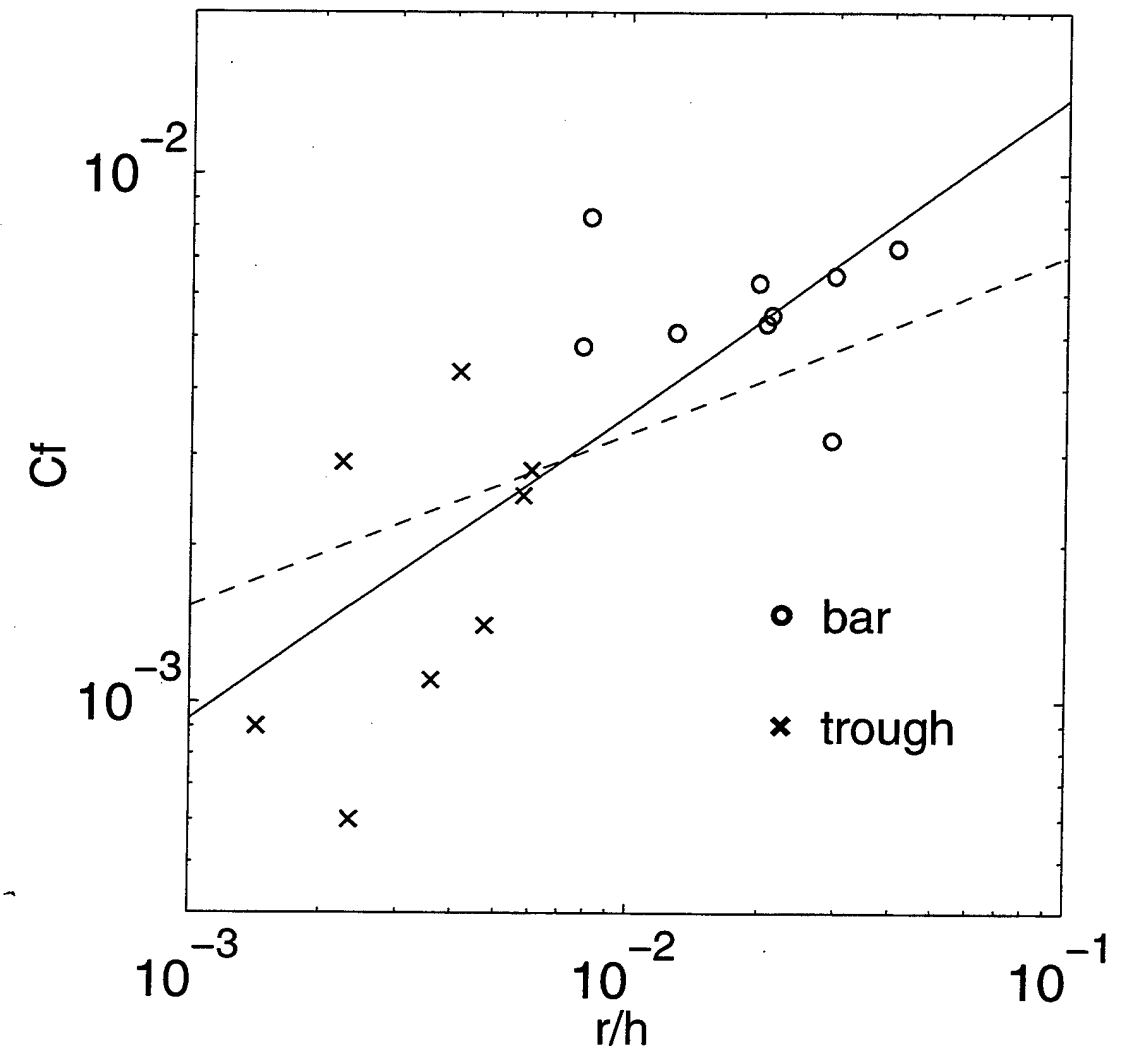

Figure 13. Bed shear stress coefficient (C_f) versus *rms* bottom roughness normalized by mean water depth ($\frac{r}{h}$). The dashed line is the Manning-Strickler equation (22) and the solid line is obtained by adjusting the coefficients of (22) by applying a linear-regression least-squares method to the data.

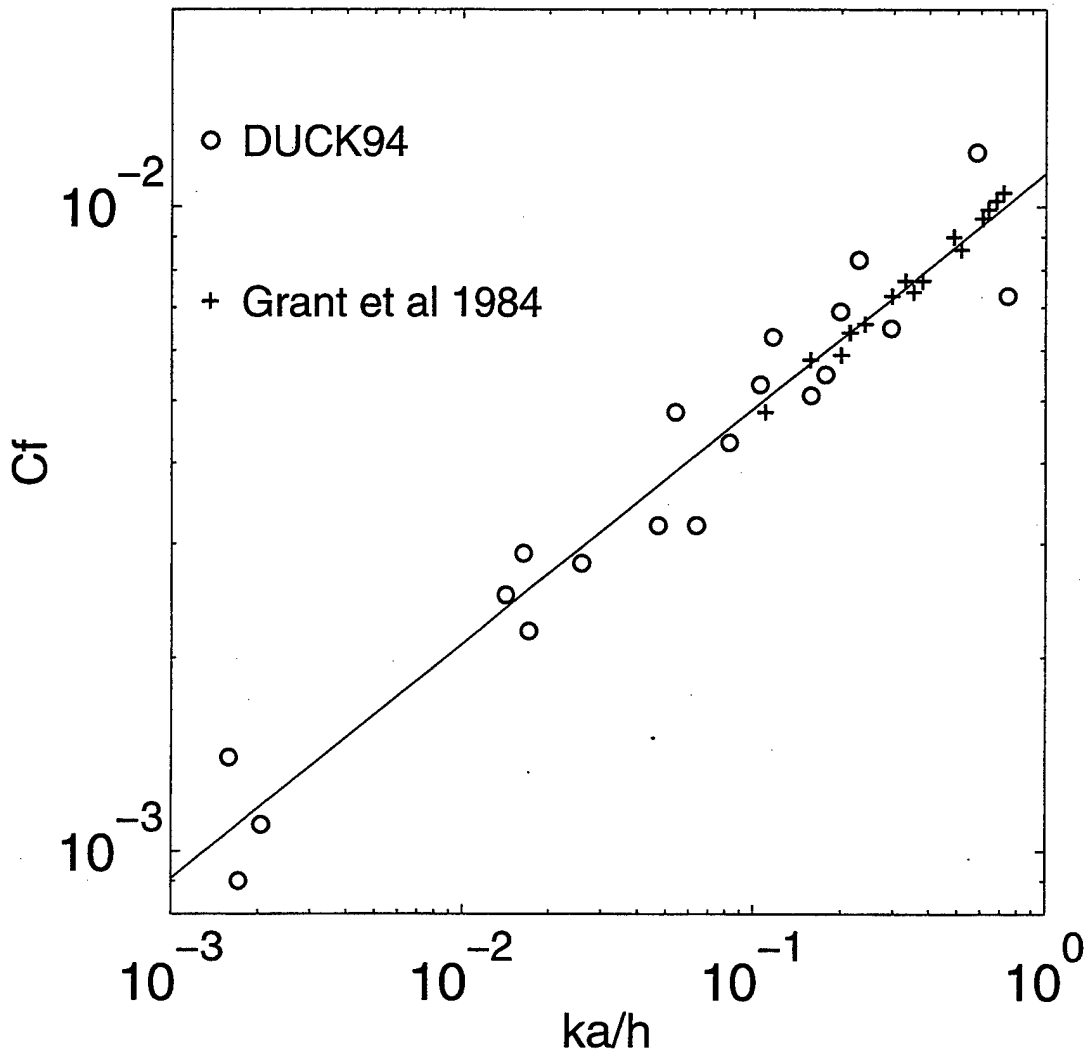

Figure 14. Bed shear stress coefficient (C_f) versus apparent bed roughness length scale normalized by mean water depth ($\frac{k_a}{h}$). The line represents predicted C_f by equation 23.

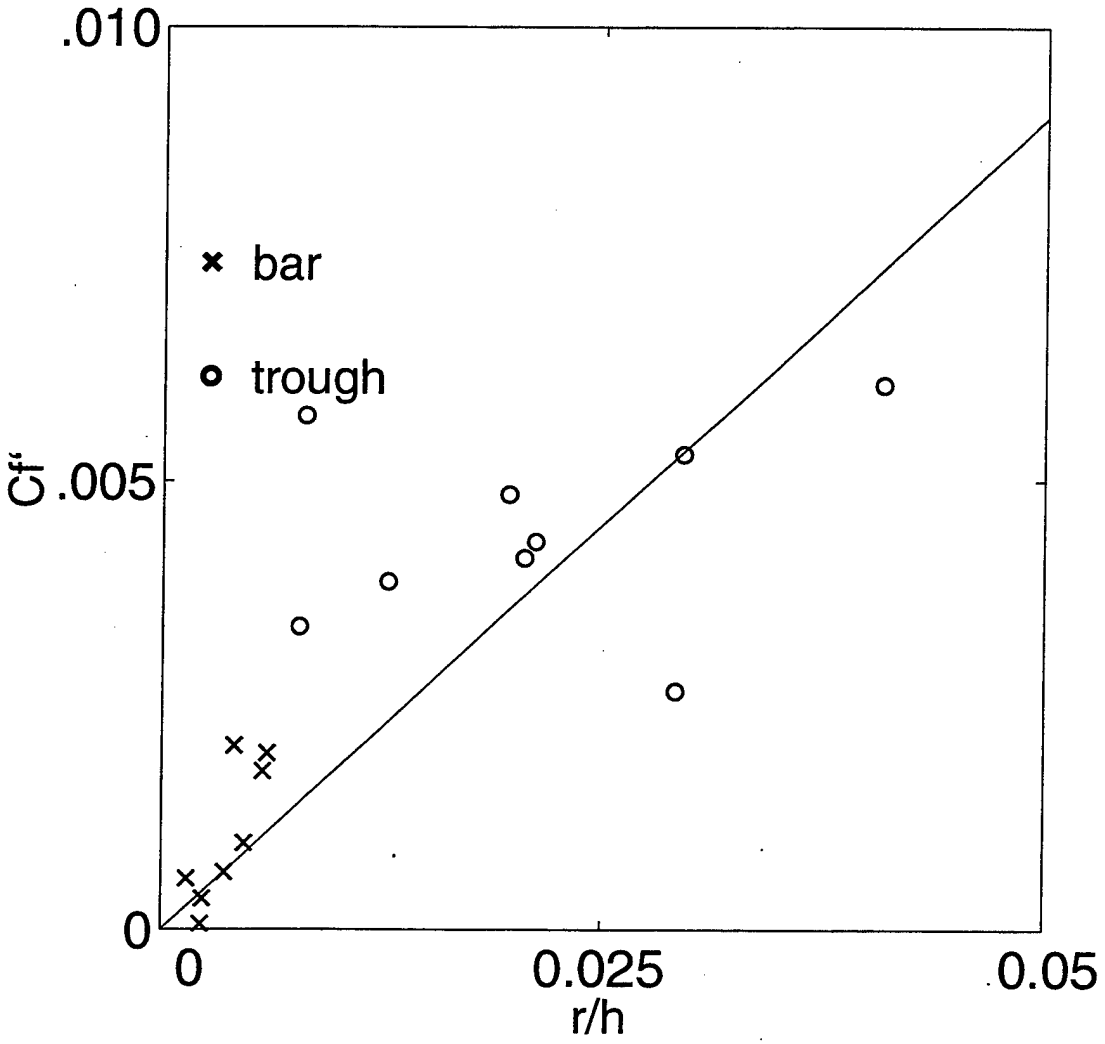

Figure 15. Bed shear stress coefficient without skin friction contribution (C_f') versus *rms* bottom roughness normalized by mean water depth ($\frac{r}{h}$). The line represents a linear regression with a regression coefficient of 0.76.

Table 1. Logarithmic Profile Fitting Results.

Day	Run	Cross-shore Position (m)	Depth h (m)	*rms* Wave height H_{rms} (m)	$\gamma = \frac{h}{H_{rms}}$	*rms* Bottom roughness r (cm)	Apparent roughness height z_a (cm)	Shear stress velocity v_* (cm/s)	Bed shear stress coeff. C_f	Skin friction shear stress velocity v_* (cm/s)
10	1	291	3.80	1.11	0.29	1.8	0.02	2.6	0.0014	1.5
10	2	261	3.24	1.12	0.35	0.8	0.0002	1.7	0.0006	1.1
10	3	231	3.26	1.15	0.35	2.0	0.3	5.1	0.0028	2.8
10	4	201	3.45	0.89	0.26	2.7	0.6	7.1	0.0048	3.9
10	5	185	3.18	0.75	0.24	2.6	2.4	7.0	0.0083	3.9
10	6	170	2.57	0.63	0.25	3.3	1.4	3.2	0.0051	1.6
10	7	156	1.98	0.55	0.28	5.8	0.3	1.8	0.0032	0.7
11	1	292	3.66	1.30	0.36	0.8	0.2	5.6	0.0029	5.5
11	2	270	3.16	1.27	0.40	1.8	0.2	4.7	0.0025	2.5
11	3	244	3.16	1.12	0.35	1.3	0.9	5.6	0.0043	4.0
11	4	230	3.75	0.98	0.26	7.4	1.5	6.3	0.0063	3.0
11	5	187	3.24	0.89	0.27	6.7	1.1	5.2	0.0053	2.4
11	6	171	3.05	0.84	0.28	9.0	3.0	4.0	0.0065	1.7
11	7	157	2.50	0.76	0.30	16.0	0.5	2.7	0.0032	1.1
11	8	146	1.63	0.66	0.40	2.2	3.2	2.3	0.0048	1.1
12	1	298	3.51	1.23	0.35	0.5	0.02	1.6	0.0009	1.0
12	2	273	2.93	1.30	0.44	1.1	0.02	2.3	0.0011	1.5
12	3	252	2.98	1.21	0.41	1.2	0.2	3.6	0.0022	2.2
12	4	225	3.54	1.04	0.29	4.2	6.9	8.1	0.0121	5.0
12	5	210	3.51	0.97	0.28	3.3	2.3	6.1	0.0069	3.7
12	6	188	2.99	0.90	0.30	6.3	1.8	4.7	0.0055	2.2
12	7	172	2.74	0.84	0.31	11.0	6.8	3.2	0.0073	1.3

Table 2. 95 percent confidence bands on v_* , z_a , and C_f . Run 8 of 11 Oct is not included as only two ems are used for profile fitting.

Day	Run	Number of ems used for the regression n	Student's t distribution $t_{(n-2,1-\alpha/2)}$	Correlation coefficient between observations and log-profile predictions C	95 % Confidence Band Shear stress velocity v_* (%)	Apparent roughness height z_a (×/÷)	Bed shear stress Coefficient C_f (%)
10	1	7	2.015	0.983	17	2.3	33
10	2	5	2.353	0.953	43	7.2	99
10	3	5	2.353	0.952	44	7.4	102
10	4	6	2.132	0.992	14	1.9	27
10	5	6	2.132	0.992	13	1.9	26
10	6	5	2.353	0.999	5	1.3	6
10	7	4	2.920	0.991	28	3.5	56
11	1	6	2.132	0.969	27	3.6	58
11	2	5	2.353	0.963	38	5.8	87
11	3	5	2.353	0.975	31	4.1	68
11	4	6	2.132	0.987	17	2.4	35
11	5	6	2.132	0.991	15	2	28
11	6	5	2.353	0.998	9	1.5	14
11	7	5	2.353	0.996	12	1.8	21
12	1	6	2.132	0.966	29	3.9	59
12	2	4	2.920	0.968	53	10	128
12	3	5	2.353	0.989	20	2.5	41
12	4	6	2.132	0.998	6	1.3	10
12	5	6	2.132	0.997	8	1.5	14
12	6	5	2.353	0.995	14	1.9	25
12	7	5	2.353	0.992	17	2.2	30

Table 3. Sensitivity of the ems to elevation from the bed as inferred from the zero-shifting method.

Day	Run	Number of ems used for the regression n	zero-shift (cm)	Correlation coefficient between observations and log-profile predictions C	95% Confidence Band Shear stress velocity v_* (%)	Apparent roughness height z_a (×/÷)
10	7	3	0	0.985	72	2.1
10	7	3	-1	0.986	66	2.0
10	7	3	-2	0.986	60	2.0
10	7	3	-3	0.986	55	2.0
10	7	3	-4	0.987	49	1.9
10	7	4	-5	0.991	31	1.8
10	7	3	+5	0.984	107	2.2
11	7	4	0	0.993	87	3.0
11	7	4	-1	0.994	81	2.9
11	7	4	-2	0.994	75	2.9
11	7	4	-3	0.994	69	2.8
11	7	4	-4	0.994	64	2.8
11	7	5	-5	0.996	53	2.7
11	7	4	+5	0.992	124	3.2
12	3	4	0	0.987	37	4.1
12	3	4	-1	0.988	34	4.1
12	3	4	-2	0.988	31	4.0
12	3	5	-3	0.988	20	3.7
12	3	5	-4	0.988	19	3.7
12	3	5	-5	0.989	17	3.6
12	3	4	+5	0.985	56	4.4

III. MEAN CROSS-SHORE CURRENTS OVER A BARRED BEACH

(This chapter consists of work to be submitted

to the *Journal of Geophysical Research*)

CROSS-SHORE MEAN FLOW OVER A BARRED BEACH

A.F. Garcez Faria, E.B. Thornton, T.C. Lippmann[1], T.P. Stanton

Naval Postgraduate School, Monterey, California 93940

ABSTRACT

The spatial distribution of the mean cross-shore flow (undertow) over a barred beach is examined with field data obtained on three energetic wave days during the DUCK94 experiment. The vertical structure of the undertow is modeled using a turbulent eddy viscosity closure and includes the important effects of wave breaking (described using the roller concept) and convective acceleration of the current. Other than a more realistic description of observed turbulence variations, a depth dependent eddy viscosity does not improve the agreement between predicted and observed undertow profiles. The effects of using different boundary conditions is investigated by extending the monochromatic formulations of Stive and Wind (1986) and Svendsen *et al.* (1987) to random waves by ensemble averaging over the wave height distribution. The contribution of breaking wave rollers to the surface mass flux can be of the same order of the contribution associated with the organized wave motion and should not be neglected. The largest discrepancies between model predictions and observations occur over the sand bar, where the observed strong undertow jet is not predicted by the model. It is postulated that the downward momentum mixing induced by wave breaking produces a constricted return flow layer that enhances undertow velocities, a process not accounted for in the model. Better agreement is obtained for this region with an empirical relation that correlates the surface mass flux with the mean rate of wave-energy dissipation per unit area.

---

[1]Scripps Institution of Oceanography, La Jolla, California 92903

INTRODUCTION

The influence of the mean cross-shore return flow, or undertow, on sediment transport and beach profile evolution has long been believed to be important (*e.g.*, Bagnold, 1940). A local vertical imbalance between the wave setup pressure gradient, that is uniform with depth, and the depth-varying wave radiation stress is conceptually responsible for driving the undertow (Dyhr-Nielsen and Sørensen, 1970). In the last two decades several theoretical models for the vertical structure of the undertow for two-dimensional beaches have been developed (*e.g.*, Dally, 1980; Svendsen, 1984; Dally and Dean, 1984; Stive and Wind, 1986; Svendsen and Buhr Hansen, 1988; Deigaard *et al.*, 1991; Stive and DeVriend, 1994; Haines and Sallenger, 1994). All models use an eddy viscosity closure scheme, and solve for the depth dependent undertow by integrating the cross-shore momentum equation twice over depth, which requires two boundary conditions to evaluate the integration constants.

There is a general consensus throughout the literature of using local conservation of mass over the vertical as one boundary condition. Commonly, the second boundary condition is either the stress at the trough level (Stive and Wind, 1986) or the no-slip condition at the bottom combined with the steady streaming generated by the bottom boundary layer (Svendsen, 1984). Despite significant physical differences, both approaches reduce to the same form between the trough level and the top of the bottom boundary layer within the surf zone, as contributions from steady streaming and bed shear stress are outweighed by mean water slope and wave forcing gradients.

The wave-induced onshore mass flux in the region between the wave crest and trough

is critical to predicting the magnitude of the undertow, which is predicted heuristically by adding the contribution from breaking wave rollers to the mass transport given by an inviscid wave theory plus (Svendsen, 1984). Dally and Brown (1995) found better agreement for laboratory generated regular waves breaking over a planar beach using stream function theory (Dean, 1974) compared with linear wave theory (LWT, hereafter), which tended to over-predict the depth-averaged undertow. On the other hand, Masselink and Black (1995), using field measurements from experiments at two planar beaches, found good agreement using shallow water LWT.

Observations of onshore mass transport by waves in the crest-trough region are scarce owing to difficulties associated with making measurements in this region. As a result, the performance of surface mass flux models is usually evaluated by assuming that mass is conserved over the vertical and comparing model predictions with measured return mass flux. This procedure dictates *a priori* determination of the height of the cross-shore return flow layer. Direct determination of the height of this layer requires measurements of the vertical distribution of mean cross-shore flow with a vertical resolution that so far has only been achieved in laboratory experiments with monochromatic waves using Laser Doppler Velocimeters (*e.g.*, Nadaoka *et al.*, 1989).

Most existing undertow models show good agreement with laboratory data for monochromatic waves breaking over planar beaches when the depth-averaged mean return flow is adjusted to fit the data (instead of using predicted mass flux) and the magnitudes of the two largest dynamical forcing terms (wave setup and radiation stress gradients) are determined from data.

Validation of these models with field data has been limited by the lack of data. Smith *et al.* (1992), compared a model based on Putrevu and Svendsen (1991) solution for the vertical structure of the undertow to data from the 1990 DELILAH experiment on a barred beach near Duck, North Carolina, and found large discrepancies over the bar, where the model under-predicted observed velocities. This strong "undertow jet" over the bar was also present during an earlier field experiment (Sallenger et al., 1983) at the same site.

Within the surf zone, wave-breaking generated turbulence dominates bottom boundary layer processes, with the turbulent shear stress maximum at the surface decreasing to a minimum at or near the bottom. King and Kirby (1994), using LDV data from a wave flume experiment, showed that the primary turbulence generating mechanism in the surf zone is due to wave-breaking at the wave-roller interface and that turbulence intensities decrease with distance from the surface. Cox and Kobayashi (1997), using laboratory LDV measurements of regular waves spilling on a rough, plane slope, observed that the shear stress distribution within the surf zone varies linearly with depth until the top of the bottom boundary layer, and that the eddy viscosity is small near the trough level, increases to a maximum about one-third of the depth below the trough level, and then decreases toward the bottom. Svendsen (1984), investigated the effect of introducing an exponentially varying eddy viscosity (μ_z) to the predicted vertical profile of the undertow. In his formulation, two free parameters are necessary to define the magnitude and decay rate with depth of μ_z, and despite the more realistic depth-variation of μ_z, only marginal improvements are obtained for the vertical profile of the undertow (Svendsen and Buhr Hansen, 1988).

In this paper, field observations of vertical profiles of the mean cross-shore current

obtained over a naturally barred beach are used to test various models. Wave height transformation is based on an energy flux balance including the effects of rollers to describe wave breaking and a probabilistic description of wave heights. The mass flux is investigated using both linear and higher-order wave theories, and including the contribution from surface rollers, to estimate the cross-shore distribution of the undertow. The influence of depth-dependent formulations for the eddy viscosity and different choices of boundary conditions on the vertical structure of the undertow is examined.

THEORY

In the following, a right-handed coordinate system with origin at the shoreline (x positive offshore) and z positive upward from the sea surface is used. Solutions for the surface mass flux, setup and the vertical profile of the undertow are described assuming stationary wave conditions, straight and parallel depth contours, and random waves that are narrow-banded in both frequency and direction.

Wave Transformation

Wave transformation is determined from a probabilistic breaking wave model that includes roller energy gradients in the energy flux balance (Lippmann *et al.*, 1996, LBT hereafter). This model assumes that wave heights both inside and outside the surf zone can be reasonably described by the Rayleigh distribution (Thornton and Guza, 1983) and has been shown to give accurate results for random waves breaking over both planar and barred beaches. The model has two free parameters: σ, the mean angle of the wave-roller interface, and γ, a measure of breaking wave intensity $\gamma = \frac{H_{rms}}{h}$, where H_{rms} is the *rms* wave height and h is the local depth. Although the model is insensitive to the interfacial angle (kept

constant at $\sigma = 10^o$ for all runs) based on the results obtained by LBT at the same location of the DUCK94 experiment, it is necessary to adjust γ to fit the data.

Wave properties are ensemble averaged by integrating wave heights through the assumed Rayleigh distribution, p(H). Following Thornton and Guza (1983), the fraction of waves that are breaking is found by integrating through the breaking wave distribution $p_b(H) = W(H)\ p(H)$, where the weighting function, W(H), is given by Whitford (1988).

Surface Mass Flux

The conservation of mass for straight and parallel contours with the boundary condition of no flow through the beach is given by

$$\overline{\int_{-h}^{\eta} \rho[U(z) + \tilde{u}(z) + \acute{u}(z)]\,dz} = 0 \qquad \textbf{(1)}$$

where overbar indicates time averaging, η is surface elevation, ρ is water density, and the onshore horizontal velocity has been partitioned into mean, wave and turbulence contributions. In an Eulerian reference frame and assuming irrotational flow below the trough level, there is a net shoreward mean mass transport by waves limited to an upper region between the crest and trough that is given by

$$q_w = \overline{\int_{\eta_t}^{\eta_c} \rho\,\tilde{u}(z)\,dz} \qquad \textbf{(2)}$$

where subscripts (c, t) refer to (crest, trough). There is an additional contribution to the mean mass transport (per surface area) above the wave trough (surface layer) that arises from the

presence of turbulent wave rollers (Svendsen, 1984), that is defined by

$$q_r = \rho_r A \frac{c}{L_r} \tag{3}$$

where ρ_r is the roller density, L_r is the length along the wave covered by the roller cross-sectional area A, and c is the velocity that the roller mass is advected landward, assumed to be given by the wave phase speed. The roller contribution (3) to the surface mass flux is based on the calculated cross-sectional area of the roller. Earlier models (Svendsen, 1984; Deigaard et al., 1991) assume that this area is proportional to the *rms* wave height. As a consequence, the largest mean return flow would be predicted to occur at the breaker point, which is contrary to laboratory observations (Nadaoka and Kondoh, 1982). Dally and Brown (1995) solve for the area of the roller for the case of monochromatic waves breaking over a planar beach by simultaneously solving the depth-integrated and time-averaged energy, continuity, and cross-shore momentum equations and found good agreement with existing laboratory data. However, their model requires observations of the cross-shore distribution of either the mean return flow or setup to constrain the model, and therefore cannot be applied to the present data.

Another recent roller model (Lippmann and Thornton, 1997; LT97 hereafter) presents an independent method for calculating q_r, and is calibrated with video observations of the cross-shore variation of the fraction of waves that are breaking. The LT97 model is based on the energy flux balance and describes energy dissipation following Deigaard (1993). Two free parameters in the model, B, the vertical fraction of wave height covered by the roller,

and ψ, a measure of the average wave face angle, are adjusted to give a *rms* best fit to breaking observations.

The onshore mass transport in the upper region is balanced locally by a mean return flow below the trough (undertow)

$$q_w + q_r = -\overline{\int_{-h}^{\eta_t} \rho U(z)\,dz} = -\rho U_R h_t \qquad (4)$$

where U_R is the depth-averaged return flow and h_t is the depth below the trough.

Undertow

The time-averaged cross-shore momentum equation, neglecting molecular viscous stresses, and for the assumed straight and parallel contours and stationary wave conditions, is given by

$$\frac{\partial \rho \overline{u^2}}{\partial x} + \frac{\partial \rho \overline{uw}}{\partial z} = -\frac{\partial \bar{p}}{\partial x} \qquad (5)$$

The horizontal and vertical velocities (u,w) are expanded into mean, turbulent, and wave-induced components, $u = U + \acute{u} + \tilde{u}$ and $w = \acute{w} + \tilde{w}$, where the mean vertical velocity is assumed equal to zero. The time-averaged pressure, $\bar{p} = \rho[g(\bar{\eta} - z) - \overline{\tilde{w}^2} - \overline{w'^2}]$, is obtained from the depth integrated vertical momentum equation, after neglecting contributions from the cross-shore gradient of the vertically integrated wave and turbulent shear stress (Stive and Wind, 1982). After substituting for the time-averaged pressure, (5) can be further simplified for the region between the top of the bottom boundary layer and trough level (middle layer),

with the aid of the following assumptions: 1) wave and turbulent velocity components are statistically independent; 2) turbulence is near isotropic (Stive and Wind, 1982); 3) the wave shear stress is given by $\frac{\partial \rho \overline{\tilde{u}\tilde{w}}}{\partial z} = -\frac{1}{2}\frac{\partial \rho}{\partial x}[\overline{\tilde{u}^2} - \overline{\tilde{w}^2}]$ (Rivero and Arcilla, 1995); and 4) a first order eddy viscosity closure for the turbulent shear stress $-\rho\overline{\acute{u}\acute{w}} = \rho\mu_z\frac{\partial U}{\partial z}$. Applying these assumptions, (5) reduces to

$$\frac{\partial}{\partial z}[\rho\mu_z\frac{\partial U}{\partial z}] = \frac{1}{2}\frac{\partial \rho}{\partial x}[\overline{\tilde{u}^2} - \overline{\tilde{w}^2}] + \rho g\frac{\partial \bar{\eta}}{\partial x} + \frac{\partial \rho \overline{U^2}}{\partial x} = F(x) \qquad \textbf{(6)}$$

where μ_z is the time-invariant turbulent eddy viscosity. The forcing, F(x), in (6) is due to the cross-shore gradients of radiation stress, setup (setdown), $\bar{\eta}$, and convective acceleration of the depth-averaged undertow respectively. Here, F(x) is assumed to be independent of depth based on empirical evidence from laboratory studies (Nadaoka and Kondoh, 1982; Stive and Wind, 1982 and 1986).

A solution for the vertical distribution of the mean undertow can be determined by integrating (6) twice over depth, to give

$$U(z) = F(x)\int\frac{z}{\rho\mu_z}dz + C_1(x)\int\frac{dz}{\rho\mu_z} + C_2(x) \qquad \textbf{(7)}$$

where $C_1(x)$ and $C_2(x)$ are spatially varying integration constants. Both, the Stive and Wind (1986) and Svendsen *et al.* (1987) solutions are used, with modifications to their original developments to improve the derivation. In both these original works, a different solution for the undertow forcing (F) is used as they assume that the wave contribution to stress is small

compared with the Reynolds stress ($\rho\overline{\tilde{u}\tilde{w}} \ll \rho\overline{\acute{u}\acute{w}}$) resulting in an over estimation of the forcing by $\frac{1}{2}\frac{\partial \rho}{\partial x}[\overline{\tilde{u}^2} - \overline{\tilde{w}^2}]$ (Rivero and Arcilla, 1995). Here, (6) will be used instead.

Although different formulations for the eddy viscosity variation with depth are investigated (Appendix), the simplest solution for a depth-independent eddy viscosity (μ) is outlined here. For this case, (7) simplifies to:

$$U(z) = \frac{1}{2\rho\mu}F(x)\,z^2 + \frac{1}{\rho\mu}C_1(x)\,z + C_2(x) \qquad \textbf{(8)}$$

First, following Stive and Wind (1986), $C_1(x)$ is determined by integrating (6) once over depth and solving for the shear stress at the trough level, and $C_2(x)$ by applying conservation of mass over the vertical (see Appendix for details) to give

$$U(z) = U_R + \frac{1}{\rho\mu}F(x)\,[\frac{z^2}{2} + h\,z + \frac{3h^2 - h_t^2}{6}] + \frac{\overline{\tau}_{bx}}{\rho\mu}[z + h - \frac{h_t}{2}] \qquad \textbf{(9)}$$

where $\overline{\tau}_{bx}$ is the mean cross-shore bed shear stress that is calculated using a quadratic formulation ($\overline{\tau}_{bx} = \rho\, C_f\, \tilde{u}_b\, U_b$, where $C_f = 0.01$ is a constant friction factor and $\tilde{u}_b$ is the amplitude of the near-bottom wave-induced velocity). This monochromatic solution is quadratic in z with coefficients independent of wave height $A_2 = \frac{1}{2}$, $A_1 = h$, and $A_0 = \frac{3h^2 - h_t^2}{6}$, which can be extended to random waves by ensemble averaging over the wave distribution

$$\langle U(z)\rangle = U_R + (A_2 z^2 + A_1 z + A_0)\frac{1}{\rho\mu}\int_0^\infty F(x)p(H)\,dH + \frac{\overline{\tau}_{bx}}{\rho\mu}(z + h - \frac{h_t}{2}) \qquad \textbf{(10)}$$

In the cross-shore direction, $\bar{\tau}_{bx}$ is small compared with wave-breaking dissipation (Thornton and Guza, 1983; Svendsen, 1984; Dally and Brown, 1995), and hence the vertical structure of the undertow is mostly determined by the coefficients A_2, A_1 and A_0. The amount of curvature in the profile is a function of both F (calculated from wave quantities) and the eddy viscosity, μ. Large values of F produce more vertical shear resulting in a parabolic profile, whereas large values of μ reduce the vertical shear producing a more uniform velocity profile with depth.

The influence of the boundary condition choice to the vertical structure of the mean undertow is investigated by comparing the results obtained by (10) with the Svendsen *et al.* (1987) model that uses a no-slip condition at the bottom to replace the stress at the trough level as the second boundary condition. This no-slip condition is obtained by coupling the undertow model with a bottom boundary layer model (BBL, hereafter). Within the BBL, the flow is a combination of the steady streaming induced by the oscillatory motion and the undertow above the BBL, which results in a mean velocity at the top of this layer (U_b) that is obtained by requiring continuity in velocity and shear stress between these two regions to give (see Svendsen *et al.*, 1987 for details)

$$<U(z)> = U_b + (A_2 z^2 + A_1 z + A_3)\frac{1}{\rho\mu}\int_0^{\infty} F(x)p(H)dH + \frac{\bar{\tau}_{bx} - \bar{\tau}_{bs}}{\rho\mu}(z + h) \qquad \textbf{(11)}$$

where $A_3 = \frac{h^2}{2}$ is another coefficient independent of wave height and $\bar{\tau}_{bs}$ is related to the steady streaming in the BBL ($\bar{\tau}_{bs} = -\frac{1}{2}\rho\mu_{bl}\sqrt{\frac{\pi f}{\mu_{bl}}}\frac{\tilde{u}_b^{\,2}}{\sqrt{gh}}$, where f is wave frequency and μ_{bl} is the eddy viscosity inside the BBL). Their model further assumes that μ_{bl} is much smaller

than the eddy viscosity in the middle layer, which was recently verified in a laboratory experiment using LDV (Cox and Kobayashi, 1997). Following Putrevu and Svendsen (1993), the eddy viscosity inside the BBL is estimated by $\frac{\mu_{bl}}{h\sqrt{gh}} = 0.32\, C_f^2 \left(\frac{H}{h}\right)^2$.

Setup

The setup gradient is a dominant driving force for the undertow. The setup is calculated by depth-integrating the time-averaged cross-shore momentum equation (5) from the bottom to the mean water level, to give

$$\frac{\partial S_{xx}}{\partial x} + \frac{\partial M_r}{\partial x} + \rho(\bar{\eta} + h)\frac{\partial U_R^2}{\partial x} = -\rho g(\bar{\eta} + h)\frac{\partial \bar{\eta}}{\partial x} \qquad \textbf{(12)}$$

where S_{xx} is the wave radiation stress (Longuet-Higgins and Stewart, 1964), $M_r = cq_r$ is the momentum flux associated with wave rollers, and the last term on the lhs is the convective acceleration of the depth-averaged undertow. In the derivation of (12), it is assumed that the mean bed shear stress (Longuet-Higgins and Stewart, 1964) and the cross-shore wind stress (owing to small observed onshore winds in the data described later) are negligible.

DATA

Field measurements were acquired as part of the DUCK94 experiment (*e.g.* Garcez Faria *et al.*, 1997 [Chapter 1]) conducted at the U.S. Army Corps of Engineers Field Research Facility (FRF) in Duck, North Carolina. The data selected for analysis are from 10-12 Oct. when strong cross-shore currents (0.05-0.4 m/s) caused by a storm with predominant winds and waves from the north were present.

The vertical structure of the current was measured with a vertical stack of seven two-component Marsh-McBirney electromagnetic current meters (ems, hereafter) mounted on a mobile sled at elevations 0.4, 0.7, 1.0, 1.5, 1.8, 2.2, and 2.6 m above the bed. The ems were horizontally displaced at least 1 m from the sled, and oriented such that the vertical stack was in the up-drift direction of the longshore current to minimize interference by the sled structure. The em offsets were determined *in situ* and found to be accurate within 1 cm/s.

The sled orientation was determined using a digital compass mounted on the sled with accuracy O(1 degree). Measured two-component velocities were rotated to a shore normal right-handed coordinate system by using compass data and adding at each sled position any deviation of the bottom contour line from a shore parallel direction. A precise determination of the rotation angle is important to avoid contamination of cross-shore velocities by the observed strong longshore currents O(1 m/s). Velocity errors associated with the rotation of the coordinate system were comparable to the determined offsets, and therefore are neglected.

For the first run on each day, the sled was towed by the Coastal Research Amphibious Buggy (CRAB) to its farthest offshore location seaward of the bar (approximately 160 m from the shoreline). A forklift on the beach pulled the sled shoreward 10 to 30 meters for subsequent measurement runs that are referred to in the text by sequential numbers within each day. Each data run was nominally one hour, and seven to eight runs were made across a transect during each day spanning the high tide during this period.

Waves and mean water level were measured using an array of five pressure sensors mounted on the sled. Directional wave spectra were also acquired using a linear array of 10

pressure sensors in 8 m depth. Additionally, a 13 element cross-shore array of pressure sensors was used to measure wave heights spanning the width of the surf zone (Elgar *et al.*, 1997). The fixed array was located approximately 25 m to the north of the sled transect. These data were continuously sampled at 2 Hz. Video observations were used to measure the fraction of wave breaking along the same transect using the method of Lippmann and Holman (1991).

Meteorological information of wind and atmospheric pressure were recorded simultaneously at the seaward end of the 600 m long FRF pier and atop the FRF building in front of the pier. The bathymetry was measured daily using the CRAB and it was found that the depth contours were nearly straight and parallel for the three days under consideration.

RESULTS AND DISCUSSION

Measured and modeled undertow flows are maximum on top and on the shoreward slope of the bar, with increasing magnitude from 10 to 12 Oct. as wave forcing increased with the approach of a storm (Fig. 1). The vertical structure over this region is the classic parabolic shape associated with strong wave-breaking turbulence (Svendsen, 1984; Stive and Wind, 1986). In the inner trough, the return flow is weak, and almost no vertical structure is seen. At the seaward slope of the bar, observed profiles on 10 Oct. (Fig. 1a) are nearly uniform with depth. It is noted there is significant bottom roughness in the trough of the barred profiles related to the development of lunate and long-crested mega-ripples as a result of the strong longshore currents (Thornton *et al.*, 1997). The bar migrated off-shore during this period O(20 m), which was found by Gallagher et al. (1997) to be associated with the strong undertow.

Model/data comparisons are evaluated by calculating absolute and relative root-mean-square (*rms*) errors. Absolute error has dimensional units and is defined by

$$\varepsilon_{abs} = \sqrt{\frac{1}{N}\sum_{i=1}^{N}(P_i - O_i)^2} \qquad \textbf{(13)}$$

where P_i is model prediction, O_i is the observed quantity, and N is the number of observations. The relative or percent error is calculated by

$$\varepsilon_{rel} = 100\,[\sqrt{\frac{1}{N}\sum_{i=1}^{N}(\frac{P_i - O_i}{O_i})^2}\,] \qquad \textbf{(14)}$$

and weights the difference between model predictions and observations against a measure of expectation that is represented by the observation. This statistic is not well-behaved for small O_i, which sometimes is the case for observed mean cross-shore velocities. Thus measurements smaller than the *in situ* determined offsets (+/- 1 cm s^{-1}) are excluded from (14).

In the following, the accuracy of the wave transformation model is described first, which is then used to predict the surface mass flux, setup and vertical profiles of the undertow including contributions from surface rollers.

Wave Transformation

The *rms* wave height is approximated by $H_{rms} = \sqrt{8\sigma^2}$ where σ^2 is the variance calculated from the surface elevation time series. Surface elevation was calculated by Fourier transforming a one-hour pressure record, applying a LWT transfer function to the complex

Fourier amplitudes in the frequency domain, band-pass filtering by zeroing coefficients outside the range of interest (0.05Hz < f < 0.5 Hz), and inverse transforming to obtain the surface elevation time series (Thornton and Guza, 1982).

The sensitivity of the models for surface mass flux, setup, and undertow to errors associated with the use of a random wave transformation model (LBT) is investigated by comparing with results using measured wave heights interpolated with cubic splines. The difference between model output and data interpolation methods is shown in Fig. 2 for the first run of 11 Oct., which has the largest *rms* relative error (7 percent).

A plot of measured versus modeled H_{rms} for the three days analyzed (10-12 Oct.) shows good agreement (Fig. 3). The mean ε_{rel} is 5 percent for all runs, with largest errors at any cross-shore position within 12 percent. Best fit values for γ and ε_{rel} are summarized in Table 1. In general the transformation model well represents measured wave heights.

Surface Mass Flux

Estimating Surface Mass Flux from velocity measurements

The surface mass flux is inferred from the measured return flow, which is sensitive to the depth of the return flow layer. For field experiments as well as for modeling efforts, the height of the return flow layer is assumed to be coincident with the trough level, h_t. Here, h_t is calculated using both linear and non-linear wave theories and compared to surface elevation estimates. Laitone's second order approximation (Laitone, 1961) to cnoidal wave theory (Korteweg and de Vries, 1895) is used as this theory provides an analytical solution to h_t, and the conditions for all runs being examined are within the range of validity of this theory determined by the Ursell number, $\frac{H/(2*h)}{(kh)^2} > 0.6$, where k is wavenumber (Laitone,

1962). The use of a non linear wave theory generally gives higher trough levels than LWT, and consequently smaller mean return flows (U_R) for the same onshore mass transport (Fig. 4). However, the effect on the calculated total return mass flux is minimal as an increase in h_t is counterbalanced by a decrease in U_R. No statistically significant difference at the 97 percent confidence level is found between the results obtained using cnoidal and linear wave theory for all 22 runs (Fig. 5).

A problem associated with practical applications of cnoidal wave theory is related to its mathematical complexity, as it contains both the Jacobian elliptic functions and the complete elliptic integrals of the first and second kinds. An attractive alternative is the use of its asymptotic approximation, or hyperbolic wave theory (Iwagaki, 1968), which is valid when the complete integral of the second kind (K) is greater than 3, and the Ursell number is greater than 0.6 (Svendsen, 1974), which is the case for the data examined here. The calculated difference between observed surface mass flux given by LWT and Iwagaki's approximation is ε_{rel} = 7.9 percent, indicating that the hyperbolic wave theory is accurate enough to replace the more complex cnoidal wave theory. Applying Iwagaki's solution, an expression for h_t similar to LWT is derived that is a function of only local depth and *rms* wave height.

$$h_t = \frac{1}{2}\left[\left(h-\frac{H_{rms}}{3}\right) + \sqrt{\left(h-\frac{H_{rms}}{3}\right)^2 + \frac{H_{rms}^2}{3}} \right] \qquad \textbf{(15)}$$

The observed mean trough level is obtained by applying a zero-up-cross method to the measured surface elevation time series to define individual waves and then averaging the

minima between each up-cross interval. A comparison with measured mean trough level (Fig. 6), shows that this simple expression (15) provides a better estimate for the mean trough level within the surf zone (*rms* over-prediction of 4 cm) than LWT (*rms* under-prediction of 17 cm). It can also be noticed in Fig. 6 that discrepancies between predicted and observed mean trough level increase with *rms* wave height for LWT, while (14) provides an estimate of h_t that does not appear sensitive to H_{rms}.

Surface Mass Flux model

The inferred surface mass flux obtained by numerically integrating the observed cross-shore mean currents from the bottom to the trough level given by (14) are compared to model estimates (4). q_r is determined from the calibrated LT97 model and q_w is determined first using linear wave theory and then with non linear theory for comparison. Predicted q_r are dependent on the percentage of breaking waves in the LT97 model. For the 22 profiles examined, best fit values of B range 0.60-0.95 and ψ range 1.1-1.9 (Table 1), and the error between observed and modeled percentage of breakers is ε_{rel}= 5.6 percent. An example of observed and predicted percentage of breakers is shown in Fig. 7 for the third run of 12 Oct., which has the largest *rms* error (9 percent).

Inferred and predicted surface mass flux using linear wave theory are compared for the entire ensemble in Fig. 8. Due to significant changes associated with wave-breaking characteristics, the data have been divided into four regions: shoreward slope of the bar, seaward slope of the bar, trough, and foreshore. The *rms* relative error between observations and predictions using only q_w, given by linear theory is 40 percent. Including the mass flux contribution from wave rollers, q_r, improves the overall agreement (*rms* error = 28 percent).

Largest values of q_r occur at the shoreward slope of the bar (Fig. 8, lower panel), where wave-breaking is most intense. In this region, q_r is on average 72 percent of q_w, but can be as large as 144 percent (fourth run of 12 Oct.). This is in accordance with earlier model studies (Svendsen, 1984; Dally and Brown, 1995), but contrary to Masselink and Black (1995) who contend that the roller contribution to the mass transport is of secondary importance based on the results from field experiments at two near planar beaches.

The impact of using a non linear wave theory to calculate q_w is examined next. For this investigation, stream function theory (SFT, hereafter) is used as it provides a higher order solution for q_w than cnoidal wave theory, and it has already been shown to give accurate results with laboratory data (Dally and Brown, 1995). Surface mass fluxes were calculated using SFT both including and excluding q_r. For the field data examined, there is little difference between the use of LWT or SFT, with LWT giving values on average 8 percent larger than SFT (Fig. 9).

Errors in surface mass flux predictions could also arise from the misfit in estimating wave heights with a transformation model. Calculated *rms* relative error in mass flux between using LBT model predicted H_{rms} and applying a cubic spline to the measurements for all runs is 9 percent, with a maximum relative error of 19.5 percent (third run of 12 Oct.). These results suggest that the surface mass flux is not overly sensitive to the choice of the random wave transformation model.

Undertow Jets

The onshore transport is observed to extend below the mean through level during high wave conditions and where a high percentage of wave-breaking occurs, such as over

of the bar (Fig. 4b), which violates a basic assumption of existing surface mass flux models. Inferred downward momentum mixing produced from breaking-injected turbulence is probably responsible for this anomalous onshore flow in the upper layer penetrating beneath the trough level (Masselink and Black, 1995; Garcez Faria *et al.* 1997 [Chaper 1]). To conserve mass, undertow velocities in this constricted return flow layer are enhanced resulting in an undertow jet. This phenomenon was qualitatively observed by Nadaoka *et al.* (1989) in a laboratory experiment using flow visualization techniques and a fibre-optic LDV system. In their experiment, obliquely descending eddies behind the breaking wave crest were observed to substantially transport vorticity into an otherwise nearly irrotational velocity field, resulting in an increased mass transport.

On the shoreward slope of the bar where strong wave-breaking was observed (Fig. 7), the model considerably under-predicts mass transport (Fig. 8). The effect of the constricted return flow layer is estimated for this region by $\frac{q_{obs} - [q_w + q_r]}{q_{obs}}$. Enhanced undertow velocities account for an average of 39 percent of the calculated surface mass flux, and are in qualitative agreement with Nadaoka *et al.* (1989).

These observed strong jets are not believed to be associated with three-dimensional circulation cells, as measured bathymetry was essentially uniform alongshore during the period being analyzed and no qualitative evidence of stationary rip currents was observed in the video.

Empirical estimate for Surface Mass Flux

It was found empirically that the inferred surface mass flux ($Q = \rho U_{obs} h_t$) is significantly correlated at the 99.5 percent confidence level (linear correlation of 0.89 and

ε_{rel} = 27 percent) with the mean rate of wave-energy dissipation per unit area, D (Fig. 10)

$$Q = 5.27 \frac{\rho^{1/3} D^{2/3} h_t}{\sqrt{g h}} \tag{16}$$

The spatially varying D is estimated from the energy balance equation using the LT97 model. This empirical relation provides a simple alternative to estimate the surface mass flux within the surf zone that easily can be incorporated into nearshore current models for field applications with the same accuracy of existing surface mass flux models. A better agreement is obtained for the region of the shoreward slope of the bar with this relation (Fig. 8-10).

Setup

Setup is calculated using a finite centered difference method to numerically solve (12), with the condition that the setup is assumed zero at the most offshore grid point. Contributions from each term of (12) are examined for the fourth run of 12 Oct. (Fig. 11), which corresponds to the most energetic period. The cross-shore gradient of the momentum flux associated with wave rollers is calculated using the LT97 model, the radiation stress term is calculated using linear wave theory (Longuet-Higgins and Stewart, 1964), and the convective acceleration of the current ($\frac{\partial \rho U^2}{\partial x}$) is estimated by applying cubic splines to measured depth-integrated cross-shore mean return flow. The largest contributions are due to the radiation stress and roller terms. The convective acceleration term, although generally an order of magnitude smaller than the other terms, cannot be neglected, as it can be of the same order as the sum of the larger terms.

The effects on setup by contributions from the roller momentum flux and using non

linear wave theory to calculate the radiation stress are examined with one example from each day (Fig. 12). The effect of the roller is to redistribute momentum laterally into the trough of the bar, shifting the point where the setup begins onshore. This shift has a significant impact on the setup/setdown profile within the surf zone. The use of a non linear wave theory (SFT is used here) to estimate the wave radiation stress does not appear to alter the setup profile dramatically (Fig. 12).

Undertow

Cross-shore variation of the eddy viscosity

An implicit assumption of the closure model used in the undertow solution is that the eddy viscosity coefficient (μ) is proportional to turbulence intensity. Conceptually, large cross-shore variation of this parameter is expected throughout the surf zone over a natural barred beach associated with significant changes in wave-breaking generated turbulence. Haines and Sallenger (1994), in an earlier field experiment limited to 3 ems over the vertical at this same beach, used a different model for the vertical variation of the undertow and found that best fit μ for each location varied by more than an order of magnitude across the surf zone (μ = 0.0055 - 0.075 $m^2 s^{-1}$) in qualitative agreement with theoretical expectations. Smith *et al.* (1992) on the other hand applied a constant μ across the surf zone (μ = 0.05 $m^2 s^{-1}$) and found good agreement with the DELILAH data.

In order to investigate the cross-shore variation of the eddy viscosity, best fit μ (Table 2) were calculated using (10) by minimizing both the ε_{abs} and ε_{rel} at each cross-shore position occupied by the sled (Fig. 1). For all 22 runs, ε_{abs} = 2.2 cm s^{-1} (ε_{rel} = 19 percent) with maximum ε_{abs} = 6.1 cm s^{-1} (ε_{rel} = 44 percent) for the fourth run of 12 Oct. Observed

mean undertow velocities (U_{obs}) and splined *rms* wave heights were used in the calculations to isolate effects due to the choice of μ. Using modeled *rms* wave heights (LBT96), ε_{abs} = 2.5 cm s^{-1} (ε_{rel} = 22 percent), which indicates that the vertical profile of the undertow is not sensitive to errors associated with the use of a random wave transformation model. Using the surface mass flux model to estimate U_R results in *rms* errors of 5.1 cm s^{-1} and 48 percent, which suggests that largest errors in the vertical profile of mean undertow are related to failure of existing models to correctly predict the surface mass flux in breaking waves.

Models for the vertical structure of the undertow that use an eddy viscosity closure to solve for the turbulent shear stress (Reynolds stress), independent of the choice of boundary conditions and depth-dependence of the eddy viscosity, result in a general solution of the form:

$$U(z) = U_{ref} + \frac{<F(x)>}{\rho \mu} S(z) \qquad \textbf{(17)}$$

where U_{ref} is a reference velocity that could be either the depth-averaged undertow or the velocity at the top of the bottom boundary layer. A nearly uniform vertical profile of undertow, as observed in the inner trough and seaward slope of the bar (Fig. 1), requires either no forcing ($F = 0$) or an infinite eddy viscosity to be correctly reproduced. An example of the spatial distribution of each term and the total F(x) for the first run of 10 Oct. is shown in Fig. 13. The dominance of the setup gradient term is evident, and hence the model predicts offshore directed flow throughout the entire surf zone, which agrees with observations. It can also be noticed that modeled total forcing, although small offshore of the bar and within the trough where the undertow was near uniform, was never nil within the

cross-shore transect occupied by the sled, which was also the case for all the other runs during the period being analyzed. Minimum *rms* errors over these regions are obtained for large eddy viscosity values (Table 2), with a maximum cutoff level arbitrarily set at $\mu = 0.5$. These unrealistically large values of μ are associated with the sensitivity of the eddy viscosity model to small errors in the dynamical forcing, which is calculated as the difference between two large numbers (setup and radiation stress gradients).

The parameterization for the eddy viscosity is of the form $\mu \approx l\,C$, where l and C are characteristic length and velocity scales (Battjes, 1975). Several dimensionally consistent parameters for μ are found in the literature, such as $(\frac{H}{2})^2 f$ [Thornton,1970]; $h(\frac{D}{\rho})^{1/3}$ [Battjes, 1975]; $h\sqrt{gh}$ [Stive and Wind, 1986]; $\frac{(kh)^2}{f}(\frac{D}{\rho})^{2/3}$ [Haines and Sallenger, 1984]. An attempt was made to relate best fit μ with these parameters after excluding from the ensemble runs that reached the cutoff level (Table 2). No statistically significant correlation at the 95 percent confidence level was obtained between these parameters and best fit μ. On the bar crest and shoreward slope of the bar the mean undertow profile assumes a parabolic shape and best fit eddy viscosity approaches a constant value ($\mu \approx 0.04$). Although contrary to theoretical expectations, these results suggest that the use of a constant eddy viscosity across the surf zone provides a reasonable approximation for the modeling of the vertical structure of the undertow.

Vertical variation of the eddy viscosity

Here, the impact of both a depth varying μ_z and different boundary conditions on the vertical structure of the undertow under field conditions are investigated. It is expected from measurements (King and Kirby, 1994; Cox and Kobayashi, 1997) that μ_z should increase

from the bottom towards the surface with increasing levels of wave-breaking generated turbulence. Several mathematical formulations for the vertical variations of μ_z were investigated and the three solutions that give best agreement with data are described in the Appendix. A comparison between the solutions for a linear (A6) and quadratic (A11) μ_z that give the smallest overall *rms* errors for the entire ensemble, together with the undertow solution (10) for a constant eddy viscosity with depth are shown in Fig. 14 for the two stations within each day that have largest observed vertical structure of the undertow. No significant improvement in the *rms* relative or absolute errors between observations and the solutions using variable μ_z with depth is observed. These results confirm earlier modeling findings that a depth-dependent eddy viscosity does not substantially improve the description of the vertical structure of the mean undertow (Svendsen and Buhr Hansen, 1988; Nadaoka *et al.*, 1989).

The influence of the boundary condition choice to the vertical structure of the mean undertow in the middle layer is investigated next. Comparison between predictions by (10) that uses conservation of mass over the vertical and the stress at the trough level as boundary conditions and (11) that uses a no-slip condition at the bottom to replace the stress at the trough level as the second boundary condition are shown in Fig. 15 for the same stations used in Fig. 14. Again, no significant improvement in the total *rms* errors between observations and predictions by these two solutions is obtained, although there are noticeable differences in the predicted currents by each model as a function of depth. Equation (10) shows better overall comparison with data, while (11) better represents the structure of the flow in the lower half of the water column. Although models coupling the middle layer and BBL flows

(11) are expected to provide a more realistic description of the undertow structure close to the bed (Battjes et al., 1990), their applicability to field conditions is still limited by the lack of data to constrain their free parameters.

CONCLUSIONS

The predicted spatial distribution of mean cross-shore currents (undertow) over a barred beach are compared with field observations during the DUCK94 experiment to quantify the relative importance of contributions from the various terms in the cross-shore momentum equation and to identify physical mechanisms not yet incorporated in existing nearshore models.

The surface mass flux model based on conservation of mass over the vertical and including contributions associated with wave rollers is compared with field observations obtained by integrating the measured return flow over depth. It was found that the roller contributions to the mass transport can be larger than the contributions from the organized wave motion when high energetic waves are present. An increase of 8 percent in the surface mass flux prediction is obtained using linear wave theory combined with contributions from wave rollers compared to the solution given by non linear streamfunction wave theory.

The largest discrepancies between model predictions and observations of undertow velocities occur over the sand bar, associated with the failure of existing models to correctly predict the surface mass flux under breaking waves. It is postulated that the downward mixing produced from breaking-injected turbulence penetrating beneath the trough level results in a constricted return flow layer and enhanced undertow velocities (undertow jet), a process not accounted for in the model. Good agreement with data is obtained for this

region with an empirical relation that correlates the surface mass flux with the mean rate of wave-energy dissipation per unit area. This empirical relation provides a simple alternative to estimate the surface mass flux within the surf zone that can be easily incorporated into nearshore current models for field applications with the same accuracy of existing surface mass flux models.

Setup (setdown) is a dominant forcing mechanism for the undertow and is calculated from the depth-integrated and time-averaged cross-shore momentum balance. It is found that despite the dominance of the setup (setdown) and radiation stress gradients in this balance, the contribution from the convective acceleration of the mean current is significant during energetic wave events. It is also shown that the inclusion of contributions from wave rollers results in an onshore shift of the point where the setup begins, which has a significant impact on the dynamical balance of forces within the surf zone.

The vertical structure of the undertow is modeled using a turbulent eddy viscosity closure, and it is found that a depth-dependent eddy viscosity does not substantially improve the agreement with data under field conditions. The effects of using different boundary conditions to solve for the vertical structure of the mean undertow is investigated by extending the monochromatic formulations of Stive and Wind (1986) and Svendsen *et al.* (1987) to random waves by ensemble averaging over the wave distribution (Equations 10, and 11, respectively). No significant improvement in the total *rms* errors between observations and predictions given by these two solutions is obtained. Despite the better representation of the undertow structure close to the bed obtained by using (11), which couples the middle layer and bottom boundary layer flows, its applicability to field

conditions is still limited by the lack of data to constrain their free parameters.

In the inner trough and seaward slope of the bar, the measurements show almost no vertical structure for the mean undertow, which would require a local balance between setup gradient and wave forcing ($F = 0$) or a large eddy viscosity ($\mu \rightarrow \infty$) to be properly modeled. Although small, model predicted forcing was never nil within these regions, so that unrealistically large values of μ are required to model the observed uniform profile of the undertow. These unrealistically large values of μ are associated with the sensitivity of the eddy viscosity model to small errors in the dynamical forcing, that is calculated as the difference between two large numbers (setup and radiation stress gradients).

On the bar crest and shoreward slope of the bar, where strong wave-breaking was observed, the mean undertow profile assumes a parabolic shape and best fit eddy viscosity approaches a constant value ($\mu \approx 0.04$). These results suggest that the use of a constant eddy viscosity across the surf zone provides a reasonable approximation for the modeling of the vertical structure of the undertow.

The absence of both setup measurements and observations of currents close to the bed are major limitations of the present study. Setup is an integral measure of the dynamic response of the mean water level to cross-shore gradients of momentum fluxes, and its gradient is an important driving force for the undertow within the surf zone. The lack of current measurements close to the bed prevents a quantitative evaluation of the effect of applying different boundary conditions to solve for the vertical profile of the undertow.

APPENDIX

In this appendix, the solution for the case of an eddy viscosity that varies linearly with

depth, as suggested by Okayasu *et al.* (1988) is derived in more detail. Following Stive and Wind (1986), the stress at the trough level and conservation of mass over the vertical are used as boundary conditions. The final solutions for other depth-dependent formulations for the eddy viscosities investigated in this study are also included.

1. Linear: $\mu_z = \alpha + \beta z'$

In this solution, a normalized vertical coordinate is introduced $z' = \frac{(z+h)}{h_t}$, and the primes are omitted hereafter for simplicity of notation. Assuming the undertow forcing to be constant over depth and using the eddy viscosity closure for the turbulent shear stress, a solution for the vertical distribution of the mean undertow is obtained by integrating (6) over depth, to give

$$\rho \mu_z \frac{\partial U(z)}{\partial z} = \bar{\tau}(z) = F(x) z + C_1 \qquad \text{A1}$$

where C_1 is an integration constant that is solved by evaluating (A1) at the bottom ($z = 0$)

$$C_1 = \bar{\tau}_b \qquad \text{A2}$$

Integrating A1 a second time and using A2, gives

$$U(z) = \frac{F(x)}{\rho\beta}[z - \frac{\alpha}{\beta}\ln(\alpha + \beta z)] + \frac{\bar{\tau}(z)}{\rho\beta}\ln(\alpha + \beta z) + C_2 \qquad \text{A3}$$

where C_2 is an integration constant that is solved by applying conservation of mass over the vertical, to give

$$C_2 = U_r - \frac{F(x)}{\rho\beta}\left[\frac{d_t}{2} - \frac{\alpha}{\beta}C_0\right] - \frac{\bar{\tau}(z)}{\rho\beta}C_0 \qquad \text{A4}$$

where

$$C_0 = \frac{\alpha}{\beta d_t}\ln\left(\frac{\alpha+\beta d_t}{\alpha}\right) + \ln(\alpha+\beta d_t) - 1 \qquad \text{A5}$$

substituting A4 in A3, the final solution for the vertical profile of the undertow is given by

$$U(z) = U_r + \frac{F(x)}{\rho\beta}\left[\left(z - \frac{d_t}{2}\right) - \frac{\alpha}{\beta}\left[\ln(\alpha+\beta z) + C_0\right]\right] + \frac{\bar{\tau}(z)}{\rho\beta}\left[\ln(\alpha+\beta z) - C_0\right] \qquad \text{A6}$$

2. Quadratic: $\mu_z = \alpha + \beta (z)^{1/2}$

$$U(z) = U_r + \frac{F(x)}{\rho\beta}\left[M_1(z) - \frac{4d_t^{3/2}}{15} - \frac{\alpha^2}{\beta^2}M_3\right] + \frac{\bar{\tau}(z)}{\rho\beta}\left[M_2(z) + \frac{2\alpha d_t^{-1/2}}{\beta} - M_3\right] \qquad \text{A7}$$

where

$$M_1(z) = \frac{2}{3}z^{3/2} - \frac{\alpha}{\beta}z + \frac{2A^2}{\beta^2}z^{1/2} - \frac{2\alpha^3}{\beta^3}\ln(\alpha+\beta z^{1/2}) \qquad \text{A8}$$

$$M_2(z) = 2z^{1/2} - 2\alpha\ln(\alpha+\beta z^{1/2}) \qquad \text{A9}$$

$$M_3 = \frac{1}{\beta^3 d_t}\left[\frac{4\beta^3}{3} d_t^{3/2} + \alpha\beta^2 d_t + 2\alpha(\alpha^2 - \beta^2)\ln(\alpha + \beta d_t^{1/2}) - \alpha(2\ln(\alpha) + 1)\right] \qquad \text{A10}$$

3. Parabolic: $\mu_z = \alpha + \beta\,[z - (z)^2]$

This parabolic form for the vertical variation of the eddy viscosity was suggested by Roelvink and Reniers (1994), and observed by Cox and Kobayashi (1997) with LDV in a laboratory experiment on regular waves spilling on a rough, plane slope.

$$U(z) = U_r + \frac{F(x)}{\rho\beta\psi}\left[N_1(z) - \frac{N_3}{d_t}\right] + \frac{\bar{\tau}(z)}{\rho\beta\psi}\left[N_2(z) + - \frac{N_4}{d_t}\right] \qquad \text{A11}$$

where

$$N_1(z) = \beta\tanh^{-1}\left(\frac{2\beta z - \beta}{\psi}\right) - \frac{\psi}{2}\ln[\alpha + \beta(z - z^2)] \qquad \text{A12}$$

$$N_2(z) = 2\beta\tanh^{-1}\left(\frac{2\beta z - \beta}{\psi}\right) \qquad \text{A13}$$

$$N_3 = \psi d_t - (2\alpha + \beta d_t)\tanh^{-1}\left(\frac{2\beta d_t - \beta}{\psi}\right) - 2\alpha\tanh^{-1}\left(\frac{\beta}{\psi}\right) - \frac{\psi d_t}{2}\ln[\alpha + \beta(d_t - d_t^2)] + N_4 \qquad \text{A14}$$

$$N_4 = (2\beta d_t - \beta)\tanh^{-1}\left(\frac{2\beta d_t - \beta}{\psi}\right) - \beta\tanh^{-1}\left(\frac{\beta}{\psi}\right) - \frac{\psi}{2}\ln\left[\frac{\alpha + \beta(d_t - d_t^2)}{\alpha}\right] \qquad \text{A15}$$

$$\psi = \sqrt{\beta^2 + 4\alpha\beta} \qquad \text{A16}$$

In the above listed solutions, the eddy viscosity (μ_z) is a function of two non-dimensional parameters (α and β). The value of the eddy viscosity at the bottom ($\mu_{z=0}$) is given by α, which in this study is assumed to be represented by the molecular viscosity, due to the lack of reliable measurements of currents close to the bed under field conditions to better constraint this value. Although, the solution within the middle layer does not significantly change if the assumed constant eddy viscosity within the bottom boundary layer (Putrevu and Svendsen, 1993) is used for α.

ACKNOWLEDGMENTS

This research was funded by the Office of Naval Research, Coastal Sciences Program, under contract N00114-95-AF-002. The authors wish to express their appreciation to all those who participated in the DUCK94 experiment, particularly the staff of the U.S. Army Field Research Facility under the direction of B. Birkemeier. In addition, special appreciation is expressed to Jim Stockel and R. Wyland, Naval Postgraduate School, for their role in acquisition and processing of wave and current data.

REFERENCES

Bagnold, R.A., Beach formation by waves; some model experiments in a wave tank, *J. Inst. Civ. Eng*, 15, 27-40, 1940.

Battjes, J.A., Modelling of turbulence in the surf zone, *Proceedings of the Symposium on Modelling Techniques, ASCE*, Vol. 2, 1050-1061, 1975.

Battjes, J.A., R.J. Sobey, and M.J.F. Stive, Nearshore circulation, in *The Sea*, vol. 9, John Wiley-Interscience, pp. 467-493, 1990.

Cox, D.T., and N. Kobayashi, Undertow profiles in the bottom boundary layer under breaking waves, *Proceedings 25th Coastal Engineering Conference, ASCE*, (in press), 1997.

Dally, W.R., A numerical model for beach profile evolution, M.S. thesis, Dep. of Civil Eng., Univ. of Del., Newark, 1980.

Dally, W.R., and R.G. Dean, Suspended sediment transport and beach profile evolution, *Journal of Waterw. Port Coastal and Ocean Eng.*, 110, 1, 15-33, 1984.

Dally, W.R., and C.A. Brown, A modeling investigation of the breaking wave roller with application to cross-shore currents, *Journal of Geophysical Research*, 100 (C12), 24,873-24,883, 1995.

Dean, R.G., Evaluation and development of water wave theories for engineering applications, *Spec. Rep.* 1, U.S. Army Waterw. Exp. Stn., Vicksburg, Miss., 1974.

Deigaard, R., P. Justesen, and J. Fredsoe, Modeling of undertow by a one-equation turbulence model, *Coastal Engineering*, 15, 431-458, 1991.

Deigaard, R., A note on the three-dimensional shear stress distribution in a surf zone, *Coastal*

Engineering, 20, 157-171, 1993.

Dyhr-Nielsen, M., and T. Sørensen, Sand transport phenomena on coasts with bars, *Proceedings 12th Coastal Engineering Conference, ASCE*, 855-866, 1970.

Elgar, S., R.T. Guza, B. Raubenheimer, T.H.C. Herbers, and E.L. Gallagher, Spectral evolution of shoaling and breaking waves on a barred beach, *Journal of Geophysical Research* (in review), 1997.

Gallagher, E. L., S. Elgar, and R.T. Guza, Observations of sand bar evolution on a natural beach, *Journal of Geophysical Research* (accepted), 1997.

Garcez Faria, A.F., E.B.Thornton, T.P. Stanton, C.V. Soares, and T.C. Lippmann, Vertical profiles of longshore currents and related bed shear stress and bottom roughness, *Journal of Geophysical Research* (accepted), 1997 [Chapter 1].

Haines, J.W., and A.H. Sallenger Jr., Vertical structure of mean cross-shore currents across a barred surf zone, *Journal of Geophysical Research*, 99 (C7), 14,223-14,242, 1994.

Iwagaki, Y., Hyperbolic waves and their shoaling, *Proceedings 11th Coastal Engineering Conference, ASCE*, 124-144, 1968.

King, F.C.K., and J.T. Kirby, Observation of undertow and turbulence in a laboratory surf zone, *Coastal Engineering*, 24, 51-80, 1994.

Korteweg, D.J., and G. De Vries, On the change of form of long waves advancing in a rectangular canal, and on a new type of long stationary waves, *Phil. Mag.*, 39, 5, 422-443, 1895.

Laitone, E.V., The second approximation to cnoidal and solitary waves, *Journal of Fluid Mechanics*, 9, 430-444, 1961.

Laitone, E.V., Limiting conditions for cnoidal and Stokes' waves, *Journal of Geophysical Research*, 67, 1555-1564, 1962.

Lippmann, T.C., and R.A. Holman, Phase speeds and angle of breaking waves measured with video techniques, *Proc. Coastal Sediments 91, ASCE,* 542-556, 1991.

Lippmann, T.C., A.H. Brookins, and E.B. Thornton, Wave energy transformation on natural profiles, *Coastal Engineering*, 27, 1-20, 1996.

Lippmann, T.C., and E.B.Thornton, The spatial distribution of wave breaking on a barred beach, *Journal of Geophysical Research* (in review), 1997.

Longuet-Higgins, M.S., and R.W. Stewart, Radiation stresses in water waves: A physical discussion, with applications, *Deep Sea Res.*, 11, 529-562, 1964.

Masselink, G., and K.P. Black, Magnitude and cross-shore distribution of bed return flow measured on natural beaches, *Coastal Engineering*, 25, 165-190, 1995.

Nadaoka, K., and T. Kondoh, Laboratory measurements of velocity field structure in the surf zone by LDV, *Coastal Engineering Jpn.*, 25, 125-145, 1982.

Nadaoka, K., M. Hino, and Y. Koyano, Structure of the turbulent flow field under breaking waves in the surf zone, *Journal of Fluid Mechanics*, 204, 359-387, 1989.

Okayasu, A., Shibayama, T., and K. Horikawa, Vertical variation of undertow in surf zone, *Proceedings 21st Coastal Engineering Conference, ASCE*, 478-491, 1988.

Putrevu, U. and I.A. Svendsen, Wave induced nearshore currents: a study of the forcing, mixing and stability characteristics. *Research Report* No. CACR-91-11, Center for Applied Research, University of Delaware, 1991.

Putrevu, U. and I.A. Svendsen, Vertical structure of the undertow outside the surf zone,

Journal of Geophysical Research, 98(C12), 22707-22716, 1993.

Rivero, F.J. and A.S. Arcilla, On the vertical distribution of $<\tilde{u}\tilde{w}>$, *Coastal Engineering*, 25, 137-152, 1995.

Roelvink, J.A., and A.J.H.M. Reniers, Upgrading of a quasi-3D hydrodynamic model, *Book of abstracts of the Mast-II overall workshop*, Gregynog, UK, 1994.

Sallenger, A.H., Jr., P. Howard, C. Fletcher, and P. Howd, A system for measuring bottom profile, waves and currents in the high-energy nearshore environment, *Marine Geology*, 64, 237-257, 1983.

Smith, J.K., Svendsen, I.A., and U. Putrevu, Vertical structure of the nearshore current at DELILAH: measured and modeled, *Proceedings 23rd Coastal Engineering Conference, ASCE*, 478-491, 1992.

Stive, M.J.F., and H.G. Wind, A study of radiation stress and set-up in the nearshore region, *Coastal Engineering*, 6, 1-25, 1982.

Stive, M.J.F., and H.G. Wind, Cross-shore mean flow in the surf zone, *Coastal Engineering*, 10, 325-340, 1986.

Stive, M.J., and H.J. De Vriend, Shear stress and mean flow in shoaling and breaking waves, *Proceedings 24th Coastal Engineering Conference, ASCE*, 594-608, 1994.

Svendsen, I.A., Cnoidal waves over a gently sloping bottom, PhD dissertation, Institute of Hydrodynamics and Hydraulic Engineering, Technical University of Denmark, 1974.

Svendsen, I.A., Mass flux and undertow in a surf zone, *Coastal Engineering*, 8, 347-365, 1984.

Svendsen, I.A., H.A. Schäffer, and J. Buhr-Hansen, The interaction between the undertow

and the boundary layer flow on a beach, *Journal of Geophysical Research*, 92(C11), 11845-11856, 1987.

Svendsen, I.A., and J. Buhr Hansen, Cross-shore currents in surf-zone modelling, *Coastal Engineering*, 12, 23-42, 1988.

Thornton, E.B., Variation of longshore currents across the surf zone, *Proceedings 12th Coastal Engineering Conference, ASCE*, 291-308, 1970.

Thornton, E.B., and R.T. Guza, Energy saturation and phase speeds measured on a natural beach, *Journal of Geophysical Research*, 87(C12), 9499-9508, 1982.

Thornton, E.B., and R.T. Guza, Transformation of wave height distribution, *Journal of Geophysical Research*, 84(C8), 4931-4938, 1983.

Thornton, E.B., J.L. Swayne, and J.R. Dingler, Small-scale morphology related to waves and currents across the surf zone, *Marine Geology* (accepted), 1997.

Whitford, D.J., Wind and wave forcing of longshore currents across a barred beach, Ph.D. Thesis, Naval Postgraduate School, Monterey, CA, 1988.

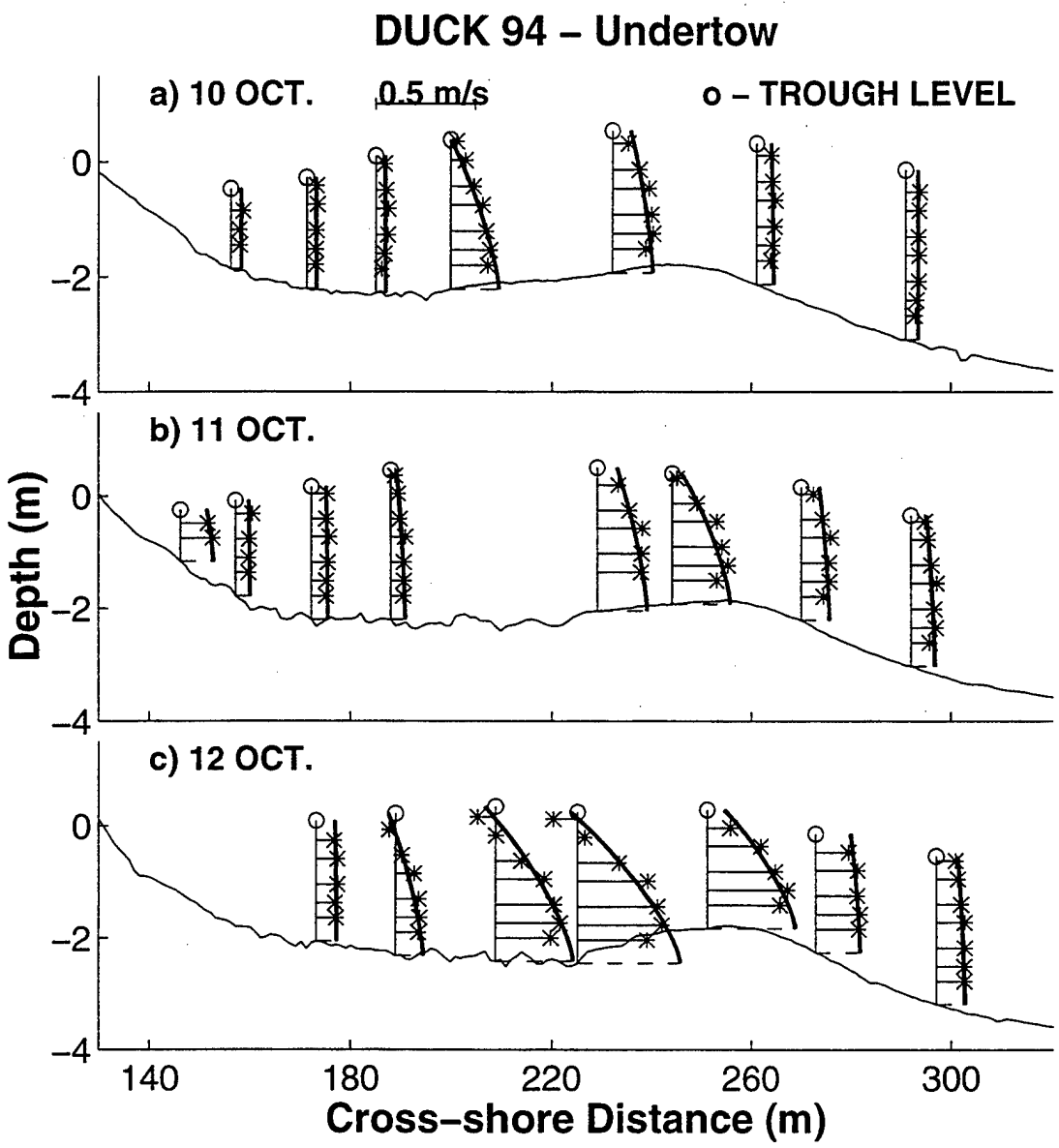

Figure 1. Measured (*) and *rms* best fit model predicted (Equation 10) vertical profiles of mean cross-shore return currents (heavy line) superposed on bottom profile with meantrough level indicated by (o) for the entire period being examined.

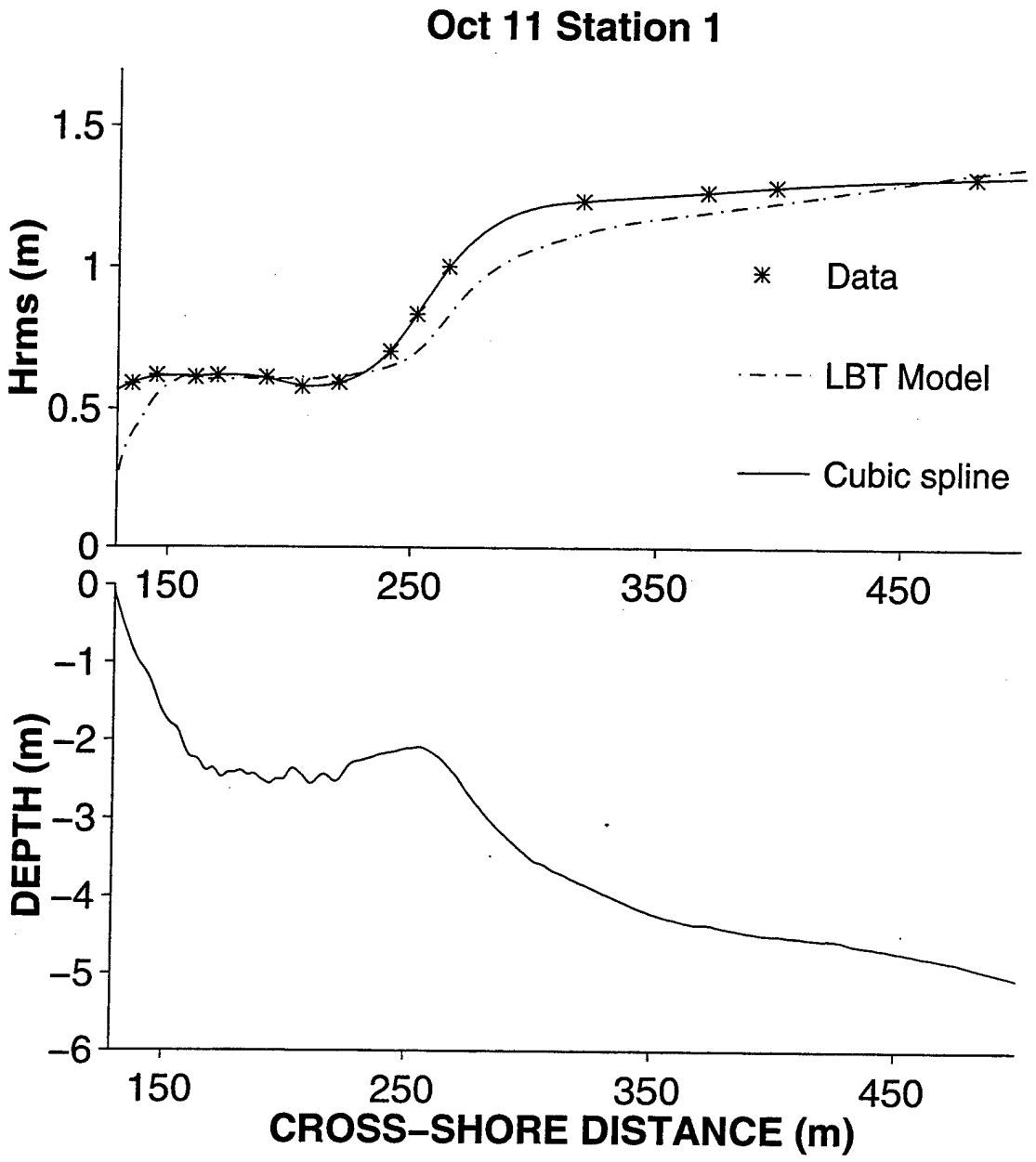

Figure 2. LBT "worst case" model prediction of H_{rms} versus cross-shore distance (dash-dotted line) compared with cubic spline interpolation (solid line) of observations (*), first run of 11 Oct. (upper panel). The bottom profile is shown in the lower panel.

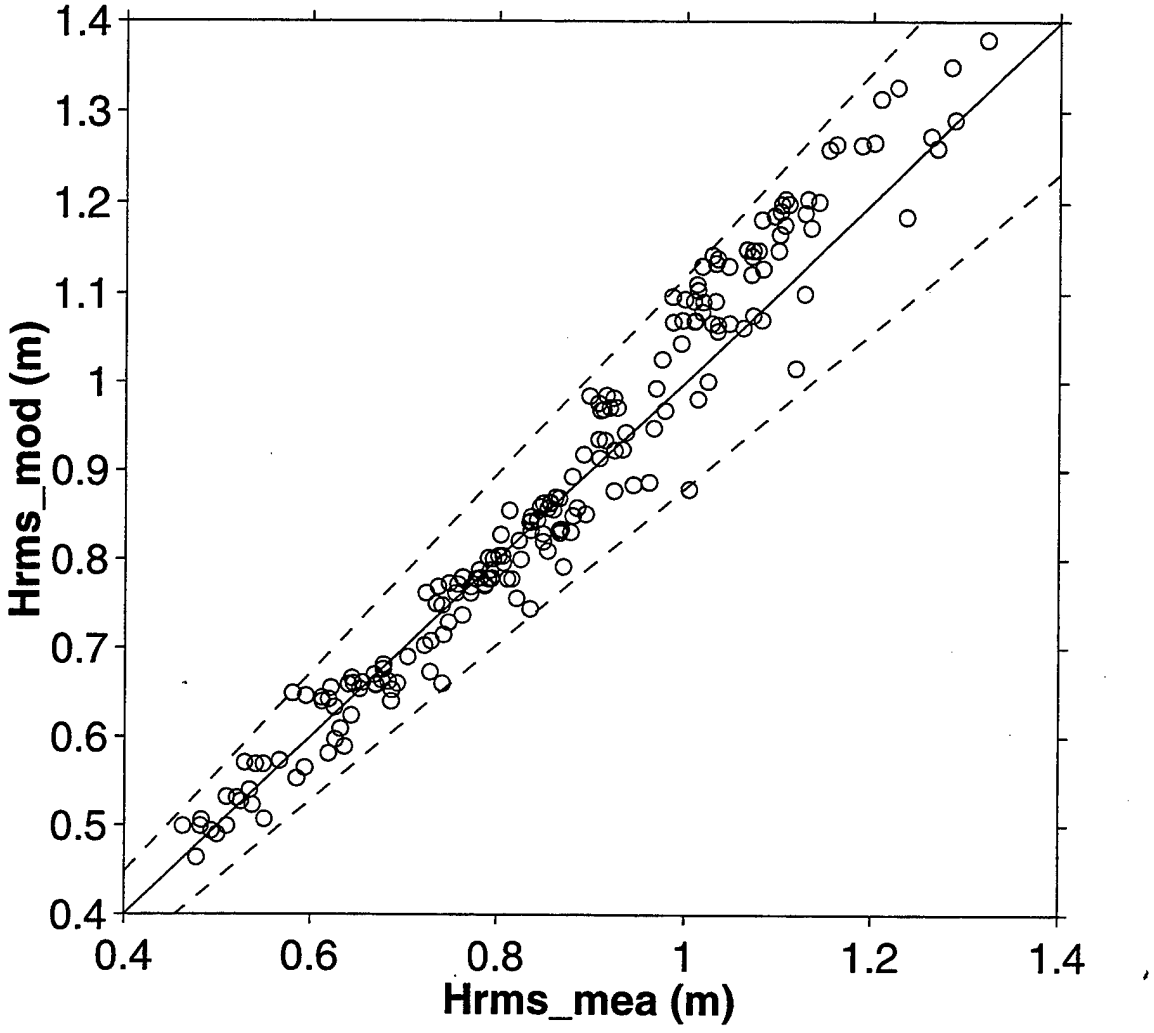

Figure 3. Predicted (LBT model) versus observed H_{rms}. The solid line represents perfect agreement and the dashed lines the ± 10 percent error bounds.

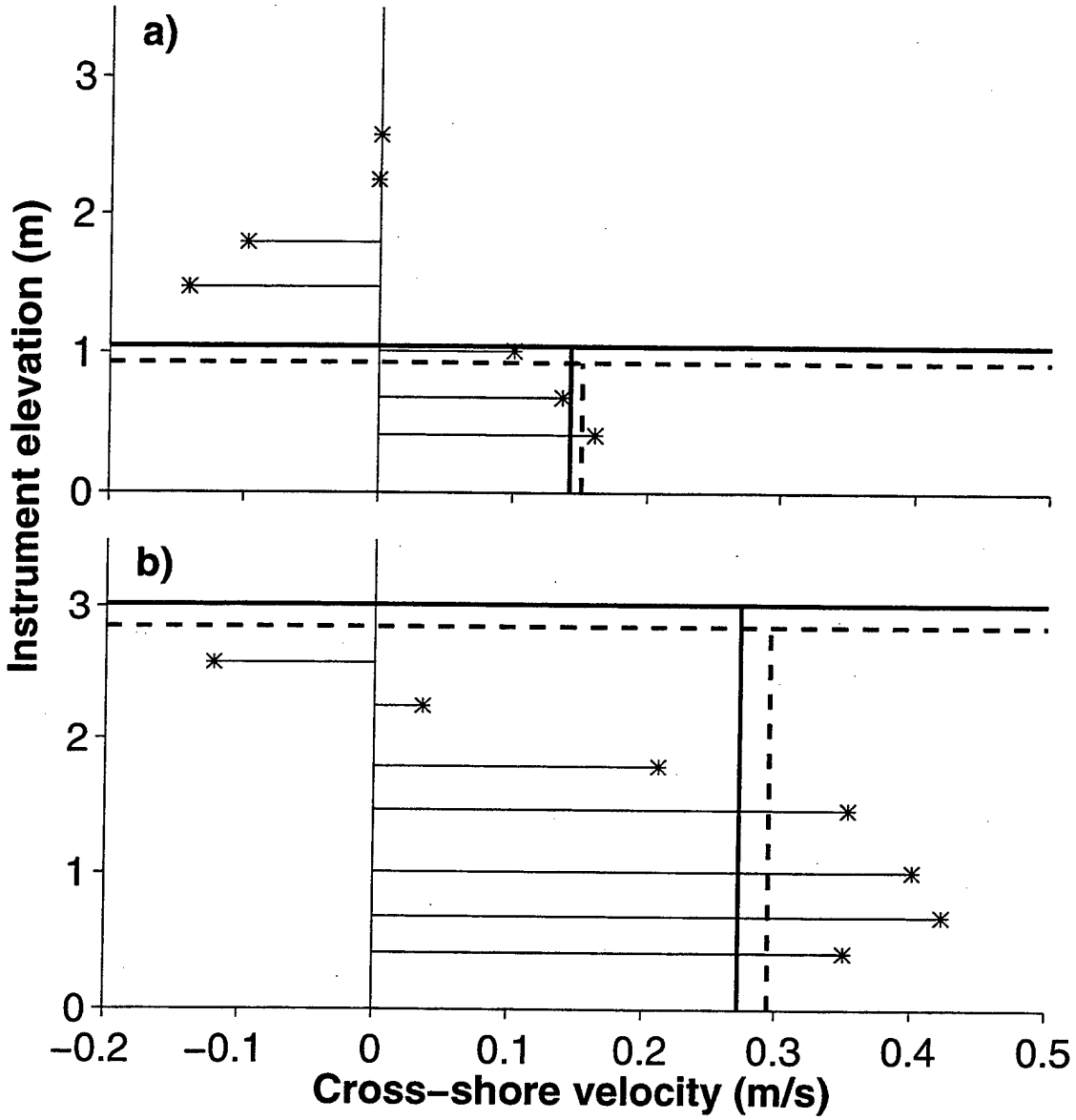

Figure 4. Observed vertical profiles of mean cross-shore currents (*) for the eighth run of 11 Oct. (a) and for the fourth run of 12 Oct. (b). Horizontal heavy lines represent mean trough level (h_t) and vertical heavy lines the depth averaged undertow (U_r) calculated using linear (dashed) and cnoidal (solid) wave theories.

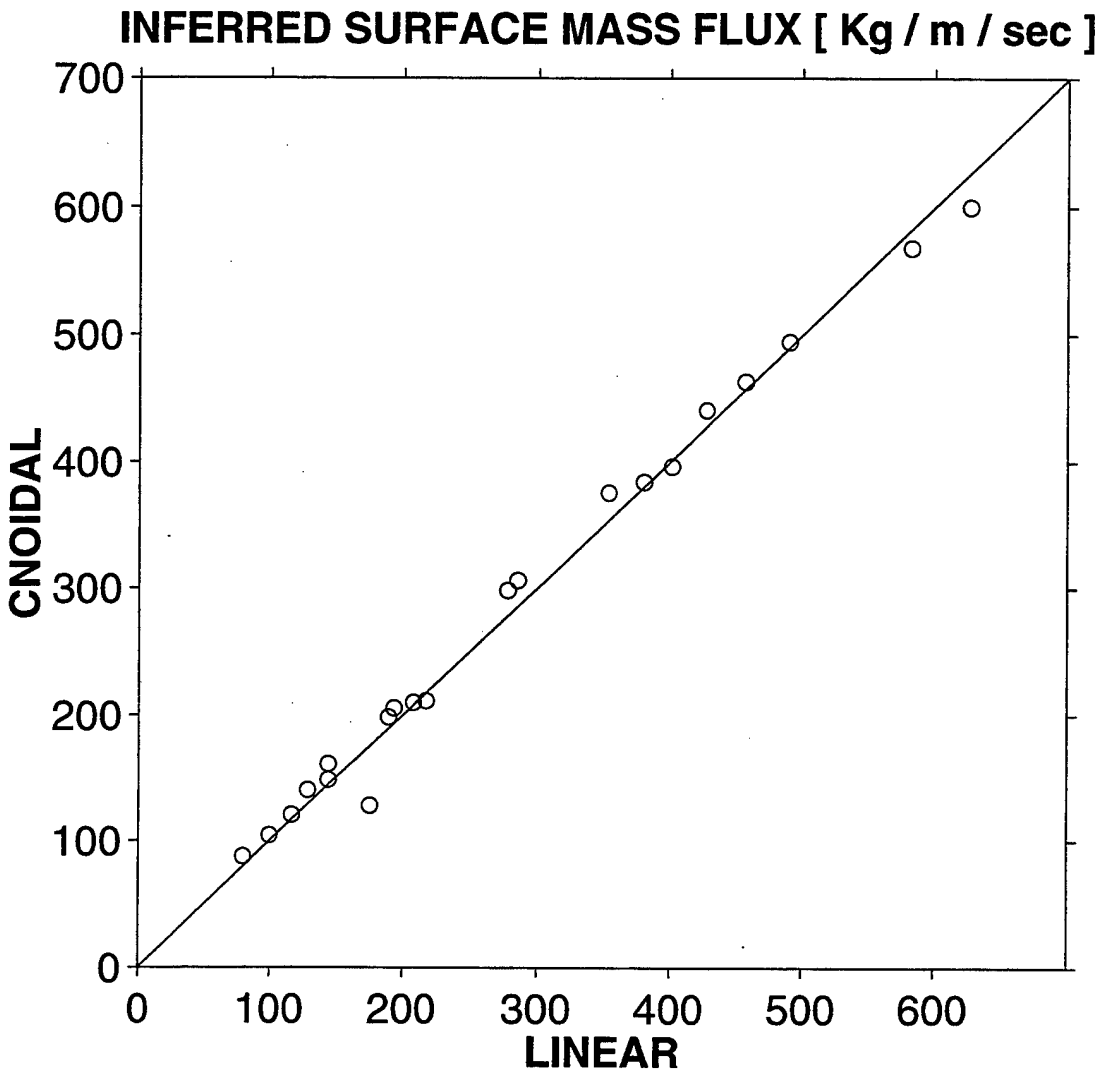

Figure 5. Comparison between inferred surface mass flux ($\rho\, U_{obs}\, h_t$) from mean velocity measurements using linear and cnoidal wave theories to estimate the mean trough level, h_t.

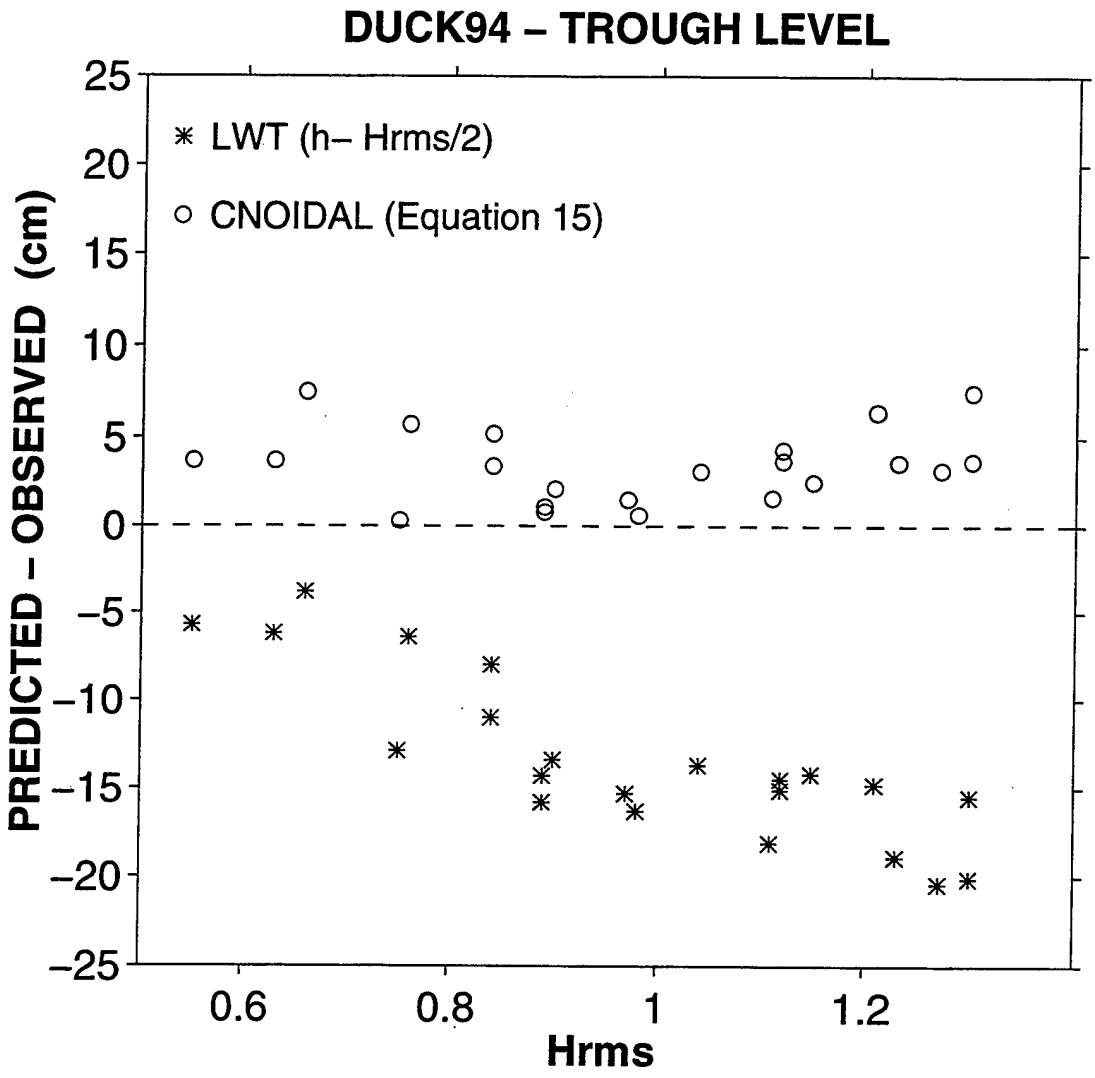

Figure 6. (Predicted - Observed) mean trough level, h_t, versus observed H_{rms}. Positive values represent over prediction.

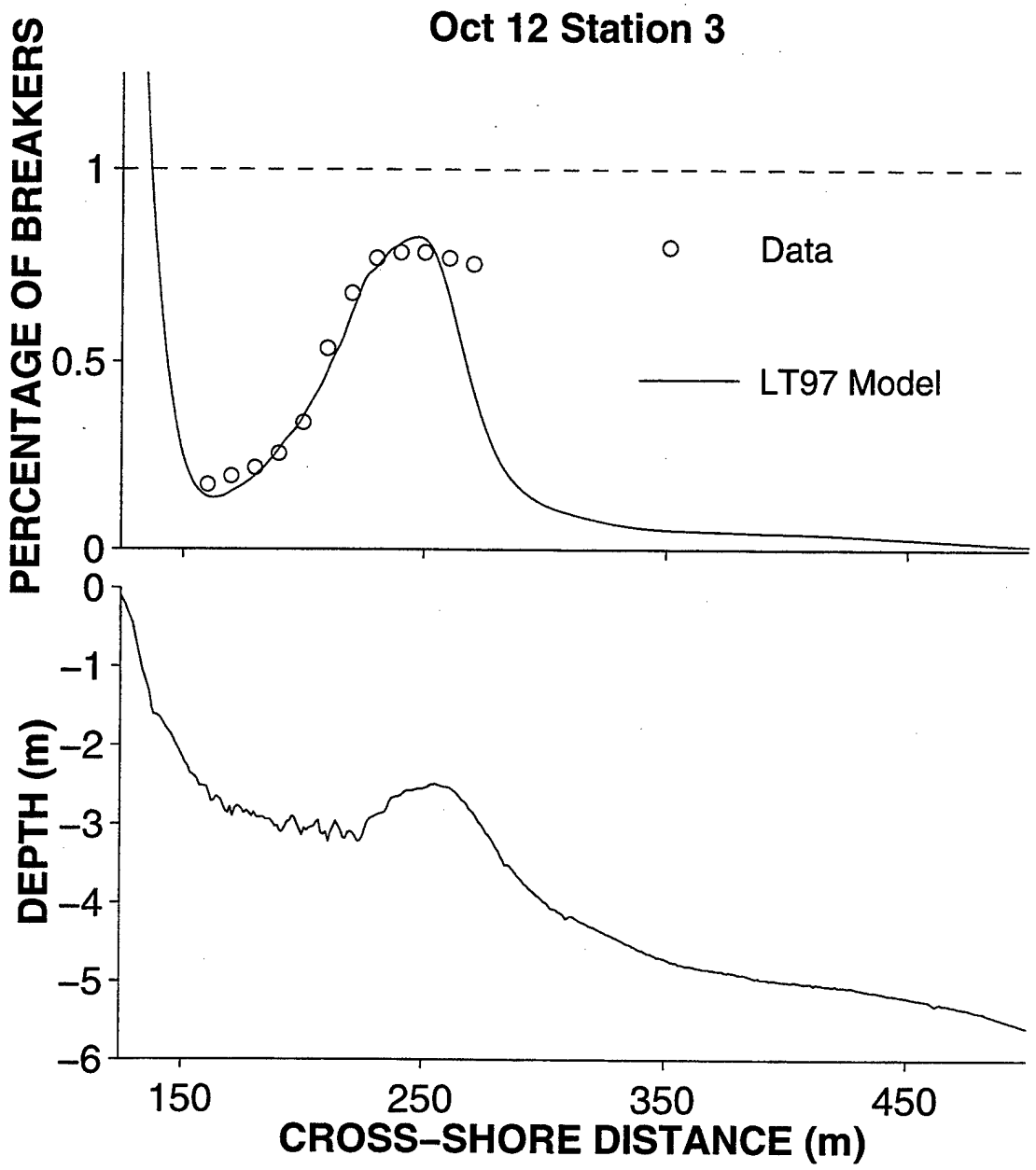

Figure 7. Lippmann and Thornton (1997) model predictions (solid line) and observed (o) percentage of waves breaking versus cross-shore distance for the third run of 12 Oct. (upper panel). The bottom profile is shown in the lower panel.

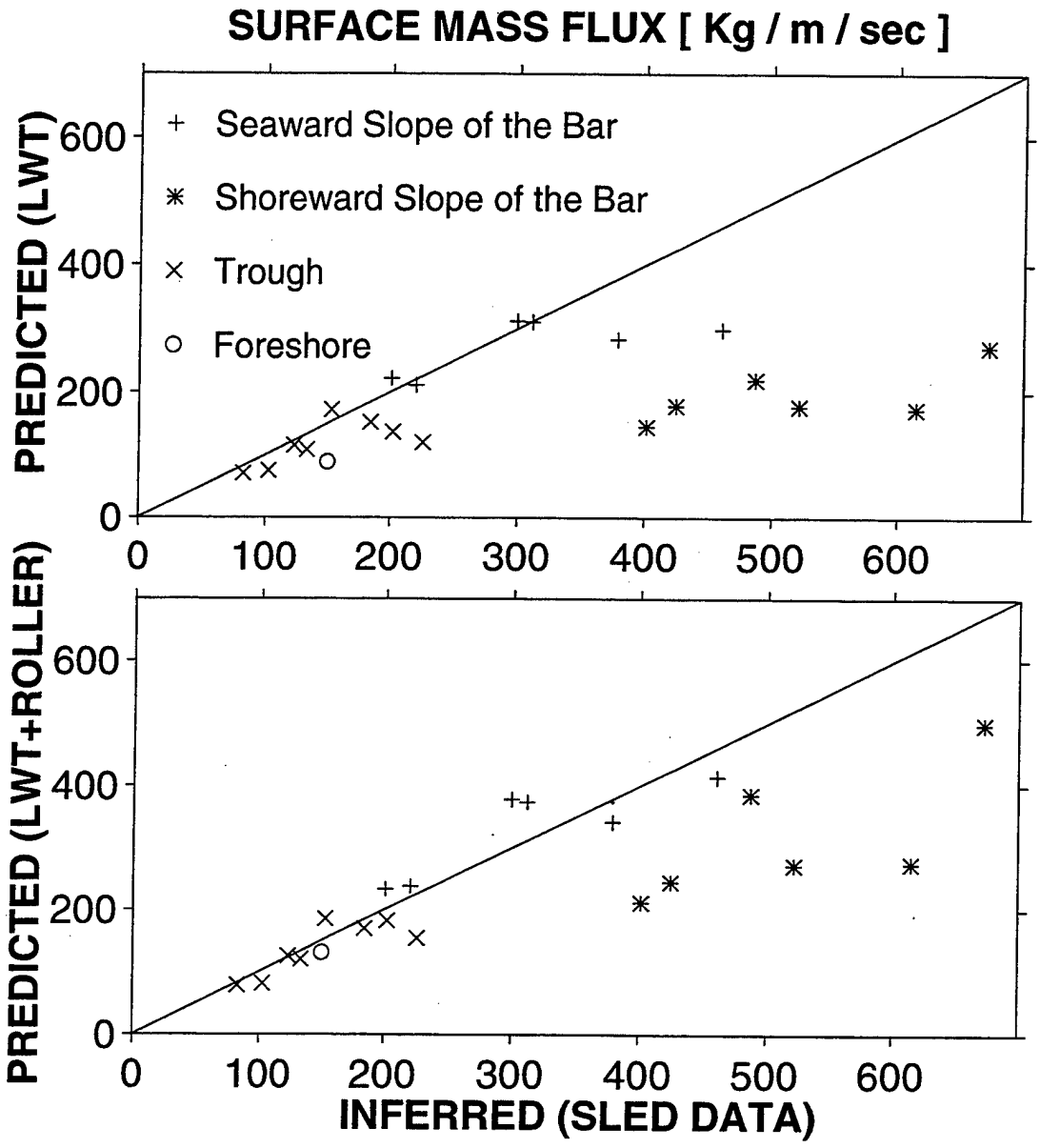

Figure 8. Inferred ($\rho\, U_{obs}\, h_t$) versus linear wave theory predicted surface mass flux (q_w, only) for the entire ensemble of 22 runs (upper panel). The lower panel shows the effect of including contributions from wave rollers ($q_w + q_r$).

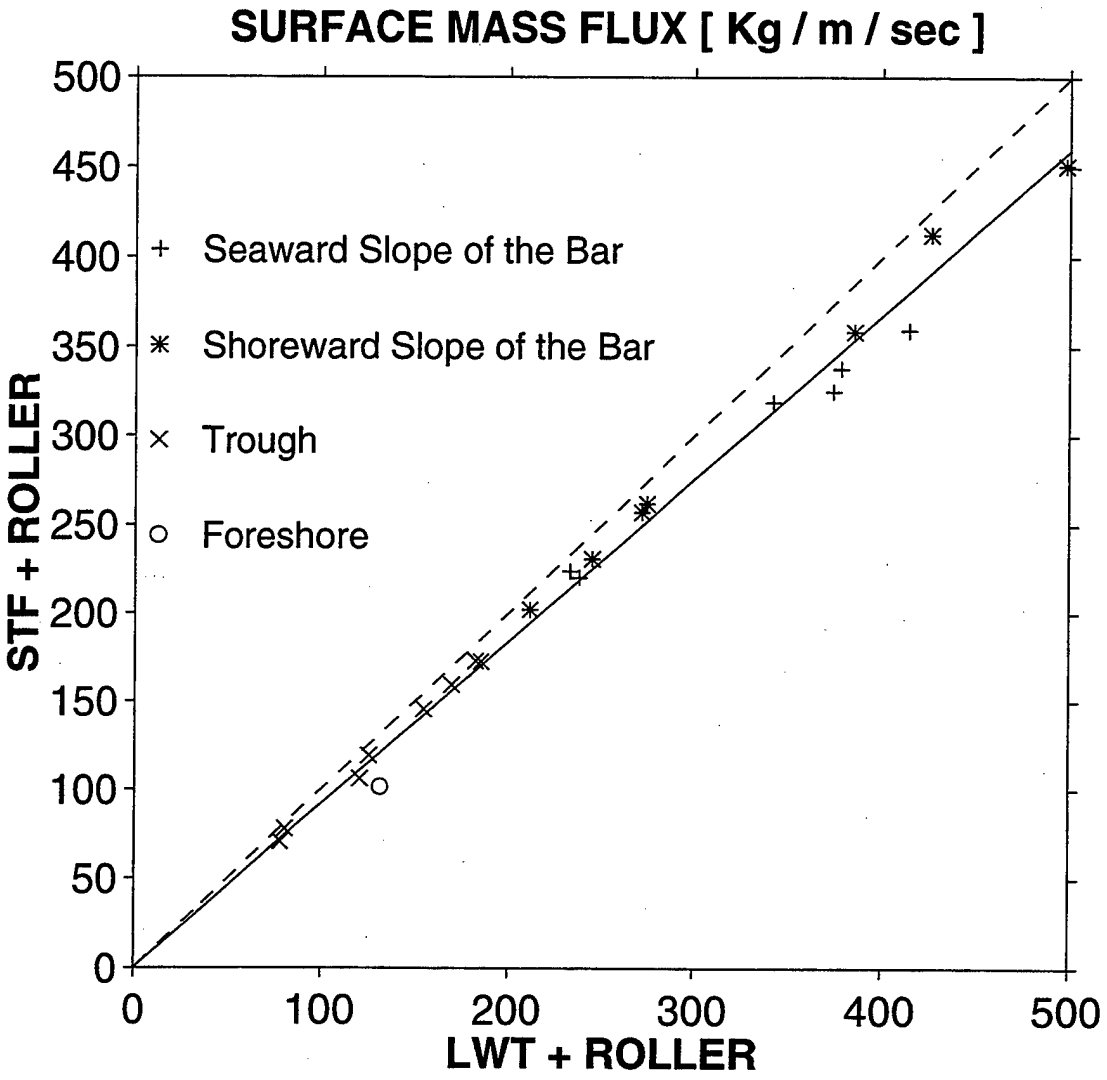

Figure 9. Comparison between predicted surface mass flux ($q_w + q_r$) given by linear and streamfunction (Dean, 1974) wave theories. The dashed line represents perfect agreement, and the solid line represents a linear regression with a slope of 0.92.

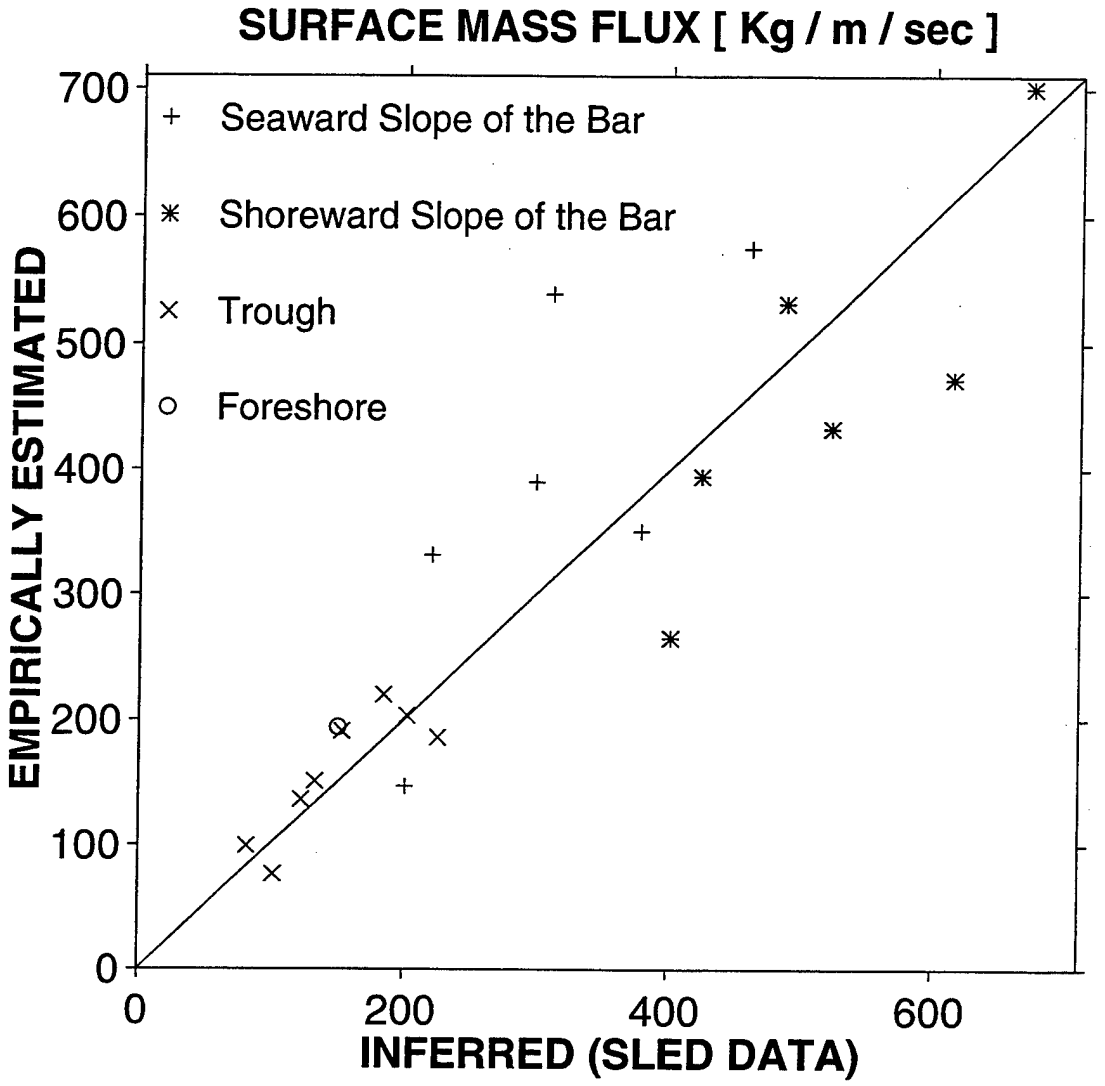

Figure 10. Inferred versus empirically estimated (Equation 16) surface mass flux. The line represents perfect agreement.

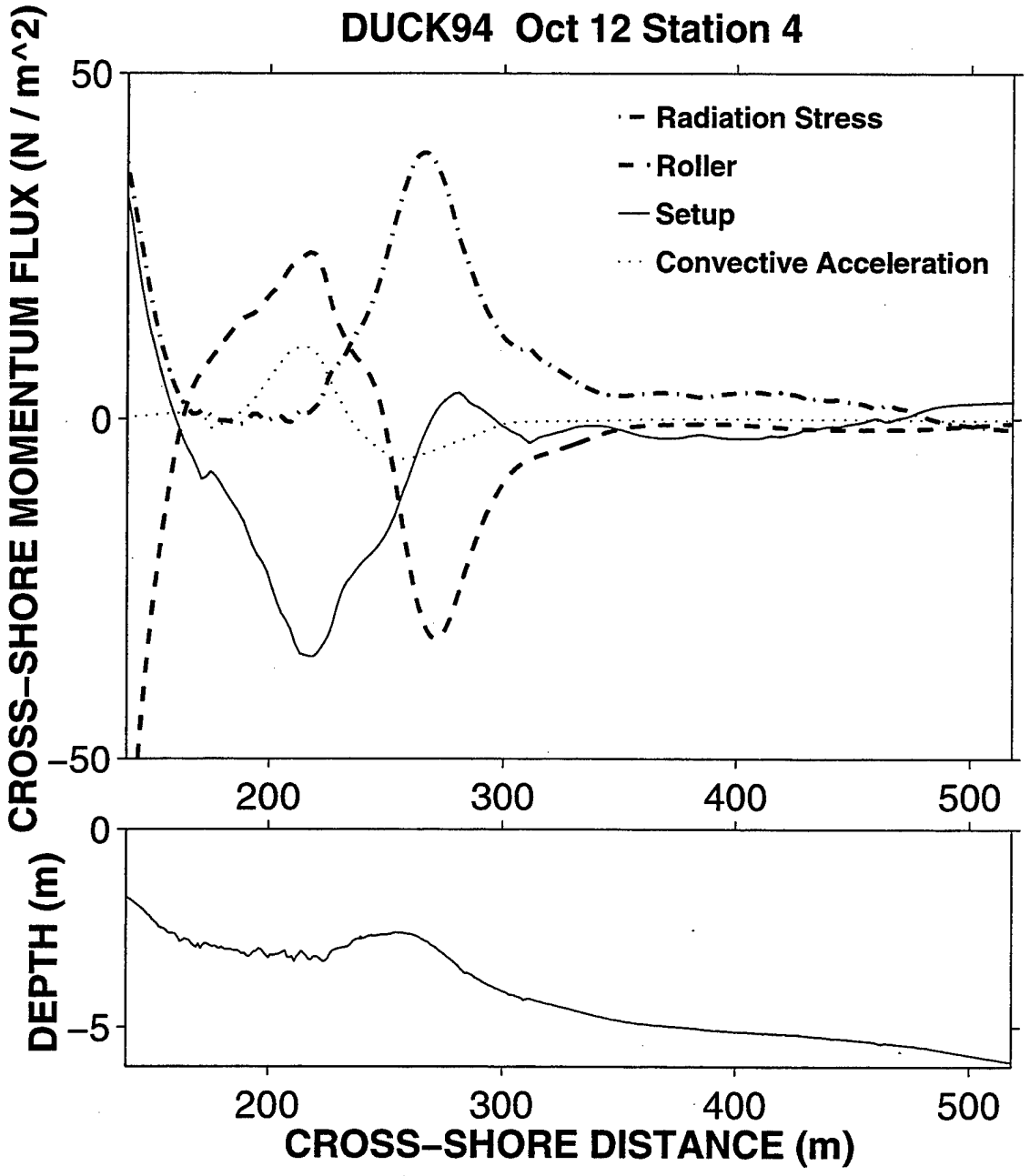

Figure 11. Terms of the momentum balance equation (12) versus cross-shore distance for the fourth run of 12 Oct. (upper panel). The bottom profile is shown in the lower panel.

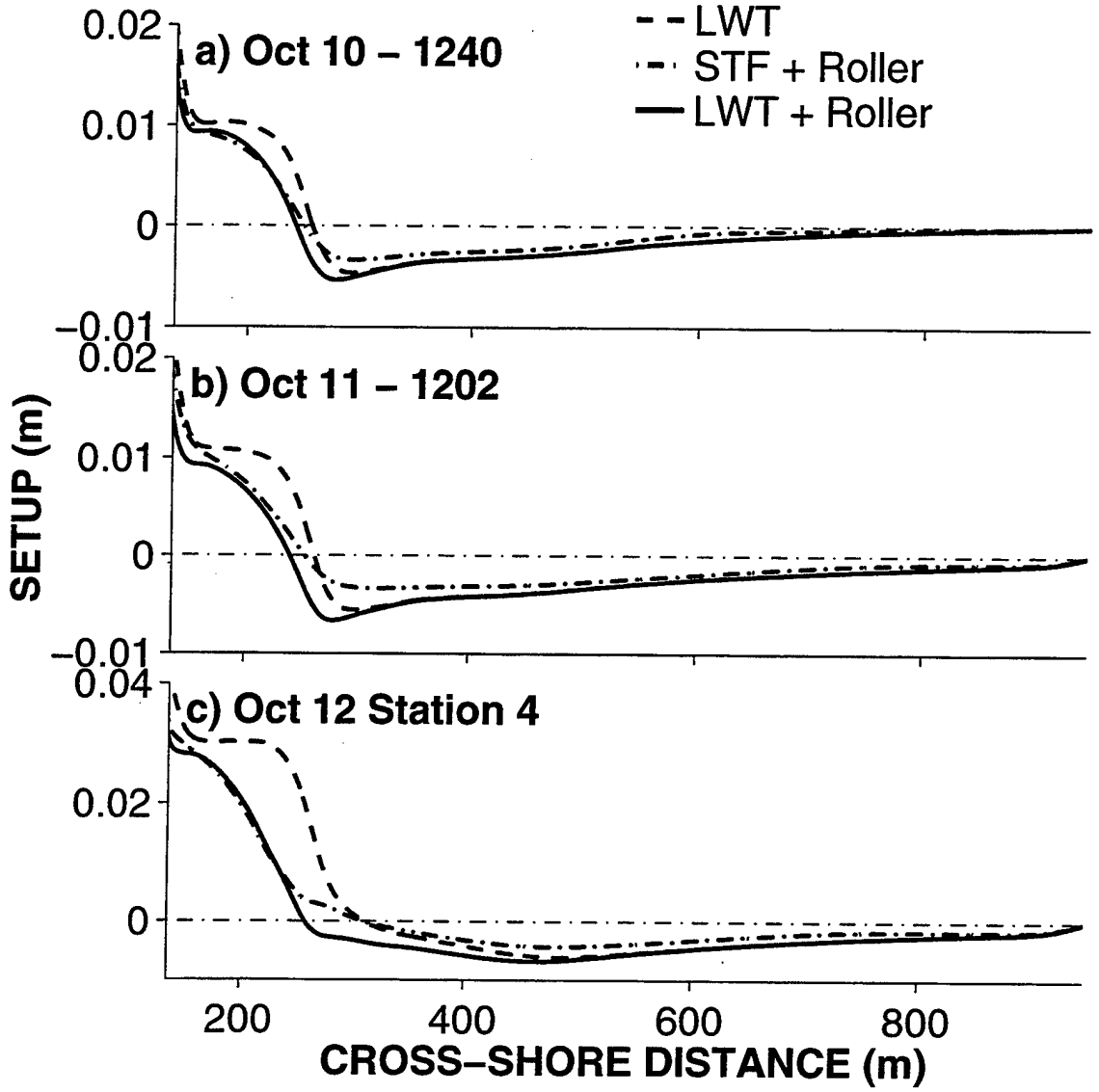

Figure 12. Setup calculated using linear wave theory (dashed line), streamfunction theory with roller (dash-dotted line) and linear wave theory with roller (solid line) versus cross-shore distance for the fourth run of each day.

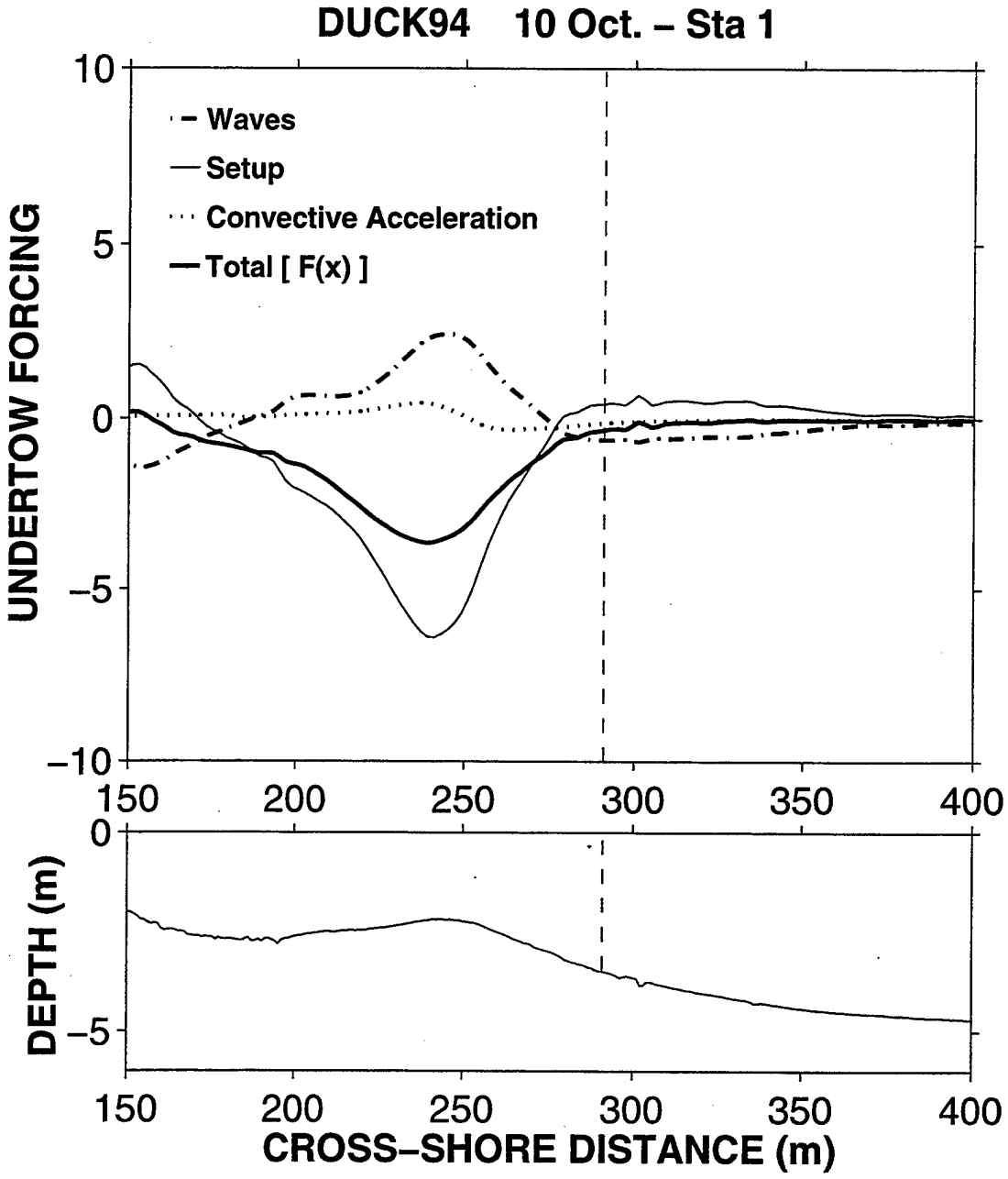

Figure 13. Undertow dynamical forcing terms (6) versus cross-shore distance for the first run of 10 Oct. (upper panel). The bottom profile is shown in the lower panel. The vertical dashed line indicates the cross-shore position occupied by the sled.

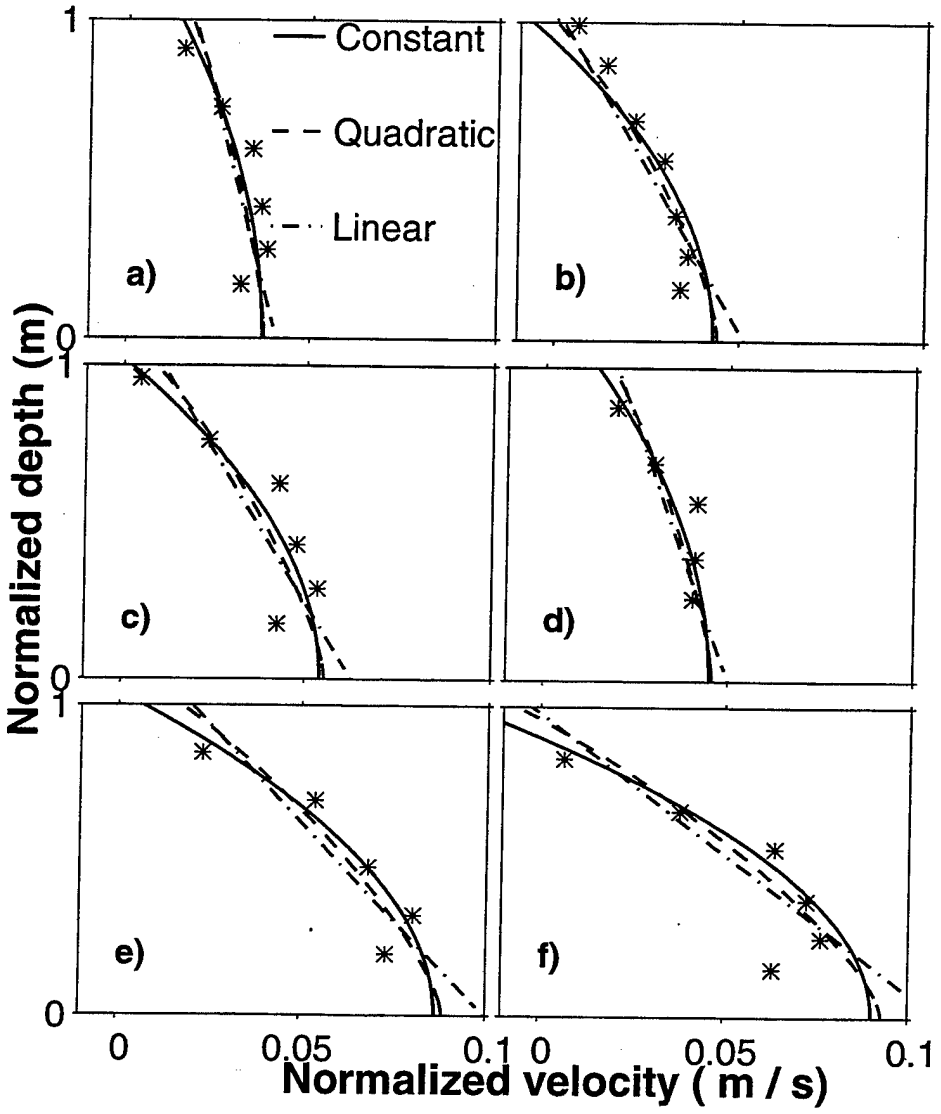

Figure 14. Comparison between measured undertow (*) and predictions using different formulations for the vertical variation of the eddy viscosity (constant = solid line; linear = dash-dotted line; and parabolic = dashed line) for the third and fourth runs of Oct. 10 (a, and b), Oct. 11 (c, and d), and Oct. 12 (e, and f).

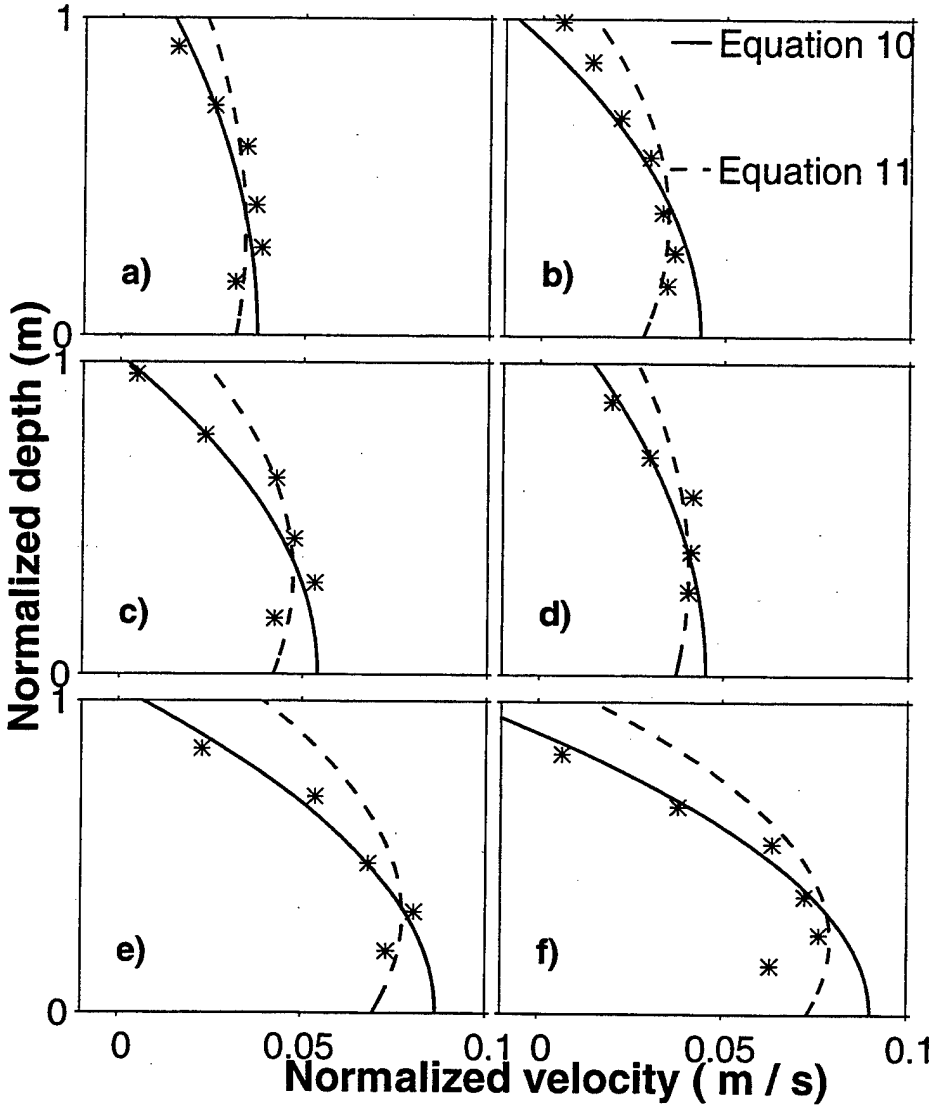

Figure 15. Same as Figure 14, but comparing predictions given by Equation 10 (solid line) and Equation 11 (dashed line).

Table 1. Best fit model parameters

Model:		Wave Transformation (LBT 86)			Roller (LT 97)		
Day	Run	σ ($^{\circ}$)	γ	error (%)	B	ψ	error (%)
10	1	10	0.33	2.3	0.70	1.3	2.0
10	2	10	0.32	4.9	0.60	1.6	3.8
10	3	10	0.32	4.5	0.60	1.2	3.5
10	4	10	0.32	4.9	0.70	1.1	5.2
10	5	10	0.32	4.1	0.65	1.7	4.2
10	6	10	0.31	4.1	0.75	1.7	4.7
10	7	10	0.31	5.0	0.75	1.9	4.3
11	1	10	0.32	7.0	0.85	1.4	7.5
11	2	10	0.33	4.7	0.65	1.7	6.5
11	3	10	0.33	4.3	0.70	1.1	7.3
11	4	10	0.33	3.9	0.65	1.2	5.7
11	5	10	0.32	4.8	0.60	1.7	3.8
11	6	10	0.32	4.1	0.85	1.2	7.3
11	7	10	0.32	5.5	0.70	1.9	3.4
11	8	10	0.31	6.5	0.85	1.8	5.0
12	1	10	0.34	5.9	0.90	1.3	3.8
12	2	10	0.33	5.1	0.80	1.6	7.8
12	3	10	0.34	5.2	0.80	1.3	9.0
12	4	10	0.34	4.1	0.80	1.1	8.2
12	5	10	0.34	4.6	0.75	1.3	7.8
12	6	10	0.35	5.8	0.65	1.7	5.3
12	7	10	0.34	5.8	0.95	1.4	7.0
	mean			4.9			5.6

Table 2. Wave conditions and undertow measurements

Day	Run	*rms* wave height H_o (m)	peak frequency f_p (Hz)	mean direction α_o (°)	tide (m)	depth-averaged undertow U_{obs} (m s^{-1})	*rms* best fit eddy viscosity μ (m^2 s^{-1})
10	1	1.70	0.171	44	0.40	0.06	0.500
10	2	1.81	0.162	38	0.79	0.08	0.500
10	3	1.81	0.162	38	0.98	0.16	0.058
10	4	1.68	0.152	36	0.77	0.14	0.017
10	5	1.68	0.152	36	0.44	0.05	0.500
10	6	1.44	0.162	24	0.04	0.05	0.500
10	7	1.44	0.162	24	-0.12	0.05	0.500
11	1	2.11	0.142	18	0.22	0.10	0.240
11	2	1.88	0.142	16	0.64	0.12	0.250
11	3	1.75	0.142	17	0.86	0.19	0.033
11	4	1.70	0.142	18	0.92	0.19	0.049
11	5	1.70	0.142	18	0.85	0.05	0.063
11	6	1.70	0.142	18	0.62	0.08	0.500
11	7	1.60	0.142	16	0.32	0.07	0.500
11	8	1.60	0.142	16	0.03	0.15	0.140
12	1	1.91	0.162	18	0.05	0.13	0.130
12	2	2.29	0.142	12	0.34	0.20	0.240
12	3	2.29	0.142	12	0.71	0.30	0.032
12	4	2.32	0.142	10	0.83	0.30	0.036
12	5	2.32	0.142	10	0.84	0.20	0.035
12	6	2.35	0.142	10	0.69	0.07	0.020
12	7	2.35	0.142	10	0.42	0.10	0.500

H_o, f_p, and α_o were measures in 8m depth (FRF linear array)

IV. A QUASI-3D MODEL FOR LONGSHORE CURRENTS

(This chapter consists of work to be submitted

to the *Journal of Geophysical Research*)

A QUASI-3D MODEL FOR LONGSHORE CURRENTS

A.F. Garcez Faria, E.B. Thornton, T.C. Lippmann[1], T.P. Stanton, R.T.Guza[1], and S. Elgar[2]

Naval Postgraduate School, Monterey, California 93940

ABSTRACT

The spatial distribution of mean longshore currents over a barred beach is examined by comparing predictions given by a quasi three-dimension model presented here with data acquired during the nearshore dynamics experiment DUCK94 at Duck, North Carolina. The model includes forcing due to breaking waves described using the roller concept (Lippmann and Thornton, 1997), alongshore wind stress, cross-shore advection of mean momentum of the alongshore current, and a full non linear bottom shear stress with a variable bed shear stress coefficient, C_f, constrained by observations (Garcez Faria *et al.*, 1997a [Chapter 1]). Contributions from the alongshore wind stress are mostly evident offshore and over the inner trough of the sand bar due to the relative increase in the wind force to wave force ratio as wave forcing decreases over these regions. The advection of the momentum of the longshore current by mean cross-shore currents is shown to improve the agreement with observations within the surf zone, O[10 percent]. The use of a non linear bed shear stress formulation with a variable C_f is shown to improve model/data comparison, O[20 percent], compared to the use of a constant C_f. The largest overall improvement with observations is obtained by incorporating the roller contribution, O[50 percent].

---

[1]Scripps Institution of Oceanography, La Jolla, California 92903

[2]Washington State University, Pullman, WA 99164-2752

INTRODUCTION

The longshore current maximum observed in the trough of a barred beach during the nearshore dynamics experiments DELILAH and DUCK94 at Duck, North Carolina, is not predicted by present theory. The simplest longshore current models balance cross-shore changes in the alongshore wave momentum (radiation stress) with the alongshore bottom shear stress. Waves break over the bar reform in the trough and again break on the foreshore. Wave breaking results in changes in the radiation stress predicting two jets, one over the bar and the other at the foreshore, which does not agree with the observed current maximum in the trough. An example of the measured and modeled wave height and longshore current distributions using DUCK94 data are shown in Fig. 1. The predictions suggest that a transfer of momentum is required to account for the current deficit in the trough.

A number of mechanisms have been proposed to mix momentum laterally into the trough region to drive the longshore current. Traditional turbulent mixing, usually parameterized using classical eddy viscosity concepts associated with the shear of the longshore current (*e.g.*, Bowen, 1969; Longuett-Higgins, 1970; Thornton, 1970), would require up gradient mixing of the longshore current which is not feasible. Battjes (1975) formulated turbulent mixing induced by breaking waves, where the scale of the turbulent mixing is the same order of the wave height or the local depth, which are much too short length scales to explain the observations. Smith *et al* (1993) described wave breaking as rollers that propagate with the wave at the phase speed; they applied a turbulent kinetic energy equation and argued that turbulence was diffused downward into the water column generating an additional alongshore thrust. They applied their formulation to the DELILAH

data and partially explained the momentum deficit in the trough.

Changes in the bottom shear stress due to turbulence being injected from the surface by breaking waves and modifying the vertical profile of the longshore current, which in turn modify the magnitude of the longshore current, were investigated by Church and Thornton (1993). They allow a spatially variable bed shear stress coefficient dependent on the breaking wave induced near bottom turbulence levels. The model predicted cross-shore profiles of the longshore current improved agreement with observation compared with treatments using constant bed shear stress values, but did not completely account for the momentum deficit in the trough.

Instabilities of the longshore current have been identified as a mechanism for turbulent mixing of the longshore current originally suggested by Bowen and Homan, (1989). Dodd and Thornton (1990) showed that if shear instabilities exist, there is an accompanying cross-shore mixing of momentum. Putrevu and Svendsen (1992) carried out a numerical study of shear instabilities over various topography and using an order of magnitude analysis concluded that even a weak shear in the longshore current might be capable of producing significant mixing. Significant shear instabilities of the longshore current have been observed in the field (Oltman-Shay *et al*, 1989). Dodd *et al.* (1997) calibrated the amplitude of the shear instabilities using field measurements, and then calculated the Reynolds' stress associated with the instabilities. They found that the mixing predicted due to shear instabilities to be in qualitative agreement with that required for modeled longshore current profiles to agree with observed profiles.

Putrevu *et al.* (1995), using an order of magnitude analysis, suggested that alongshore

pressure gradients induced by alongshore variation in bottom topography could contribute substantially to the forcing for longshore currents. Reniers *et al.* (1997) examined this effect using DELILAH data and found that even a relatively small alongshore pressure gradient acting in the same direction as the wave forcing over the trough of the bar, can have a significant effect on the longshore current distribution.

The advection of the momentum of the longshore current by mean cross-shore currents as a source of momentum mixing was suggested by Putrevu and Svendsen (1993). The longshore current is strongest toward the surface and decreases to zero at the bottom. The cross-shore mean current has an onshore transport in the wave crest/trough region and an offshore transport below (undertow). Svendsen and Putrevu (1994) showed that the net interaction could induce significant mixing of the momentum of the mean currents.

The objective of this paper is to formulate a simplified quasi-three-dimension model to describe longshore currents assuming that the bottom profile has straight and parallel contours. Included in the formulation are forcing due to breaking waves described by a roller (Lippmann and Thornton, 1997) and alongshore wind shear stress, cross-shore advection of mean momentum of the alongshore current by the shear of the mean cross-shore current as suggested by Svendsen and Putrevu (1994) and a full non linear bottom shear stress. The observations acquired during DUCK94 will be used to test the model and to quantify the relative importance of contributions from the various terms of the alongshore momentum equation within the surf zone.

MODEL DEVELOPMENT

A three-dimensional model of the nearshore circulation is derived assuming

stationary wave conditions, straight and parallel bottom contours, and random waves that are narrow-banded in both frequency and direction. A right-handed-coordinate system is used with x positive onshore, y positive to the south and z positive upward from the sea surface. In the following, the energy flux balance is considered first to describe wave transformation, which includes contributions by breaking waves described with the roller concept. The random wave distributions are described, which are used to ensemble average the various equations. The conservation of mass is described next, which provides an integral condition for the solution of the vertical profile of the cross-shore velocity. The conservation of cross-shore and alongshore momentum fluxes are considered next. The depth integrated cross-shore momentum equation describes wave set-up/down, which is the primary forcing for cross-shore currents (undertow). The alongshore momentum equation contains the lateral transfer of mean momentum term that couples cross-shore and longshore currents, which requires specifying the vertical profile of U(x,z) by solving the cross-shore momentum equation. The depth integrated alongshore momentum equation is then solved to find the cross-shore distribution of the mean longshore current, V(x).

Conservation of Energy Flux

Wave heights across the surf zone are determined using the energy flux balance equation

$$\frac{\partial}{\partial x}[E_w C_g \cos(\bar{\alpha})] + \frac{\partial}{\partial x}[E_r C \cos(\bar{\alpha})] = D \qquad \textbf{(1)}$$

where the energy is partitioned into wave, E_w, and roller, E_r, contributions (Svendsen, 1984), C_g and C are the wave group velocity and phase speed described by linear theory, $\bar{\alpha}$ is the

mean incident wave angle with respect to the shore normal calculated using Snell's Law, and D represents dissipation of roller energy (Nairn *et al.*, 1990). Following Deigaard (1993), the roller dissipation is modeled as $D = C\,\bar{\tau}_s$, where $\bar{\tau}_s$ is the mean surface shear stress at the wave/roller interface.

Both cross-shore distributions of wave height and the roller dissipation, D, are calculated using the Lippmann and Thornton (1997) model. This model assumes that random wave heights are Rayleigh distributed everywhere, even when breaking (Thornton and Guza, 1983) and was shown to give good results for the DUCK94 data set (Garcez Faria *et al.*, 1997b [Chapter 2]). Therefore, wave properties in the various equations are ensemble averaged by integrating through the Rayleigh distribution, p(H), and using a weighting function, W(H), (Whitford, 1988) to calculate the percentage of waves that are breaking, $p_b(H) = W(H)\ p(H)$.

Conservation of mass flux

The conservation of mass for straight and parallel contours is given by

$$\overline{\int_{-h}^{\eta} \rho[\,U(z) + \tilde{u}(z) + \acute{u}(z)\,]\,dz} = 0 \qquad (2)$$

where the boundary condition of no flow through the beach has been utilized and the velocities have been partitioned into mean, wave and turbulent contributions. In an Eulerian reference frame, there is an onshore mass transport by waves and an additional transport by the rollers of the breaking waves (Svendsen, 1984) limited to an upper region between the crest and trough. The ensemble and time-averaged onshore mass transport in the upper region

including contributions from wave rollers is balanced by a mean return flow below the trough (undertow)

$$\langle q_x \rangle = -\langle \int_{-h}^{\overline{\eta_t}} \rho U(z)\, dz \rangle = -\rho U_r h_t \qquad (3)$$

where η_t is trough elevation, U_r is the depth-averaged return flow, h_t is the depth below the trough, and $\langle\rangle$ indicates ensemble averaging (see Garcez Faria *et al.*, 1997b [Chapter 2], for details).

Conservation of momentum flux

The depth integrated and time averaged cross-shore momentum equation is given by

$$\frac{\partial \tilde{S}_{xx}}{\partial x} + \frac{\partial M_r}{\partial x} + \rho(\overline{\eta} + h)\frac{\partial U_r^2}{\partial x} = -\rho g(\overline{\eta} + h)\frac{\partial \overline{\eta}}{\partial x} \qquad (4)$$

where $\overline{\eta}$ is the mean wave setup (down), $\tilde{S}_{xx}$ is the wave radiation stress associated with the momentum flux due to the wave motion, the second term on the lhs is the cross-shore gradient of the momentum flux associated with wave rollers, and the last term on the lhs is the convective acceleration of the depth-averaged undertow.

The depth integrated and time averaged alongshore momentum equation is given by

$$F_y + \frac{\partial \acute{S}_{xy}}{\partial x} + \frac{\partial}{\partial x}\left[\int_{-h}^{\eta_t} \rho UV dz + \int_{\eta_t}^{\eta_c} \overline{\rho(\tilde{u}+\hat{u})(V+\tilde{v}+\hat{v})dz}\ \right] = -\overline{\tau}_y^b + \overline{\tau}_y^w \qquad (5)$$

where F_y is the ensemble averaged alongshore wave forcing, which is modeled here using

a two-layer concept where waves are breaking (Lippmann *et al.*, 1996). The lower layer contains the organized wave motion and the upper layer describes wave breaking as an elevated body of turbulent fluid riding on the front face of the wave (wave roller), consistent with spilling breakers. Following Deigaard (1993), the exchange of momentum across the wave/roller interface is described by the upward and downward volume fluxes between these two layers. The downward flux produces a shear stress at the surface, $\overline{\tau}_s$, that is associated to the total wave forcing, F_y, by conservation of momentum. Therefore, following Stive and De Vriend (1994), F_y can be written in terms of the average shear stress at wave/roller interface and local mean incident wave angle

$$F_y = \frac{\partial S_{xy,w}}{\partial x} + \frac{\partial S_{xy,r}}{\partial x} = \overline{\tau}_s \sin(\overline{\alpha}) \qquad (6)$$

where $S_{xy,w}$ is the alongshore wave radiation stress and $S_{xy,r}$ is the roller contribution to the radiation stress. The surface shear stress is calculated from the roller dissipation, D, using Lippmann and Thornton (1997) model, which is calibrated with video records of the cross-shore variation of wave breaking (see Garcez Faria *et al.*, 1997b [Chapter 2], for details).

The second term on the lhs of (5) is the lateral mixing associated with the integrated turbulent Reynolds stress that is parameterized using an eddy viscosity model (Bowen, 1969; Thornton, 1970)

$$\acute{S}_{xy} = \int_{-h}^{\eta} \overline{\rho \acute{u} \acute{v}} dz = -\rho \upsilon_{tx} (h+\overline{\eta}) \frac{\partial V}{\partial x} \qquad (7)$$

where υ_{tx} is a kinematic eddy viscosity that is estimated following Battjes (1975) by $\upsilon_{tx} = N(h+\bar{\eta})\,(\frac{D}{\rho})^{1/3}$, where N is an adjustable coefficient of O(1), the turbulent length scale is order of the local depth, and the turbulent velocity scale is $(\frac{D}{\rho})^{1/3}$.

The third and fourth terms on the lhs of (5) represent the lateral mixing associated with the interaction between cross-shore and alongshore currents (Putrevu and Svendsen, 1993), which require specifying the vertical profiles of both longshore and cross-shore currents and will be addressed later.

Following Thornton and Guza (1986), the time and ensemble averaged non-linear alongshore bottom shear stress, $\bar{\tau}_y^b$, is modeled as

$$<\bar{\tau}_y^b> = \int_0^\infty [\frac{1}{T}\int_T \rho C_f \sqrt{V^2+\tilde{u}^2+2V\tilde{u}\sin(\bar{\alpha})}\;(V+\tilde{u}\sin(\bar{\alpha}))\,dt\;]\;p(H)\,dH \qquad \textbf{(8)}$$

where C_f is a bed shear stress coefficient.

The time averaged alongshore wind stress, $\bar{\tau}_y^w$, is calculated using the drag coefficient method

$$\bar{\tau}_y^w = \rho_a C_d W W_y \qquad \textbf{(9)}$$

where ρ_a is the atmospheric density, W and W_y are the total and alongshore components of wind speed and C_d is an atmospheric drag coefficient. For C_d, the value obtained by the WANDI *Group* (1988) from observations at intermediate-depth water, is enhanced by 33 percent to take into account the increased surface roughness associated with breaking waves (Whitford and Thornton, 1993, 1996).

Vertical profile of longshore velocities

Garcez Faria *et al.* (1997a [Chapter 1]) using data from DUCK94 showed that the vertical structure of mean longshore currents on a barred beach is well described by a logarithmic profile

$$V(z) = \frac{v_*}{\kappa} \ln\left(\frac{z+h}{z_a}\right) \tag{10}$$

where κ is the von Karman constant (0.4), v_* is the alongshore shear stress velocity, and z_a is an apparent roughness due to the increase in effective roughness owing to the presence of waves (Grant and Madsen, 1979). The vertical profile of the longshore current is parameterized by v_* and z_a, and the mean bottom shear stress, $\overline{\tau}_y^b$, is related to the alongshore shear stress velocity by $\overline{\tau}_y^b = \rho v_*^2$.

To compare model predicted longshore currents with measurements, the mean longshore current found by integrating (10) over depth is defined as the reference velocity given by

$$V_m(x) = \frac{1}{h} \int_{-h+z_a}^{0} \frac{v_*}{\kappa} \ln\left(\frac{z+h}{z_a}\right) dz = \frac{v_*}{\kappa} \left[\ln\left(\frac{h}{z_a}\right) + \frac{z_a}{h} - 1\right] \tag{11}$$

Vertical profile of cross-shore velocities

Garcez Faria *et al.* (1997b [Chapter 2]) extended the monochromatic wave formulation for undertow by Stive and Wind (1986) using the random wave formulation of Thornton and Guza (1983). The vertical structure of the ensemble averaged undertow is

obtained by depth-integrating the cross-shore momentum twice and solving for the integration constants by applying conservation of mass over the vertical (2) and the stress at the trough level (by integrating the vertical momentum equation from the bottom to crest elevation), to give

$$<U(z)> = U_r + \frac{1}{\rho\mu}\left[\frac{z^2}{2} + hz + \frac{3h^2 - \eta_t^2}{6}\right]\int_0^{\infty} F_x p(H)\,dH + \frac{<\bar{\tau}_x^b>}{\rho\mu}\left[z + h - \frac{\eta_t}{2}\right] \quad \textbf{(12)}$$

where μ is a depth-independent vertical eddy viscosity coefficient (Garcez Faria *et al.*, 1997b [Chapter 2]), $\bar{\tau}_x^b$ is the mean cross-shore bed stress, and F_x is the undertow forcing, given by

$$F_x = \frac{\partial \rho \overline{U^2}}{\partial x} + \frac{1}{2}\frac{\partial \rho}{\partial x}\left[\overline{\tilde{u}^2} - \overline{\tilde{w}^2}\right] + \rho g \frac{\partial \bar{\eta}}{\partial x} \quad \textbf{(13)}$$

The cross-shore bottom stress, $\bar{\tau}_x^b$, has already been shown to be small (Longuet-Higgins, and Stewart, 1964), and thus the last term on the rhs of (12) is neglected here.

Momentum transfer by mean currents

Momentum mixing is the result of the vertical shear between the cross-shore and longshore mean currents as described by the third and fourth terms on the lhs of (5). In the water column beneath the trough, the alongshore momentum of the mean longshore current, ρV, is advected offshore by the undertow, giving

$$\int_{-h}^{\eta_t} \rho UV dz = \rho <U_r> \frac{v^*}{\kappa} h_t \left[\ln\left(\frac{h_t}{z_a}\right) - 1\right] + \frac{v_*}{9\kappa\mu_z} h_t^3 <F_x> \quad \textbf{(14)}$$

which can be rewritten as a function of the reference velocity, V_m (11), neglecting the term $\frac{z_a}{h} \ll 1$, to give

$$\int_{-h}^{\eta_t} \rho UV dz = \rho <U_r> h_t V_m + \frac{\nu_*}{9\kappa\mu_z} h_t^3 <F_x> \qquad (15)$$

In the surface region between the crest and trough of the wave, the alongshore momentum of the mean longshore current, ρV, is advected shoreward due to the mean mass transport velocity of the waves and rollers of breaking waves, which is described by the fourth term on the lhs of (5). This term can be simplified assuming that waves and turbulence are uncorrelated, small incident wave angles and that the radiation stress contributions ($\rho \tilde{u}\tilde{v}$) in the crest-trough region are of higher order, giving

$$\overline{\int_{\eta_t}^{\eta_c} \rho(\tilde{u}+\hat{u})(V+\tilde{v}+\hat{v}) dz\ ]} \approx \rho V(\overline{\eta} \approx 0) \overline{\int_{\eta_t}^{\eta_c} (\tilde{u}+\hat{u})\, dz} = <q_x> \frac{\nu*}{\kappa} \ln(\frac{h}{z_a}) \qquad (16)$$

The cross-shore distribution of the mean longshore current, $V_m(x)$, is calculated by solving (5) using the Newton-Raphson iterative method, applying a centered finite differencing scheme to rewrite the partial derivatives with the boundary condition of no flow through the beach.

FIELD DATA

Field data to test the model were acquired during the DUCK94 nearshore experiment at the U.S. Army Corps of Engineers Field Research Facility (FRF), Duck, North Carolina, in October 1994. For details of the experiment see Thornton *et al.* (1997), Elgar *et al.*, 1997,

and Garcez Faria *et al.* (1997a [Chapter 1], and 1997b [Chapter 2]). The data presented here are from 10-12 Oct. when strong currents caused by a storm with predominant winds and waves from north were present and the vertical structure of both longshore and cross-shore currents have been studied by Garcez Faria *et al.* (1997a [Chapter 1], and 1997b [Chapter 2]). During this period, observations spanned the entire surf zone and conditions approximate the assumptions of steady state and straight and parallel contours.

Cross-shore transects of wave heights and currents were measured using a cross-shore array of two-component Marsh-McBirney electromagnetic current meters (ems, hereafter) and pressure sensors at each of 13 locations (See Elgar *et al.*, 1997, for details). The vertical structure of the current was measured with a vertical stack of seven ems mounted on a mobile sled, which was deployed approximately 25 m to the south of the fixed cross-shore array. Additionally, directional wave spectra were acquired using a linear array of 10 pressure sensors in 8 m depth.

For the first run on each day, the sled was towed by the Coastal Research Amphibious Buggy (CRAB) to its farthest offshore location seaward of the bar (approximately 160 m from the shoreline). A forklift on the beach pulled the sled shoreward 10 to 30 meters for subsequent measurement runs that are referred to in the text by sequential numbers within each day. Each data run was nominally one hour, and seven to eight runs were made across a transect during each day spanning the high tide during this period.

For the cross-shore array, longshore currents were measured near mid-depth, but at arbitrary elevations, z_{meas}. To make comparisons with the model, measured longshore currents, V_{meas}, are corrected to correspond to the reference mean longshore current, V_m,

using

$$V_{cor} = \frac{V_m}{V(z=z_{meas})} V_{meas}(z=z_{meas}) = \frac{\ln(\frac{h}{z_a}) + \frac{z_a}{h} - 1}{\ln(\frac{z_{meas}+h}{z_a})} V_{meas}(z=z_{meas}) \qquad (17)$$

where V_{cor} is the corrected velocity. The elevations of the ems relative to the mean water depth, z_{meas}, were adjusted using bathymetric profiles measured daily by the CRAB and the measured mean tidal elevation. The apparent roughness, z_a, at each sensor location within the cross-shore transect occupied by the sled was obtained by interpolating the values obtained at the sled locations found by fitting a logarithmic profile to the measured vertical distribution of longshore currents based on a linear-regression least-squares method (Garcez Faria *et al.*, 1997a [Chapter 1]). For sensors located off-shore of the sled transect, a constant value equal to the measured z_a at the most off-shore position occupied by the sled was used. An example of the measured and corrected mean longshore velocities during the first run of 11 Oct. are shown in the upper panel of Fig. 2. The root mean square (*rms* , hereafter) value of the velocity corrections for all 22 runs considered is 7.1 cm s^{-1} which results on a *rms* reduction of 16 percent, and maximum correction of 16.4 cm s^{-1} amounting to a 27.5 percent reduction (Fig. 2, lower panel). Data analysis showed that the velocity correction is not a strong function of z_a, but rather mostly determined by the ems' elevation and local depth. If instead of an interpolated value, a constant z_a equal to the mean of all measured values within the days being analyzed were used, the *rms* difference between the velocity corrections given by these two approaches is 2.1 cm s^{-1} (5 percent).

RESULTS AND DISCUSSION

The relative importance of the various terms in the depth integrated and time averaged alongshore momentum balance (5) is investigated by comparing model predictions with field measurements. Contributions from each term in (5) are addressed separately, first by using a constant bed shear stress coefficient (C_f), and then by specifying cross-shore variation of C_f. Model/data comparison are quantified using a relative *rms* error defined by

$$\varepsilon = 100 \left[\sqrt{\frac{\sum (V_{meas} - V_{\mathrm{mod}})^2}{\sum V_{meas}^2}} \right] \qquad \textbf{(18)}$$

In model comparisons with data, the vertical structure of mean currents is examined at the single sled location during each run, while the cross-shore distribution of mean longshore velocity is examined using the array data combined with the single sled data point. The runs used in the following figures to illustrate contributions from different terms in the alongshore momentum balance are arbitrarily chosen to cover as much of the data as possible

Alongshore wave forcing

The importance of including contributions from wave rollers is examined in a simple balance between wave radiation stress and bottom shear stress using the Lippmann and Thornton (1997) model that includes rollers. The basis for comparisons is the Thornton and Guza (1986) model that does not include rollers, which implies that dissipation of wave energy by wave breaking occurs locally; this model has good success in describing wave driven longshore currents on near planar beaches. A comparison of the two model predictions with observations of mean longshore currents for the third run of each day being

examined is shown in Fig. 3. Incorporating the roller contribution into the alongshore wave forcing significantly changes the cross-shore distribution of the mean longshore current, resulting in a better agreement with observations (Tables 1 and 2).

The effects of including wave rollers is to displace the forcing of the longshore current shoreward. The magnitude of this onshore displacement is controlled by the steepness of the front face of the breaker and wave phase speed (Nairn *et al.*, 1990; Deigaard, 1993; Thornton and Lippmann, 1997). For highly asymmetric waves, the advection distances are smaller and the longshore current maximum will be located closer to the sand bar crest than for more symmetric waves. Advection distances also increase with increasing wave phase speed, which is proportional to water depth in shallow water, and hence more current is forced in the trough at higher tidal elevations. This tidal modulation of the longshore current is consistent with observations during the DELILAH experiment (Thornton and Kim, 1993).

This good agreement with data suggests that the alongshore wave forcing within the surf zone can be modeled using the average shear stress at the wave/roller interface, $\bar{\tau}_s$, as long as model predicted shear stress is constrained by wave breaking observations.

It can also be noticed in Fig. 3 that good agreement is obtained between the sled data and the depth-corrected data from the fixed array, despite the approximate 25 meters separation in the alongshore direction between the sensors. These results support the assumption that there was no alongshore variation of the mean longshore current in the vicinity of the measurements during the period being analyzed.

Wind forcing

During the three-day period studied here the mean alongshore wind speed was 9.1

m s^{-1} (range 7.7 - 12.6 m s^{-1}) resulting in an average wind force to wave force ratio of 0.21 (0.10 - 0.50) [Chaper 1]. Despite the wave force dominance characterizing wave-driven longshore currents, wind force contribution is not negligible. The effect of including the time averaged wind stress contribution, $\bar{\tau}_y^w$, to the alongshore momentum balance is shown in the upper panel of Fig. 4 for the time period with largest wind force to wave force ratio (seventh run of 10 Oct.). Better agreement with observations offshore and within the trough is obtained, which is related to the relative increase in the wind force to wave force ratio as wave forcing is decreased over these regions.

$\bar{\tau}_y^w$ is a direct function of the wind drag coefficient, C_d, that is yet poorly constrained by measurements within the surf zone. The constant value for this parameter adopted here is questionable, as the increased surface roughness over the bar associated with wave breaking is theoretically expected to result in larger values for C_d over this region. The sensitivity of the model to uncertainties in C_d is shown in the lower panel of Fig. 4 by varying this value within the range of values obtained by Hsu (1970) for the upper swash zone of a Florida beach (C_d = 1.0 - 7.0 x 10^{-3}). These results indicate that uncertainties in C_d could lead to underestimation of the wind stress contribution to the alongshore momentum balance. Hence, under certain conditions $\bar{\tau}_y^w$ can be an O(1) term even for wave dominated conditions inside the surf zone, especially within the trough of a barred beach.

Turbulent Reynolds stress mixing

Little difference is found over most of the cross-shore transect covered by the measurements between model predictions with and without the inclusion of the turbulent Reynolds stress mixing, $\acute{S}_{xy}$, parameterized using an eddy viscosity model(Fig. 5, upper

panel). The large differences close to the shore are not of a physical nature, but rather limitations of the dissipation model as the depth approaches zero at the shoreline (see Lippmann and Thornton, 1997 for details).

The gradual change in the predicted energy dissipation given by the Lippmann and Thornton (1997) model (Fig. 5, lower panel) results in an already smooth longshore current distribution that does not require this *ad hoc* mixing to smooth current gradients. Another possible reason that this turbulent mixing term has little effect on the longshore current profile is the small turbulent mixing scale by breaking waves used, O(h) or O(H_{rms}), which is much less than the length scale of the width of the surf zone during the days considered O(50-100 h). Other turbulent mixing scales order of the surf zone, such as shear instabilities, may contribute to momentum mixing (Dodd *et al.*, 1997), but are beyond the scope of this paper.

Following these results, and to allow an independent evaluation of the importance of the momentum mixing by mean currents to the alongshore momentum balance, the turbulent Reynolds stress mixing is neglected for the remainder of the paper, by setting N to zero.

Momentum mixing by mean currents

The contribution from the momentum mixing by mean currents to the alongshore momentum balance is illustrated by comparing model predictions including and neglecting this term with observations of mean longshore currents for the second run of each day being examined (Fig. 6). The inclusion of this type of mixing results in a shoreward displacement of the peak of the predicted mean longshore current improving the agreement with observations within the surf zone for either a constant or a variable C_f by O[10 percent]

(Table 2). Outside the surf zone, where both the magnitude and vertical structure of the cross-shore current decrease, this mixing effect is not as important, although it still leads to significantly smaller errors in the case of a constant C_f (Table 1). It can also be noticed in Fig. 6 and Table 2 that better agreement with data is obtained towards the end of the three-day-period. It is postulated that this improvement in model/data comparison is due to enhanced non linear mean current interactions associated with the observed strong cross-shore currents caused by increased wave heights and smaller angles of incidence with respect to beach normal connected with the arrival of a storm (Garcez Faria *et al.*, 1997b [Chapter 2]).

The solution for the vertical structure of the undertow used in describing the momentum mixing has as a free parameter the vertical eddy viscosity coefficient, μ, that was kept constant ($\mu = 0.04$) in both the cross-shore and over the vertical, which was shown to be a reasonable approximation under field conditions (Garcez Faria *et al.*, 1997b [Chapter 2]). The robustness of this approach is shown by changing the values of μ by an order of magnitude (Fig. 7). The amount of mixing is directly proportional to μ and the model is stable for increasing values of μ. However, reducing μ by a factor larger than 5 leads to numerical instability as the vertical profile of the undertow (12) is an inverse function of μ. These results indicate that the dispersion mixing is enhanced by an increase in the vertical gradient of the undertow (decrease in μ), which is consistent with theoretical expectations, and that the model is numerically stable for a wide range of values of the free parameter μ.

Bed shear stress

The alongshore forcing by winds and waves, including the effects of wave-breaking

modeled with the roller concept, plus the momentum mixing associated with non linear mean current interactions is balanced by the bed shear stress, modeled with a non linear quadratic formulation (Thornton and Guza, 1986). Best fit values for the constant bed shear stress coefficient, C_f, listed in Table 1 are found by iteratively minimizing the error, ε, between measurements and the complete model predictions (waves, rollers and UV mixing). Only ems located shoreward of the mean breaker line (at approximately 150 m offshore) are included in the error estimate in order to avoid biasing the *rms* fit by large errors from ems outside the surf zone. Nevertheless, the values of ε listed in Table 1 are calculated using all ems in order to compare the effects of incorporating a variable C_f. Due to the non-linear formulation used in the model, the values of ε for partial solutions of the model (waves and rollers) are obtained by re-running the model until the C_f value that gives a *rms* best fit is found for each case. The average values of ε for the ems only within the surf zone are listed in Table 2.

Although a constant C_f value provides a reasonably accurate and robust numerical solution for the cross-shore distribution of mean longshore currents within the surf zone, it does not provide insight into the physics of the problem, nor does it describe the circulation outside of the surf zone well (Figs. 3-7). Feddersen *et al.* (1997), using measurements during the entire DUK94 experiment balanced cross-shore integrated wind and wave forcing with a quadratic bottom stress formulation and found that best fit C_f values within the surf zone are three times larger than the values outside of the surf zone. Garcez Faria *et al.* (1997a [Chapter 1]) equated bed shear stress calculated from logarithmic velocity profiles to a quadratic bottom shear stress formulation and found that the associated C_f values varied by

more than an order of magnitude across the surf zone (0.0006-0.012) and were positively correlated with *rms* bottom roughness estimated from sonar altimeter measurements. Their measurements show that smaller values of C_f occurred over the bar associated with small bottom roughness owing to the planning action of the intense wave-breaking in this region. Larger values of C_f were measured in the trough, where the roughness increased due to the presence of mega ripples aligned with the strong observed longshore currents. They found the following empirical relation between C_f and apparent roughness length scale of the bed, $k_a = 30 z_a$, normalized by water depth.

$$C_f = 0.011 \left(\frac{k_a}{h}\right)^{\frac{1}{2.75}} \tag{19}$$

Here, a first attempt is made to estimate the effects of a cross-shore varying C_f on the spatial distribution of mean longshore currents by comparing model predictions using this simple relation with measurements in a diagnostic approach. In order to use (19), measured z_a values for the entire three-day-period were linearly regressed as a function of cross-shore position with small values over the bar and increasing shoreward. A constant z_a equal to the furthest offshore regressed value is used for cross-shore positions offshore of the transect occupied by the sled, where no measurements were available (Fig. 8, upper panel). The points with large estimated errors ($\varepsilon > 50$ percent) in either z_a or C_f were not included in the regression. These regressed values are then used in (19) to estimate the average cross-shore variation of C_f within the period being analyzed (Fig. 8, lower panel). Despite the large data scatter resulting in low correlation between measured and regressed z_a ($r = 0.53$), a

statistically significant correlation at the 95 percent confidence level (r = 0.96) between predicted and observed C_f is obtained. This is clearly not the case if an average value for C_f (dashed line) is adopted.

The simplistic assumption that the cross-shore distribution of the bottom roughness length scale (k_a) remains unchanged during the span of these three days which have significant changes in wave and wind forcing is certainly not realistic. Therefore, it was expected that the magnitude of the estimated cross-shore distribution of C_f would have to be adjusted for each run by multiplying the results given by (19) by a factor of O(1). Nevertheless, no change was required for all the runs on 10 and 11 Oct., which suggests that the cross-shore variation of C_f is not overly sensitive to changes in k_a, and is mostly controlled by bathymetrical changes associated with tidal variation. On 12 Oct., all the runs had to be increased by a constant factor of 1.7 to match observations. This is not surprising, as the storm waves on this day increased bottom roughness within the trough (Thornton *et al.*, 1997) and enhanced the non-linear interactions between waves and currents, which are the two major factors defining the magnitude of k_a (Grant and Madsen, 1979). Increased z_a and C_f values were measured on 12 Oct. (Fig. 8), although these anomalously large values were excluded from the regression due to their large uncertainties.

A comparison between model predictions using the best fit constant C_f and the cross-shore variable C_f given by (19) is shown in Fig. 9 for the first run of each of the days examined. These results, together with smaller calculated ε (Table 1) show that despite the crude approximation adopted here, a variable C_f significantly improves the agreement with observations outside the surf zone, O[20 percent]. Even inside the surf zone, where the

constant C_f value was adjusted to give the best *rms* fit to observations, a similar or even better agreement is obtained (Table 2). The overall improvement of model/data comparison obtained by applying the quasi-three-dimensional model with a cross-shore varying C_f indicates that the bottom roughness length scale is an important factor controlling the bed shear stress. It also suggests that the empirical relation obtained by Garcez Faria *et al.* (1997a [Chapter 1]), (19), provides a reasonable estimate for the cross-shore variation of C_f under field conditions, although the prognostic use of this relation is still limited due to our present inability to predict the bottom roughness length scale.

SUMMARY AND CONCLUSIONS

The predicted cross-shore distribution of mean alongshore currents over a barred beach given by the quasi-three-dimensional model formulated here are compared with field observations acquired during the DUCK94 experiment in an attempt to improve our physical understanding of the hydrodynamic processes governing longshore currents in the surf zone. The model includes forcing due to breaking waves described using the roller concept (Lippmann and Thornton, 1997), alongshore wind stress, cross-shore advection of mean momentum of the alongshore current (Svendsen and Putrevu, 1994), and a full non linear bottom shear stress with a variable bed shear stress coefficient, C_f, constrained by observations (Garcez Faria *et al.*, 1997a [Chapter 1]).

Incorporating the roller contribution results in a shoreward displacement of the forcing of the longshore current controlled by the wave asymmetry and phase speed. Using the shear stress at the wave/roller interface, calibrated with observations of the spatial variation of wave breaking (Lippmann and Thornton, 1997), to force the longshore current

significantly shifts the longshore current maximum towards the trough of the barred beach, resulting in largest improvement with observations, O[50 percent], for the various mechanisms examined.

Improved agreement with observations offshore and over the inner trough of the sand bar is obtained by including the time averaged wind stress contribution, which is modeled using the drag coefficient method. This better agreement is related to the relative increase in the wind force to wave force ratio as wave forcing decreases over these regions. Measurements of wind stress within the surf zone are needed to better constrain the magnitude of the wind drag coefficient, C_d, and to investigate the expected cross-shore variation of this parameter with increased surface roughness associated with breaking waves.

Two mixing mechanisms for the mean longshore current were investigated. First, the turbulent Reynolds stress mixing is modeled using an eddy viscosity formulation (Battjes, 1975), and it is shown that it does not significantly improve the agreement with observations. The failure of this mechanism is possibly related to the scale used to parameterize this turbulent mixing by breaking waves, O(h) or O(H_{rms}), which is much less than the length scale of the width of the surf zone during the days considered O(50-100 h). The second mechanism, the momentum mixing by non linear mean current interactions, is modeled by combining the solutions for the vertical profiles of longshore and cross-shore currents (Garcez Faria *et al.*, 1997a [Chapter 1] and 1997b [Chapter 2]). This mechanism is shown to displace the peak of the predicted longshore current shorewards resulting in a better agreement with observations within the surf zone O[10 percent].

The use of a non linear bed shear stress formulation with a cross-shore varying bed

shear stress coefficient, C_f, constrained by observations significantly improves the agreement with observations, O[20 percent], compared with using a constant C_f value adjusted to give the best *rms* fit to observations inside the surf zone. These results indicate that incorporating the effects of a changing bottom roughness length scale through a variable C_f is an important step for understanding nearshore hydrodynamics. However, a predictive relation for the bottom roughness length scale as a function of mean currents in the presence of waves is required to accurately specify C_f values.

The overall good agreement obtained between model predictions and observations indicates that alongshore pressure gradients were weak during the period being analyzed (10-12 Oct.), and hence the circulation was essentially two-dimensional. Therefore, despite the lack of setup measurements, the DUCK94 data provide a detailed data set to verify existing 2D and quasi-3D models for longshore currents under field conditions.

ACKNOWLEDGMENTS

This research was funded by the Office of Naval Research, Coastal Sciences Program, under contract N00114-95-AF-002. The authors wish to express their appreciation to all those who participated in the DUCK94 experiment, particularly the staff of the U.S. Army Field Research Facility under the direction of B. Birkemeier. In addition, special appreciation is expressed to Jim Stockel and R. Wyland, Naval Postgraduate School, for their role in acquisition and processing of wave and current data.

REFERENCES

Battjes, J.A., Modelling of turbulence in the surf zone, *Proceedings of the Symposium on Modelling Techniques, ASCE*, Vol. 2, 1050-1061, 1975.

Bowen, A. J., The generation of longshore currents on a plane beach. *J. Mar. Res.*, 27, 206-215, 1969.

Bowen, A.J. and R.A. Holman, Shear instability of the mean longshore current. *Journal of Geophysical Research*, 94, 18023-18030, 1989.

Church, J.C., and E.B. Thornton, Effects of breaking wave induced turbulence within a longshore current model, *Coastal Engineering*, 20, 1-28, 1993.

Deigaard, R., A note on the three-dimensional shear stress distribution in a surf zone, *Coastal Engineering*, 20, 157-171, 1993.

Dodd, N. and E. B. Thornton, "Growth and Energetics of Shear Waves in the Nearshore", *Journal Geophysical Research*, 95, No. C9, pp. 16,075-16,083, 1990.

Dodd, N., E.B. Thornton, J.C. Church, and J. Oltman-Shay, Mixing by shear instabilities of the longshore current, *Journal of Geophysical Research* (in review), 1997.

Elgar, S., R.T. Guza, B. Raubenheimer, T.H.C. Herbers, and E.L. Gallagher, Spectral evolution of shoaling and breaking waves on a barred beach, *Journal of Geophysical Research* (in review), 1997.

Feddersen, F., R.T. Guza, S. Elgar, and T.H.C. Herbers, Longshore momentum balance in the nearshore, *Journal of Geophysical Research* (submitted), 1997.

Garcez Faria, A.F., E.B.Thornton, T.P. Stanton, C.V. Soares, and T.C. Lippmann, Vertical profiles of longshore currents and related bed shear stress and bottom roughness,

Journal of Geophysical Research (accepted), 1997a [Chapter 1].

Garcez Faria, A.F., E.B. Thornton, T.C. Lippmann, and T.P. Stanton, Cross-shore mean flow over a barred beach, *Journal of Geophysical Research* (submitted), 1997b [Chapter 2].

Grant, W. D. and O. S. Madsen, Combined wave and current interaction with a rough bottom, *Journal of Geophysical Research*, 84(C4), 1797-1808, 1979.

Hsu, S.A., The shear stress of a sea breeze on a swash zone, *Proceedings 12th Coastal Engineering Conference, ASCE*, 243-255, 1970.

Lippmann, T.C., E.B. Thornton, and A.J.H.M. Reniers, Wave stress and longshore current on a barred profile, *Proceedings of Coastal Dynamics'95, ASCE*, 401-412, 1996.

Lippmann, T.C., A.H. Brookins, and E.B. Thornton, Wave energy transformation on natural profiles, *Coastal Engineering*, 27, 1-20, 1996.

Lippmann, T.C., and E.B.Thornton, The spatial distribution of wave breaking on a barred beach, *Journal of Geophysical Research* (in review), 1997.

Longuet-Higgins, M.S., and R.W. Stewart, Radiation stresses in water waves: A physical discussion, with applications, *Deep Sea Res.*, 11, 529-562, 1964.

Longuet-Higgins, M.S., Longshore currents generated by obliquely incident sea waves, 2. *Journal of Geophysical Research*, 75, 6790-6801, 1970.

Nairn, R.B., J.A. Roelvink and H.N. Southgate, Transition zone width and implications for modelling surf zone hydrodynamics, *Proceedings 22nd Coastal Engineering Conference, ASCE*, 68-81, 1990.

Oltman-Shay, I., P.A. Howd and W.A. Birkemeier, Shear Instabilities of the Mean

Longshore Current,2, Field Observations., *Journal of Geophysical Research*, 94 (C12), 18031-18042, 1989.

Putrevu, U. and I.A. Svendsen, Shear instabilities of longshore currents: a numerical study, *Journal of Geophysical Research*, 97 (C5), 7283-7303, 1992.

Putrevu, U. and I.A. Svendsen, A Mixing Mechanism in the Nearshore Region, *Proceedings 23rd Coastal Engineering Conference, ASCE,* 2758-2771, 1993.

Putrevu, U. J. Oltman-Shay and I.A. Svendsen, Effect of alongshore nonuniformities on longshore current predictions, *Journal of Geophysical Research*, 100 (C8), 16119-16130, 1995.

Reniers, A.J.H.M., E.B. Thornton, and T.C. Lippmann, Effects of alongshore non-uniformities on longshore currents measured in the field, *Journal of Geophysical Research* (in review), 1997.

Smith, J.M., M. Larson, and N.C. Kraus, Longshore current on a barred beach: Field measurements and calculation, *Journal of Geophysical Research*, 98 (C12), 22717-22731, 1993.

Stive, M.J.F., and H.G. Wind, Cross-shore mean flow in the surf zone, *Coastal Engineering*, 10, 325-340, 1986.

Stive, M.J., and H.J. De Vriend, Shear stress and mean flow in shoaling and breaking waves, *Proceedings 24th Coastal Engineering Conference, ASCE*, 594-608, 1994.

Svendsen, I.A., Mass flux and undertow in a surf zone, *Coastal Engineering*, 8, 347-365, 1984.

Svendsen, I.A., and U. Putrevu, Nearshore mixing and dispersion, *Proc. R. Soc. London*,

445, 561-576, 1994.

Thornton, E.B., Variation of longshore currents across the surf zone, *Proceedings 12th Coastal Engineering Conference, ASCE*, 291-308, 1970.

Thornton, E.B., and R.T. Guza, Transformation of wave height distribution, *Journal of Geophysical Research*, 84(C8), 4931-4938, 1983.

Thornton, E.B. and R.T. Guza, Surf zone longshore currents and random waves: Field data and models, *Journal of Physical Oceanography*, 16, 1165-1178, 1986.

Thornton, E.B and C.S. Kim, Longshore current and wave height modulation at tidal frequency inside the surf zone, *Journal of Geophysical Research*, 98 (C9), 16509-16519, 1993.

Thornton, E.B., J.L. Swayne, and J.R. Dingler, Small-scale morphology related to waves and currents across the surf zone, *Marine Geology* (accepted), 1997.

WAMDI Group, The WAM Model: A third generation ocean wave prediction model, *Journal of Physical Oceanography*, 18, 1775-1810, 1988.

Whitford, D.J., Wind and wave forcing of longshore currents across a barred beach, Ph.D. Thesis, Naval Postgraduate School, Monterey, CA, 1988.

Whitford, D.J. and E.B. Thornton, Comparison of wind and wave forcing of longshore currents, *Continental Shelf research*, Vol. 13, No. 11, 1205-1218, 1993.

Whitford, D.J. and E.B. Thornton, Bed shear stress coefficients for longshore currents over a barred profile, *Coastal Engineering*, 27, 243-262, 1996.

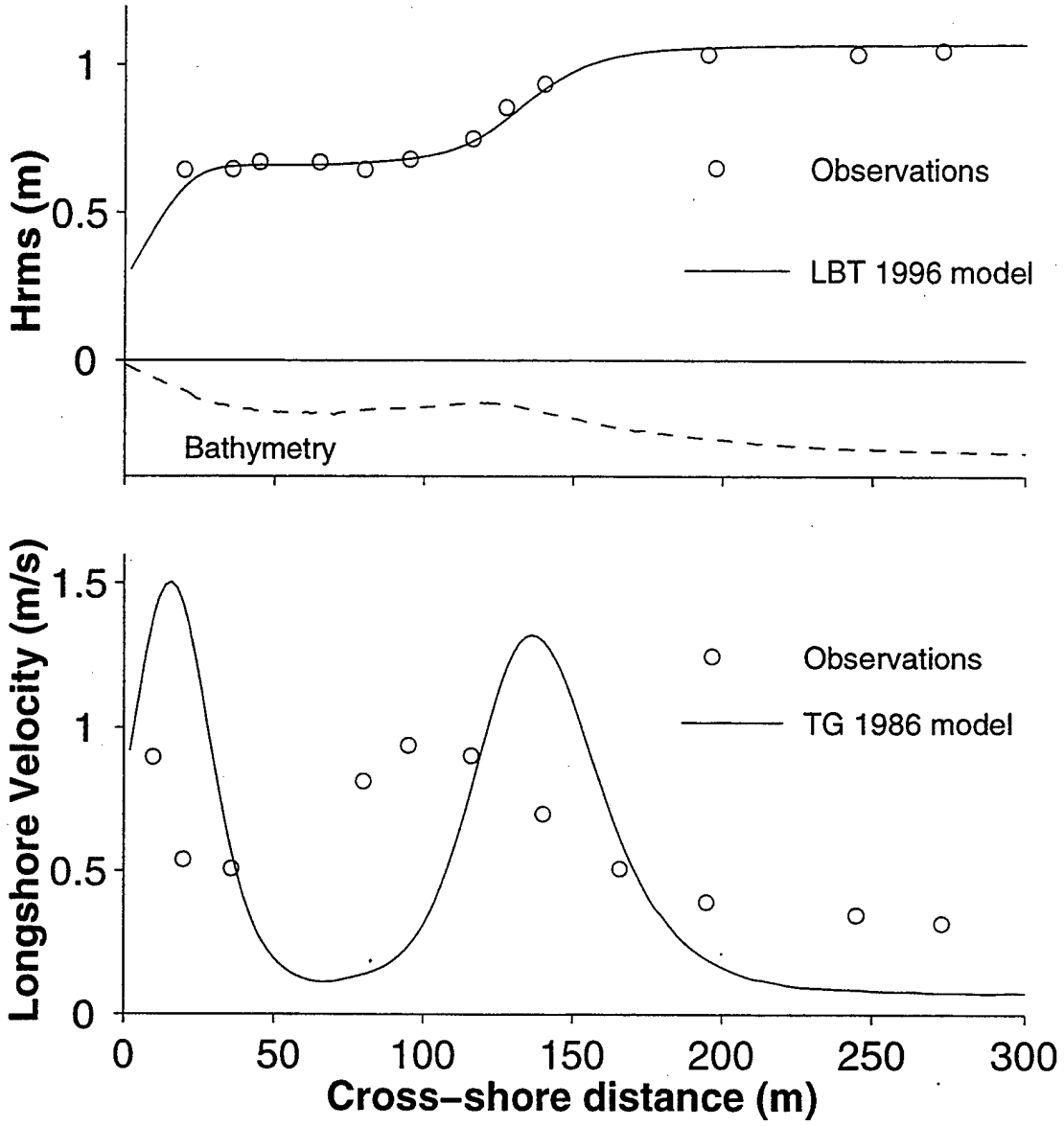

Figure 1. Cross-shore distributions of predicted (Lippmann, Brookins, and Thornton, 1996 model) H_{rms} wave heights (upper panel) and mean longshore currents (Thornton and Guza, 1986 model) V_m (lower panel). The open circles are the measured values on 10 October 1994 during DUCK94 experiment. The bottom profile (not to scale) is shown in the upper panel.

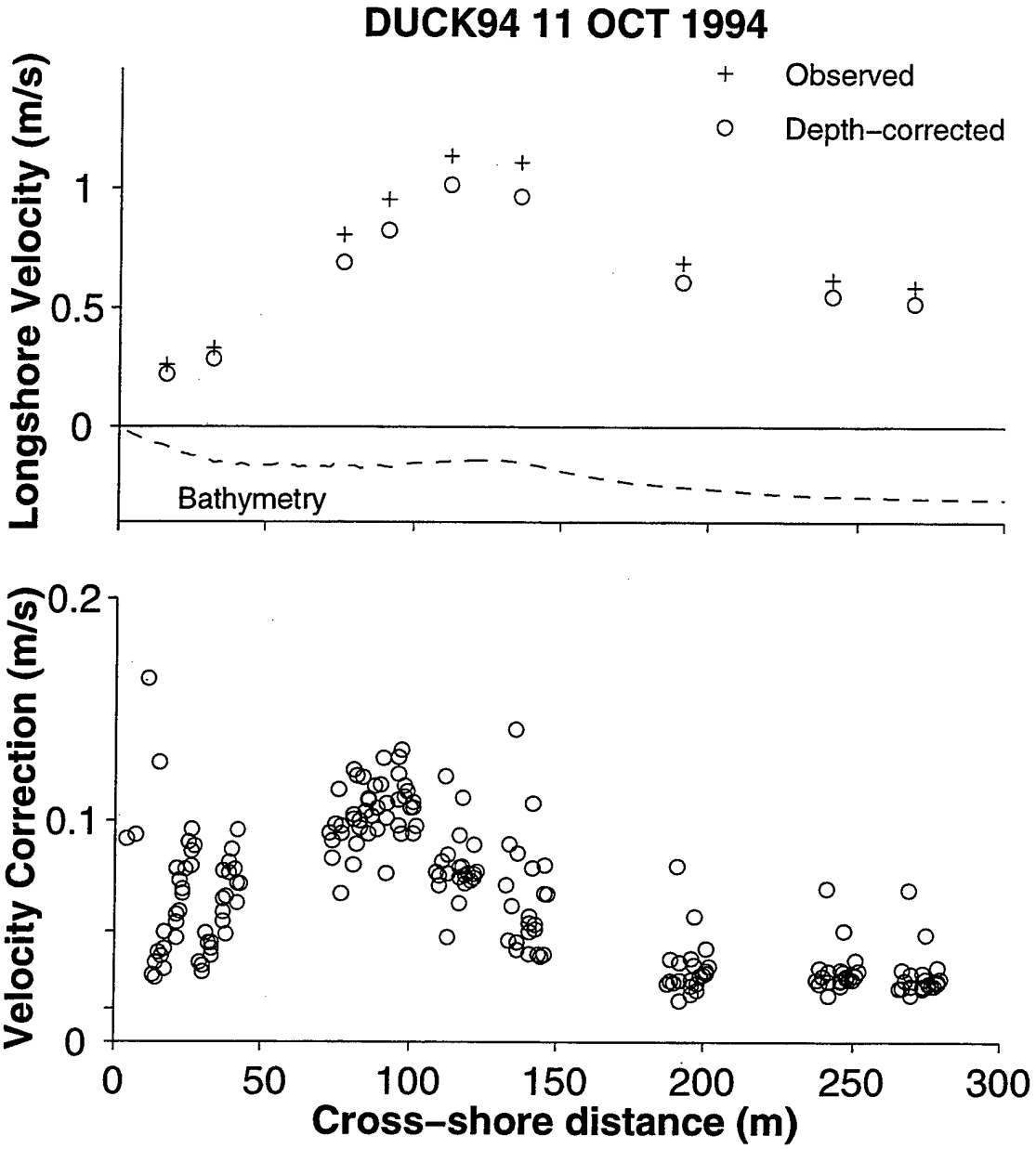

Figure 2. Cross-shore distribution of measured (+) and depth-corrected (o)mean longshore currents, V_{mm}, for the first run of 11 Oct. (upper panel). Cross-shore distribution of the calculated velocity-correction using (17) applied to the measured longshore velocities in the fixed cross-shore array for 10-12 Oct (lower panel). The bottom profile (not to scale) is shown in the upper panel.

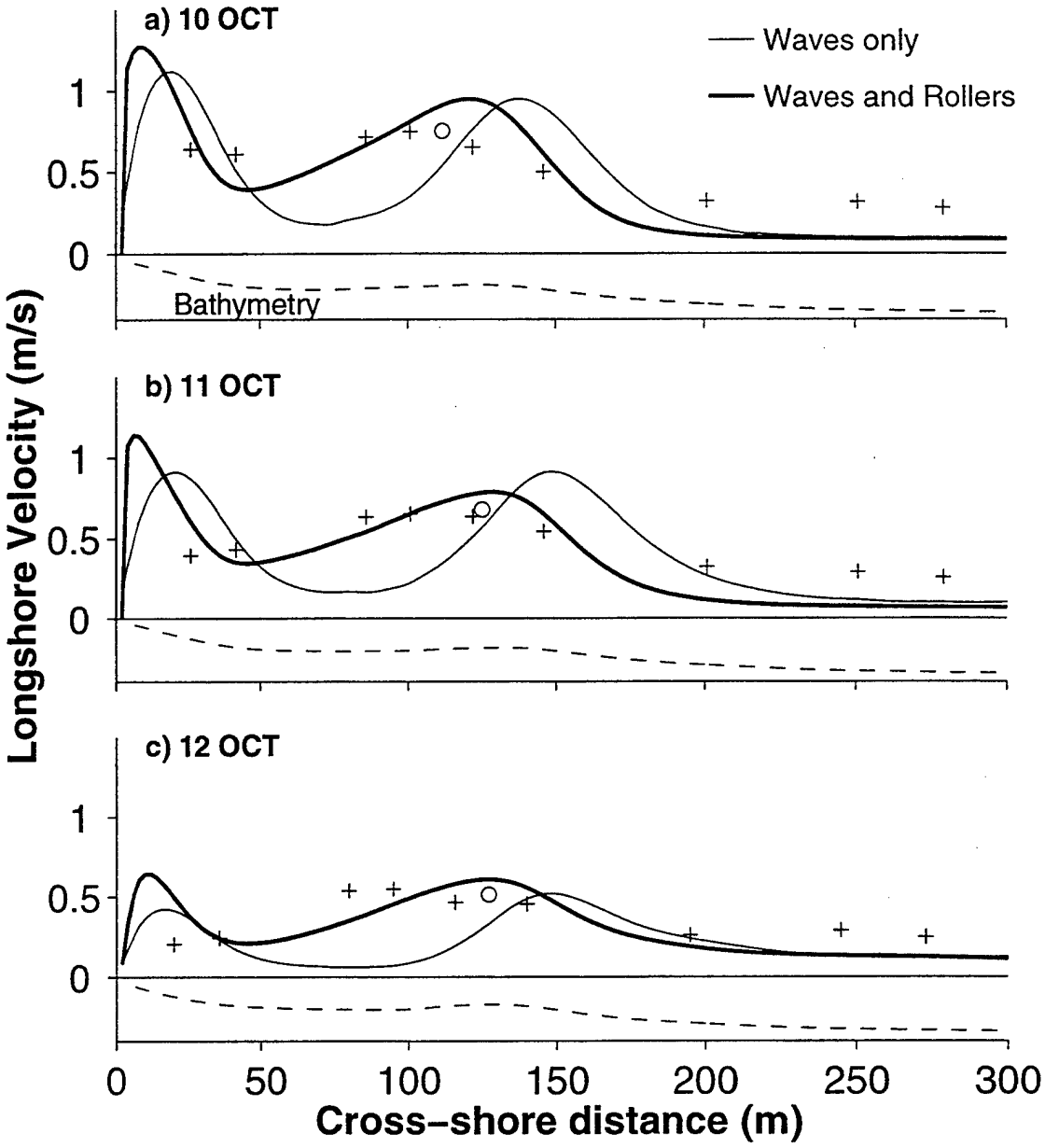

Figure 3. Comparison between measured mean longshore velocity at the sled (o) and fixed array (+) and predictions forcing the model with waves only (solid line) and waves and rollers (heavy line) for the third run of 10 Oct. (a), 11 Oct. (b), and 12 Oct. (c). Respective bottom profiles (not to scale) are shown in all panels.

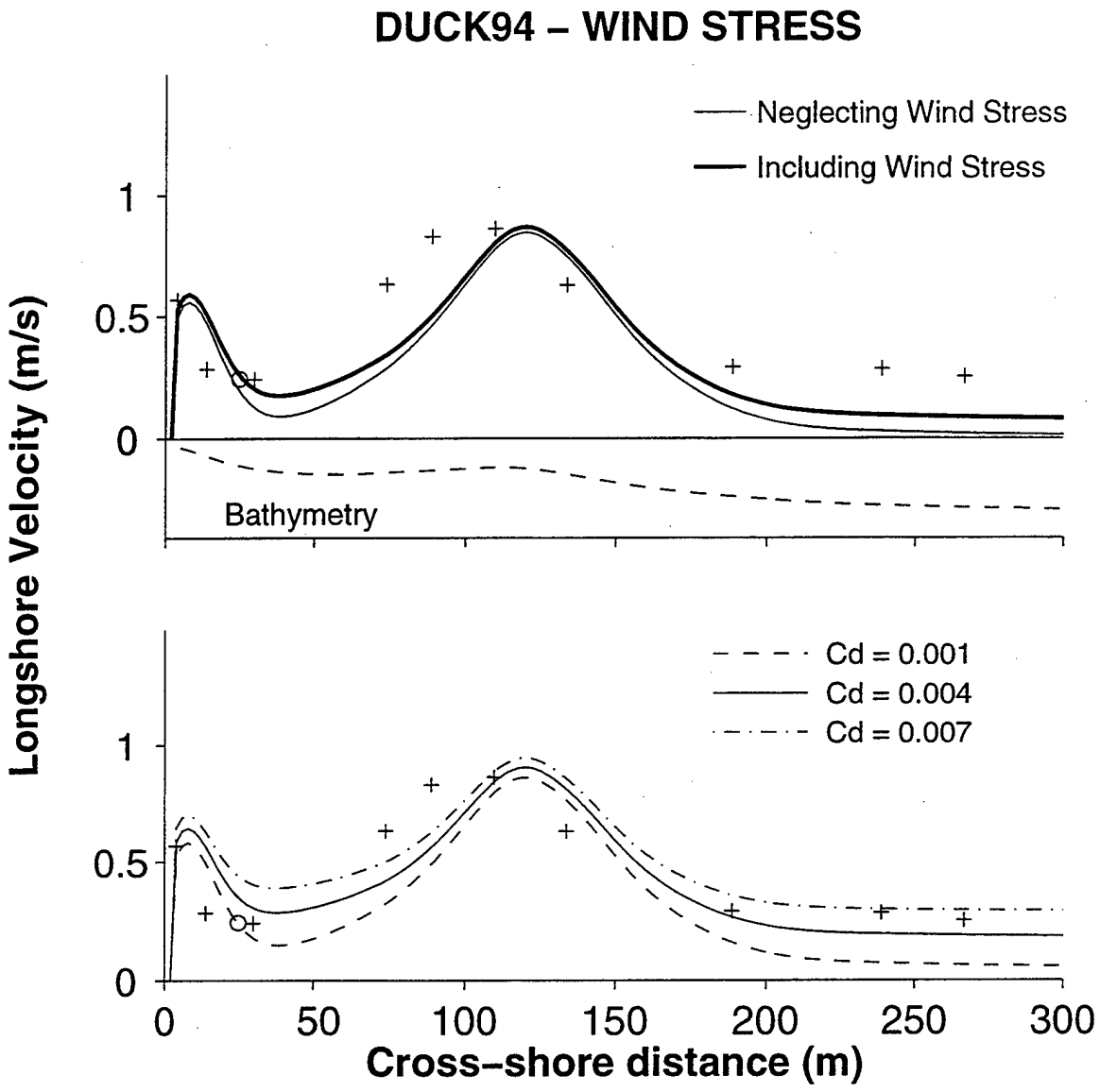

Figure 4. Comparison between measured mean longshore velocity at the sled (o) and fixed array (+) and model predictions neglecting (solid line) and including (heavy line) contributions from the alongshore wind stress for the seventh run of 10 Oct. (upper panel). Model sensitivity to the wind drag coefficient, C_d (lower panel). The bottom profile (not to scale) is shown in the upper panel.

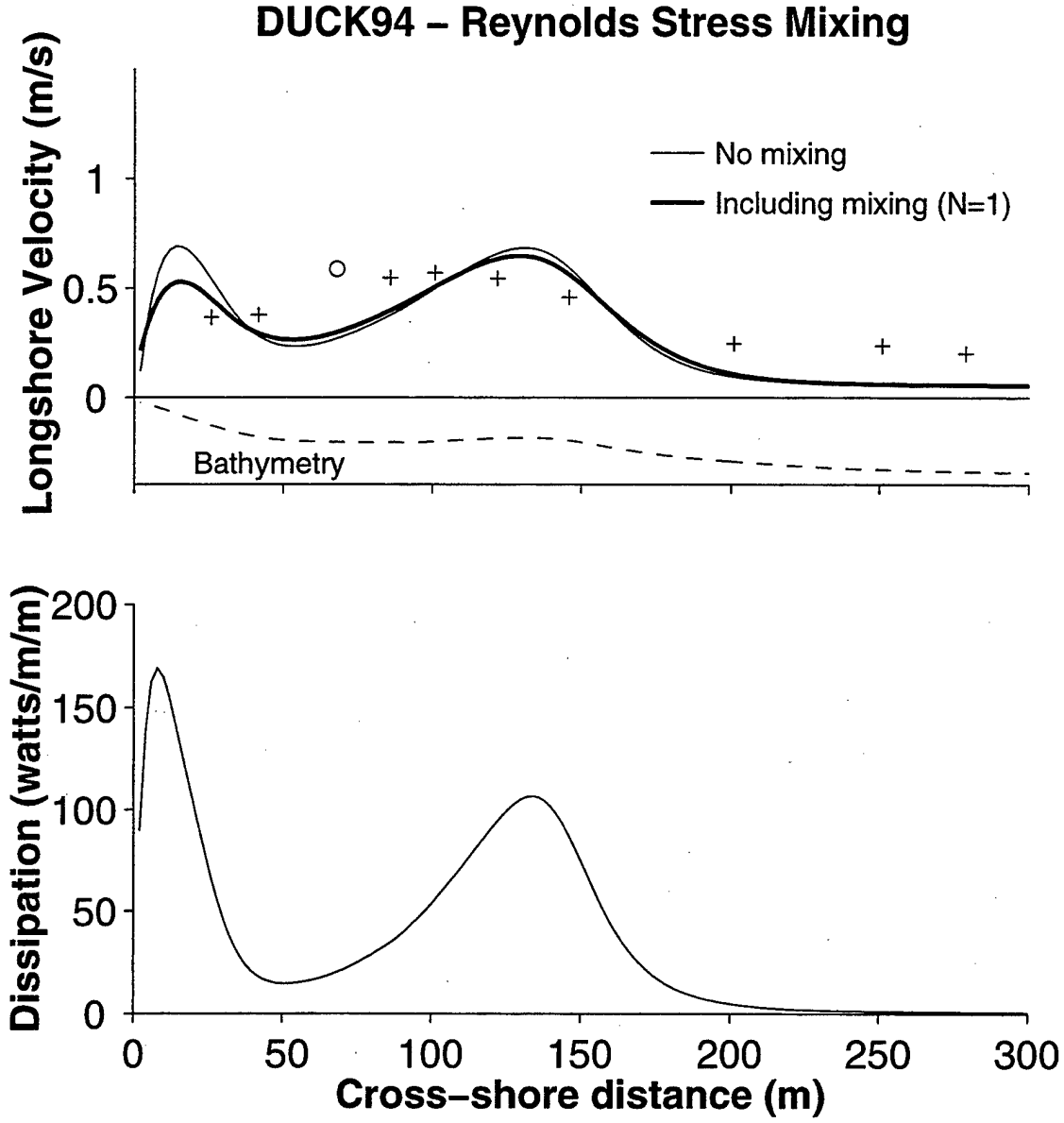

Figure 5. Comparison between measured mean longshore velocity at the sled (o) and fixed array (+) and model predictions neglecting (solid line) and including (heavy line) the Reynolds stress mixing for the fifth run of 11 Oct. (upper panel). Cross-shore distribution of predicted dissipation given by the Lippmann and Thornton (1997) model (lower panel). The bottom profile (not to scale) is shown in the upper panel.

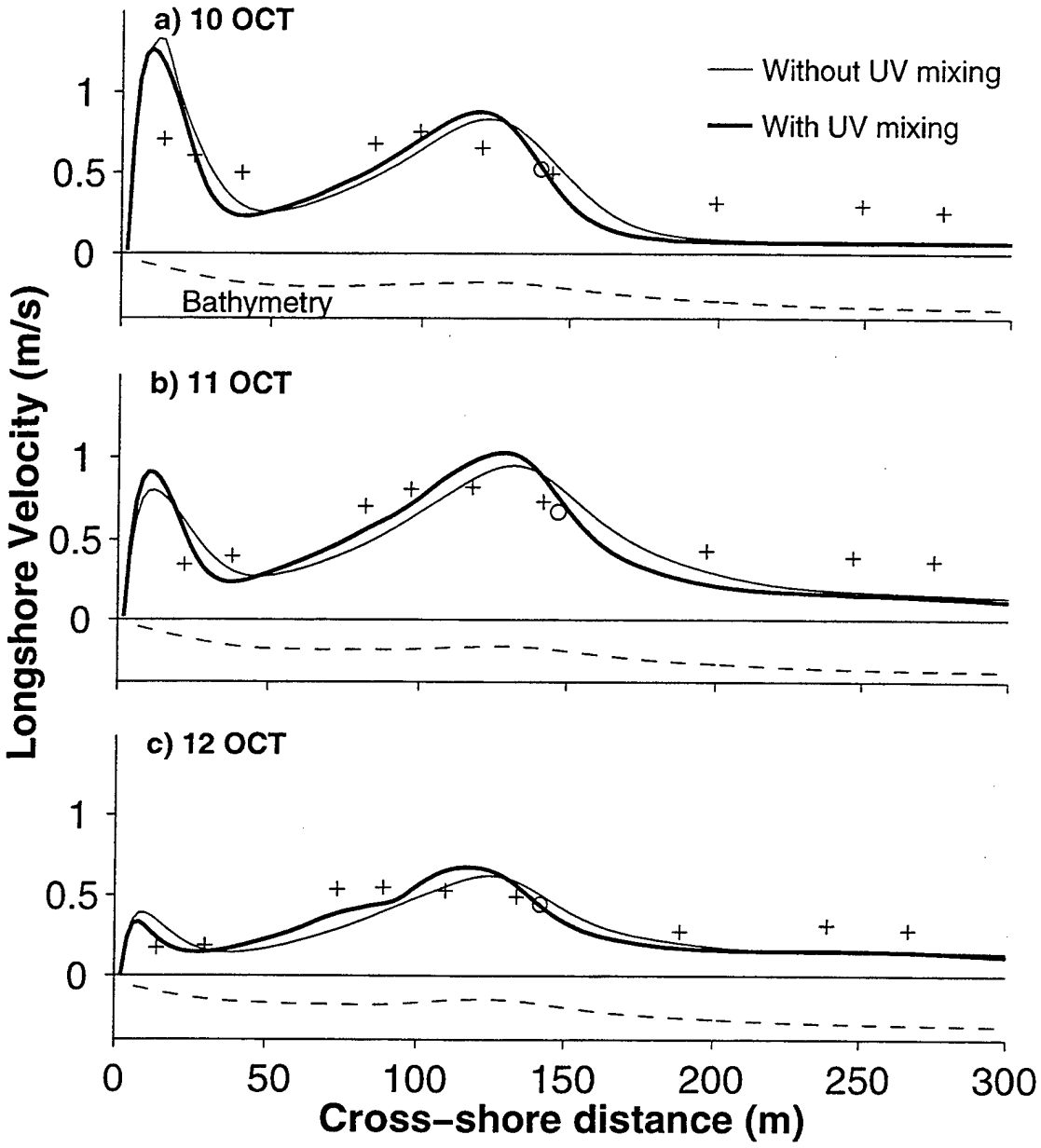

Figure 6. Comparison between measured mean longshore velocity at the sled (o) and fixed array (+) and model predictions neglecting (solid line) and including (heavy line) the momentum mixing by mean currents for the second run of 10 Oct. (a), 11 Oct. (b), and 12 Oct. (c). Respective bottom profiles (not to scale) are shown in all panels.

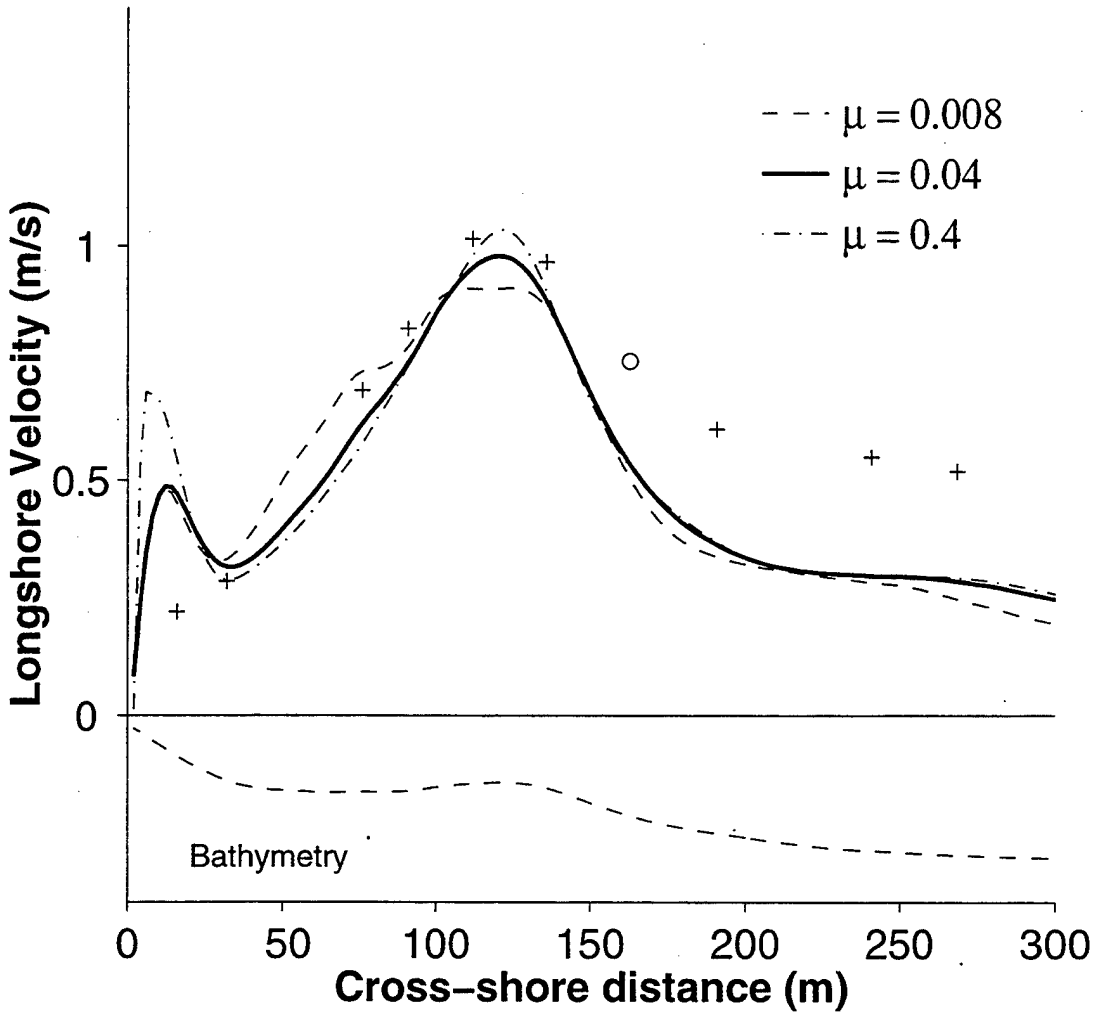

Figure 7. Model sensitivity to the vertical eddy viscosity coefficient, μ, compared with measured mean longshore velocity at the sled (o) and fixed array (+) for the first run of 11 Oct. superposed on the bottom profile (not to scale).

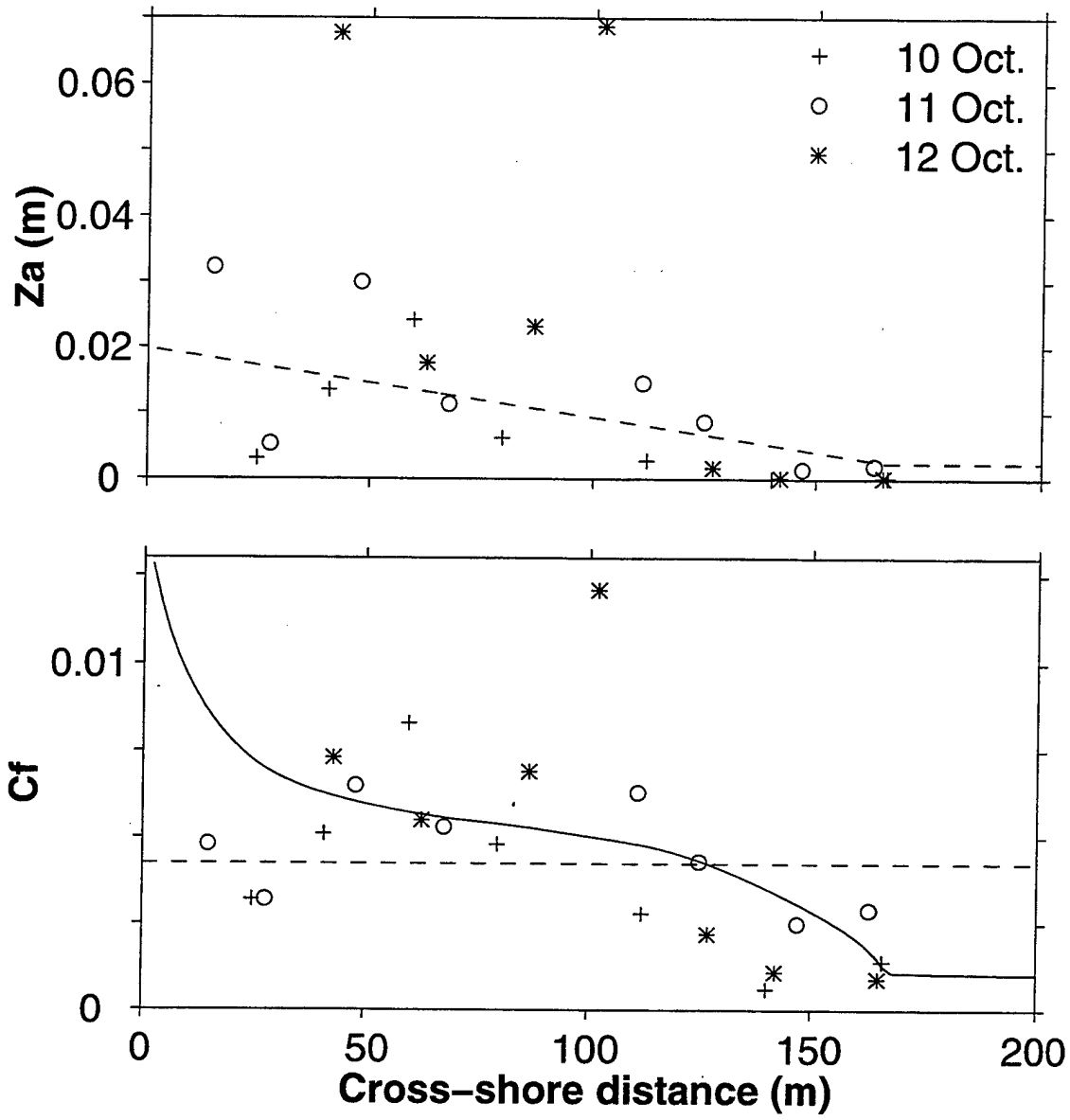

Figure 8. Apparent roughness, z_a, versus cross-shore distance (upper panel). The dashed line represents the regressed values used in (19). Bed shear stress coefficient, C_f, versus cross-shore distance (lower panel). The solid line represents predictions given by (19) using regressed z_a values shown in the upper panel and the dashed line is the average C_f.

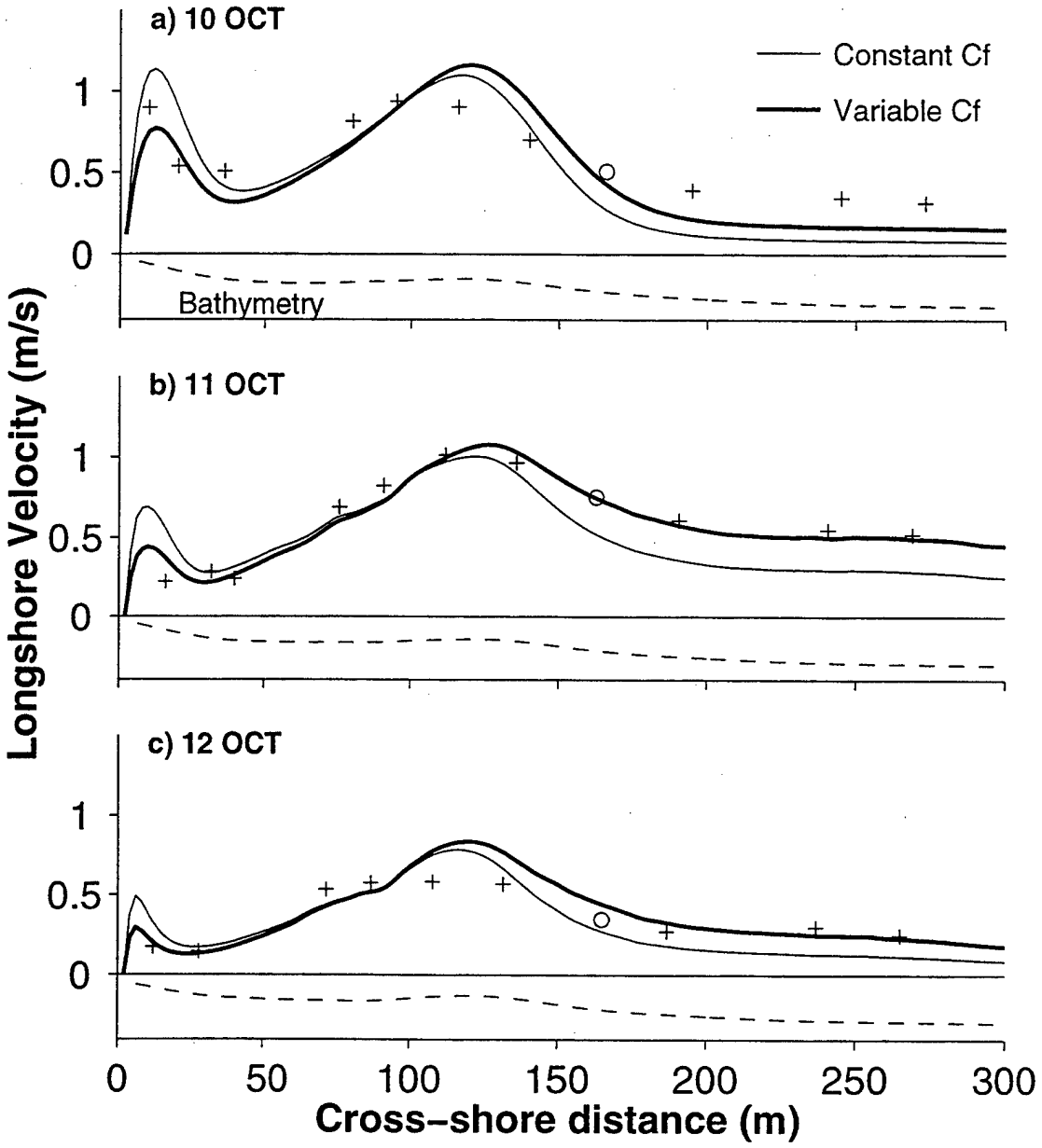

Figure 9. Comparison between measured mean longshore velocity at the sled (o) and fixed array (+) and model predictions using a constant bed shear stress coefficient, C_f, (solid line) and a variable C_f (heavy line) for the first run of 10 Oct. (a), 11 Oct. (b), and 12 Oct. (c). Respective bottom profiles (not to scale) are shown in all panels.

Table 1. Best fit model parameters and percent errors for all current meters

Day	Run	Constant C_f				Variable C_f			
			Percent Error				Percent Error		
		C_f	Waves	Rollers	UV Mixing	Average C_f	Waves	Rollers	UV Mixing
10	1	0.0050	63	50	51	0.0031	54	43	36
10	2	0.0065	65	69	50	0.0030	65	44	43
10	3	0.0050	60	43	45	0.0029	95	37	37
10	4	0.0065	70	46	45	0.0030	65	38	37
10	5	0.0060	276	52	50	0.0030	68	47	46
10	6	0.0060	72	50	50	0.0032	54	37	38
10	7	0.0055	85	55	48	0.0032	51	36	38
11	1	0.0045	98	62	50	0.0031	57	23	23
11	2	0.0055	67	41	40	0.0030	52	32	33
11	3	0.0050	68	44	44	0.0030	54	33	33
11	4	0.0060	74	47	46	0.0030	61	37	37
11	5	0.0070	78	54	48	0.0030	62	43	44
11	6	0.0065	90	61	45	0.0030	62	32	33
11	7	0.0060	65	58	54	0.0032	54	37	41
11	8	0.0090	83	64	59	0.0031	63	35	35
12	1	0.0090	74	53	41	0.0030	62	33	23
12	2	0.0085	74	45	20	0.0053	53	30	28
12	3	0.0090	66	54	35	0.0052	56	37	29
12	4	0.0065	64	48	35	0.0050	56	29	27
12	5	0.0070	66	44	40	0.0050	60	36	36
12	6	0.0090	72	62	46	0.0050	62	48	45
12	7	0.0100	68	139	98	0.0052	67	137	105
Mean		**0.0068**	**82**	**58**	**47**	**0.0036**	**61**	**41**	**39**

Table 2. Average percent errors for current meters located within the surf zone

Day	Constant C_f Percent Error			Variable C_f Percent Error		
	Waves	Rollers	UV Mixing	Waves	Rollers	UV Mixing
10	110	47	37	73	42	38
11	89	52	34	65	40	34
12	78	52	29	65	39	34
Mean	**92**	**50**	**33**	**68**	**40**	**35**

INITIAL DISTRIBUTION LIST

No. Copies

1. Defense Technical Information Center 2
   8725 John J. Kingman Rd., STE 0944
   Ft. Belvoir, VA 22060-6218

2. Dudley Knox Libary 2
   Naval Postgraduate School
   411 Dyer Rd.
   Monterey, CA 93943-5101

3. Oceanography Department 1
   Code OC/Co
   Naval Postgraduate School
   833 Dyer Rd. Rm. 328

4. Prof E. B. Thornton 2
   Oceanography Department
   Code OC/Tm
   Naval Postgraduate School
   833 Dyer Rd. Rm. 328

5. LCDR A. F. Garcez Faria 5
   Av. Governador Portela, 810
   Manejo
   Resende, Rio de Janeiro, 27520-250
   Brazil

6. Diretoria de Hidrografia e Navegação 2
   Rua Barão de Jaceguay s/n
   Ponta da Armação
   Niterói, Rio de Janeiro 24048-900
   Brazil

7. Prof. T. Stanton 1
   Oceanography Department
   Code OC/St
   Naval Postgraduate School
   833 Dyer Rd. Rm. 328

8. Prof. T. H. C. Herbers 1
Oceanography Department
Code OC/He
Naval Postgraduate School
833 Dyer Rd. Rm. 328

9. Dr. T. Lippmann 1
Center for Coastal Studies, 0209
Scripps Institution of Oceanography
9500 Gilman Dr.
La Jolla, CA 92039-0209

10. Commander 1
Naval Oceanography Command
Stennis Space Center, MS 39529-5000

11. Commanding Officer 1
Naval Oceanographic Office
Stennis Space Center, MS 39529-5001

12. Superintendent 1
Naval Research Laboratory
Marine Geosciences Div Code 7400
Stennis Space Center, MS 39529-5000

13. Chief of Naval Research 1
800 N. Quincy Street
Arlington, VA 22217

14. Office of Naval Research 1
Ocean Sciences Directorate (Code 1121 CS)
Attn: Thomas Kinder
800 N. Quincy Street
Arlington, VA 22217

15. Library 1
Scripps Institution of Oceanography
La Jolla, CA 92037

16. Dr. Dennis Whitford 1
Oceanography Department
U.S. Naval Academy
Annapolis, MD 21402

17. Director 1
U.S. Army Coastal Engineering Research Center
Kingman Building
Ft. Belvoir, VA 22060

18. Director 1
Waterways Experiment Station
Corps of Engineers
3909 Halls Ferry Rd
Vicksburg, MS 39180-6199

19. Dr. Diane Foster 1
Department of Oceanography
Dalhousie University
Hallifax, NS
Canada B3H 4J1

20. Dr. Helmut Baumert 1
Institut fuer Meereskunde
Universitaet Hamburg
Troplowitzstr. 7
D - 22529 Hamburg
Germany

21. Dr. Ad Reniers 1
Delft Hydraulics
Rotterdamseweg 185
PO Box 177
2600 MH Delft
The Netherlands